DESIGN AND ANALYSIS OF LOW PRESSURE MEMS SENSOR

A THESIS

Submitted by

SINDHANAISELVI D.

for the award of the degree of

DOCTOR OF PHILOSOPHY

in

ELECTRICAL AND ELECTRONICS ENGINEERING

DEPARTMENT OF ELECTRICAL AND ELECTRONICS ENGINEERING

PONDICHERRY ENGIINEERING COLLEGE

PONDICHERRY UNIVERSITY

PUDUCHERRY – 605 014

INDIA

JUNE 2015

DECLARATION

I hereby declare that the thesis titled **"DESIGN AND ANALYSIS OF LOW PRESSURE MEMS SENSOR"** submitted to the Pondicherry University for the award of the Degree of **DOCTOR OF PHILOSOPHY** in **Electrical and Electronics Engineering,** is a record of the original research work done by me under the supervision of **Dr. R. Ananda Natarajan,** Professor, Department of Electronics and Instrumentation Engineering, Pondicherry Engineering College, and that the work has not been submitted either in whole or in part for any other Degree/Diploma/Certificate or any other title by any University/ Institution before.

Date: ***(SINDHANAISELVI D.)***

Place : Puducherry – 14.

Dr. R. ANANDA NATARAJAN
Professor
Department of Electronics and Instrumentation Engineering
Pondicherry Engineering College
Puducherry – 605 014.

CERTIFICATE

Certify that this thesis entitled **"DESIGN AND ANALYSIS OF LOW PRESSURE MEMS SENSOR"** submitted for the award of the degree of **DOCTOR OF PHILOSOPHY** in **Electrical and Electronics Engineering** of the Pondicherry University, Puducherry is a record of the original research work done by **SINDHANAISELVI D.** during the period of study under my supervision and that the thesis has not previously formed the basis for the award to the candidate of any Degree, Diploma, Associateship, Fellowship or other similar titles. This thesis represents independent work on the part of the candidate.

Date : **(Dr. R. ANANDA NATARAJAN)**

Place: Puducherry – 14. **Supervisor**

ACKNOWLEDGEMENT

I would like to express my deep and sincere gratitude to my Research Guide, **Dr. R. Ananda Natarajan**, Professor, Department of Electronics and Instrumentation Engineering, Pondicherry Engineering College, Puducherry, for his excellent guidance and whole hearted involvement during my research work. His understanding, encouragement and personal guidance have all contributed to the present form of the thesis.

I thank **Dr. D. Govindarajulu**, Principal, Pondicherry Engineering College for his support and motivation to bring my research work a successful one.

I specially thank **Dr. P. Dhavachelvan**, Professor, Department of Computer Science, Pondicherry University, Puducherry and a member of the Doctoral Committee, for his constructive comments, and support throughout the period of this work.

I am deeply grateful to **Dr. K. Manivannan**, Professor, Department of Electrical and Electronics Engineering, Pondicherry Engineering College, and a member of the Doctoral Committee, for his constant involvement in making my research work more significant by providing constructive suggestions during the entire period of research work.

I am very much thankful to **Dr. P. Ramesh Babu**, Professor and Head, Department of Electronics and Instrumentation Engineering, Pondicherry Engineering College, Puducherry, for his support throughout the period of this work.

I am greatly indebted to **Dr. R.Joseph Daniel**, Associate Professor and Co-ordinator, NPMaSS, Department of Electronics and Instrumentation Engineering, Annamalai University for his encouragement, useful discussions and providing the MEMS design tools to complete the research work.

I extend my sincere thanks to **Dr. Alamelu Nachiappan**, Professor and Head, Department of Electrical and Electronics Engineering, Pondicherry Engineering College for her valuable suggestions, caring advice and encouragement.

I greatly acknowledge the valuable help and support rendered by all Teaching and Non-Teaching staff members of Electronics and Instrumentation Engineering Department of Pondicherry Engineering College, Puducherry.

I extend my gratefulness to the Teaching and Non-Teaching staff members of Electrical and Electronics Engineering Department of Pondicherry Engineering College, Puducherry for their support.

On my personal note, I whole heartedly acknowledge the support, encouragement and advice rendered by my late father **Thiru. R.Dhanapalan**, (School Teacher), and my mother **Tmt. M. Malarvizhi**, (Retired School Teacher), who laid the basement to buildup my carrier to this height. I also submit my gratitude to my beloved husband **Dr. T. Shanmuganantham**, Assistant Professor, Department of Electronics Engineering, Pondicherry University, and to my lovable son **Master S. Mageshwer**, the persons accompanying me throughout my path, for their commendable sacrifice, encouragement and continuous support. My heartfelt thanks are also submitted to my sister **Mrs. D. Vetriselvi** and her family members, for her affection, adjustment and support.

Finally, I am much delightful in dedicating this work to my beloved parents, whose blessing is always driving me towards success.

Sindhanaiselvi D.

ABSTRACT

Pressure measurement is certainly one of the most mature applications of Micro Electro Mechanical Systems. This is made possible by the advantage of batch fabrication micromachining technologies capable of manufacturing sensors at very low unit cost. Silicon micromachined pressure sensors are inherently smaller, lighter and faster than their macroscopic counterparts and are often more precise. Low pressure measurement is essential and need to be highly accurate. This low pressure is used in measuring indirectly the level measurement of water by hydrostatic head. The range of level measurement is 1cm to 100 cm which is equivalent to 98Pa to 9.8 kPa. The low range pressure is chosen as 0Pa to 1000Pa.

Many of the silicon micromachined pressure sensors use diaphragm as the major sensing element and piezoresistive transduction mechanism is used to convert the small deflection from the diaphragm into electrical output. The most common shapes used are the square and rectangular respectively due to their ease of fabrication and higher deflection sensitivity. Flat diaphragms are used for very high pressure measurement. The maximum sensitivity of flat diaphragms is achieved by finding minimum thickness using burst pressure analysis. Perforated thin diaphragms are used to sense medium pressure range. These diaphragms are alternate to thick diaphragms to maximize sensitivity. Very thin diaphragms are required for sensing low pressure. The reduction of diaphragm thickness leads to balloon effect which results in high non-linearity. Flat and perforated diaphragms do not offer solutions for low pressure sensing. As the diaphragm is the major key for this pressure sensor, it should be designed with acceptable linearity, high sensitivity, withstand the maximum pressure and should not break. So design of diaphragm is more critical to sense this low pressure.

Hence studies were initiated to design the special geometry diaphragms such as sculptured diaphragms with supports or rigids. These sculptured diaphragms with support increase the stiffness which limits the maximum deflection and concentrate the stress in centered region. These specialized geometries are proposed for simultaneous improvement of sensitivity and linearity. The sensitivity of the proposed

diaphragm is analyzed by suitable material, suitable shape, length/width aspect ratio and length/thickness aspect ratio. The load deflection analysis is carried out to ensure high linearity to ensure Small Scale Deflection (SSD) for less than 40%. The percentage of deflection is considered as small as possible to ensure higher linearity. Stress analysis is performed to identify the maximum stress regions for the proper placement of piezoresistors. The proposed diaphragm proves to be sensitive in low pressure range and linear. Further, the proposed diaphragm of square shape with double support yields a higher output. But rectangular shape satisfies both sensitivity and linearity. The results of the proposed diaphragms are validated with respect to developed analytical models. However, the thickness of the diaphragm is tested with respect to burst pressure approach. This technique improves the sensitivity by using a minimum range of thickness. At the same time, the dimension of rectangular shape is analyzed based on the length to width aspect ratio. Further the sensitivity of the proposed diaphragms is improved with respect to piezoresistors length and position of piezoresistors. The special case of the proposed diaphragm named as embossed diaphragm is tested for sensitivity with a diaphragm thickness 1 μm and compared for its performance.

The efficiency of the proposed diaphragms is improved by the stress enhancement using non uniform technique through a further reduction of thickness. At the same time, linearity is ensured to achieve SSD. By this technique, the proposed diaphragm with double boss sculptured square type yields 3.77mV with 24% deflection and rectangular type yields 3.842mV with 24% deflection. In addition, Silicon-On-Insulator (SOI) is a special micro machining method to enhance sensitivity is tested for the proposed diaphragms. The proposed diaphragms with double boss sculptured square shape using SOI yields 4.38mV with 28% deflection whereas double boss sculptured rectangular shape yields 4.84mV with 24% deflection which reveals that both sensitivity and small scale deflection to ensure linearity is satisfied in rectangular than square. The thickness of the diaphragm is 0.8 μm. Stress concentration is improved from 7.582MPa to 11.78MPa. The proposed diaphragm with a reduced thickness using non uniform thickness and SOI technique strongly establishes their superiority over all other existing diaphragms. Further research in this field is suggested to fine tune the diaphragms for better sensitivity and linearity.

TABLE OF CONTENTS

LIST OF TABLES

LIST OF FIGURES

LIST OF ABBREVIATIONS

AnisE	Anisotropic Etching
ASIC	Application Specific Integrated Circuit
BESOI	Bond and Etch-back Silicon –On –Insulator
CNTs	Carbon Nano Tubes
DRIE	Deep Reactive Ion Etching
FEA	Finite Element Analysis
Fig.	Figure
FSO	Full Scale Output
FSO	Full Scale Output
GPa	Giga Pascal
ICP	Intra Cranial Pressure
IMP	Intra Muscular Pressure
IOP	Intra Ocular Pressure
ISM	Industrial-Scientific-Medical
kPa	Kilo Pascal
LIGA	Lithographie Galvanoformung Abformung
LPCVD	Low-Pressure Chemical Vapor Deposition
LSD	Large Scale Deflection
MAP	Manifold Absolute Pressure
MEMS	Micro Electro Mechanical Systems
MPa	Mega Pascal
NEMS	Nano Electro Mechanical Systems
PECVD	Plasma Enhanced Chemical Vapor Deposition
PMMA	Poly Methyl MethAcrylate

PZT	Lead Zirconate Titanate
SAW	Surface Acoustical Wave
SiC	Silicon Carbide
Sicz	Single Crystal Silicon
SiNWs	Silicon Nano Wires
SOI	Silicon-On-Insulator
SoS	Silicon-on-Sapphire
SSD	Small Scale Deflection
TEM	Thermo Electro Mechanical
ZnO	Zinc Oxide

LIST OF SYMBOLS

P	Applied Pressure (Pa)
L	Length of Diaphragm (μm)
b or W	Width of Diaphragm (μm)
r	Radius of the diaphragm (μm)
h	Thickness of Diaphragm (μm)
y	Displacement or Center Deflection (μm)
y_p	Percentage of Center Deflection (%)
S_{xx} or σ_{xx} (σ_l)	Stress along X axis or Longitudinal Stress (MPa)
S_{yy} or σ_{yy} (σ_t)	Stress along Y axis or Transverse Stress (MPa)
S_{rr} or σ_{rr} ($\sigma_{\theta\theta}$)	Stress at the center for Circular Diaphragm (MPa)
E	Young's Modulus (170GPa)
ν	Poisson's ratio (0. 3 No Unit)
w	Total force acting on the plate (Newton)
α	Coefficient of Deflection (No unit)
β_1 and β_2	Coefficient of Stress (No Unit)
P_B	Burst Pressure (MPa)
R_1,R_2,R_3,R_4	Resistance of Piezoresistors (Ohm)
R_o	Resistance at Null pressure (Ohm)
ρ	Resistivity (Ohm-m)
l	Length of Resistor (μm)
A	Area of Resistor (μm^2)
G	Gauge Factor (No Unit)
ΔL	Change in Length (μm)

ΔW	Change in Width (μm)
Δh	Change in Thickness (μm)
ΔR	Change in Resistance (Ohm)
V_o	Output Voltage (Volts)
V_b	Bridge Excitation Voltage (Volts)
π_l	Longitudinal Piezoresistive Coefficient (10^{-11}/Pa)
π_t	Transverse Piezoresistive Coefficient (10^{-11}/Pa)
p11 or π_{11}	Smith Piezoresistive Coefficient (6.6×10^{-11}/Pa)
p12 or π_{12}	Smith Piezoresistive Coefficient (1.1×10^{-11}/Pa)
p44 or π_{44}	Smith Piezoresistive Coefficient (138×10^{-11}/Pa)

CHAPTER 1

INTRODUCTION

1.1 PROLOGUE

The electronic industry has, since the beginning of Integrated Circuits (IC) technology, developed fabrication processes and machinery enabling two-dimensional miniaturized structures of micrometer scales and smaller sizes. Silicon was chosen as a production material for its excellent electrical properties. The fabrication technology, used in IC production, has been further developed into the field of Micro Electro Mechanical Systems (MEMS). The Acronym Micro-Electro-Mechanical-Systems (MEMS) is the integration of mechanical elements, sensors, actuators and electronics on a common substrate through the utilization of "Microfabrication Technology" or "Microtechnology" [1, 2, 3]. This technology uses the outstanding mechanical as well as the electrical properties of the silicon material and has developed the fabrication process known as the silicon micro machining for the production of three-dimensional structures in the micrometer or even nanometer range. In the most general form, MEMS consist of mechanical microstructures, microsensors, microactuators and microelectronics, all integrated onto the same silicon chip. This is shown schematically in Fig. 1.1.

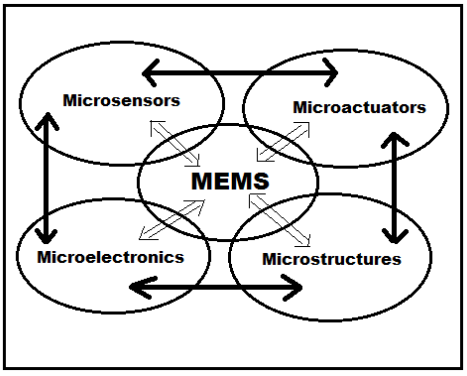

Fig.1.1 Schematic illustration of MEMS components

Microsensors detect changes in the system's environment by measuring mechanical, thermal, magnetic, chemical or electromagnetic information or phenomena. Microelectronics processes this information and signals the micro actuators to react and create some form of changes to the environment. MEMS devices are very small; their components are usually microscopic. Levers, gears, pistons, as well as motors and even steam engines have all been fabricated by MEMS. However, MEMS is not just about the miniaturization of mechanical components or making things out of silicon. MEMS is a manufacturing technology; a paradigm for designing and creating complex mechanical devices and systems as well as their integrated electronics using batch fabrication techniques. As for the IC-technology, the main benefit of MEMS is the size and cost reduction made possible by technology. The high performance that can be achieved due to the mechanical properties of the silicon material is of great importance.

In the last two decades Micro Electro Mechanical Systems (MEMS), Micro Systems, Micro Machines and their subfields, Microfluidics/lab-on-a-chip, Optical MEMS (also called MOEMS), RF MEMS, Power MEMS, Bio-MEMS and their extension into nanoscale (for example NEMS, for Nano Electro Mechanical Systems) have re-used, adapted or extended the "Microfabrication" methods. The major concepts and principles of Microfabrication are micro lithography, doping, thin films, etching, bonding, and polishing. The application of MEMS is found in several areas, including science and engineering but not limited to physics, chemistry, industry, automobile, telecommunication, civil, mechanical, biomedical, telemedicine, military and naval applications. It is also giving rise to various kinds of interdisciplinary research. Some of the major applications are listed below with a few examples.

1.2 APPLICATION OF MEMS

Automotive airbag sensors were one of the first commercial devices using MEMS. They are in widespread use today in the form of a single chip containing a smart sensor, or accelerometer, which measures the rapid deceleration of a vehicle on

hitting an object. The deceleration is sensed by a change in voltage. An electronic control unit subsequently sends a signal to trigger and explosively fill the airbag. Initial air bag technology used conventional mechanical 'ball and tube' type devices which were relatively complex, weighed several pounds and cost several hundred dollars. They were usually mounted in the front of the vehicle with separate electronics near the airbag. MEMS has enabled the same function to be accomplished by integrating an accelerometer and the electronics into a single silicon chip, resulting in a tiny device that can be housed within the steering wheel column costing only a few dollars as shown in Fig. 1.2. The accelerometer is essentially a capacitive or piezoresistive device consisting of a suspended pendulum proof mass/plate assembly. As acceleration acts on the proof mass, micromachined capacitive or piezoresistive plates sense a change in acceleration from deflection of the plates.

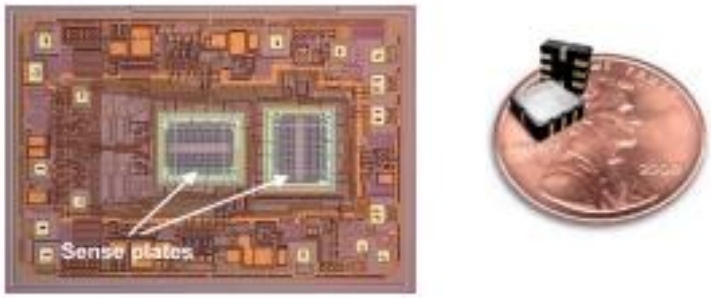

Fig.1.2 Modern day MEMS Accelerometer (left) fully packaged device (right)

The airbag sensor [1] is fundamental to the success of MEMS and micromachining technology. With over 60 million devices sold and in operation over the last 10 years and operating in such a challenging environment as that found within a vehicle, the reliability of the technology has been proven. An example of this success is today's vehicles – the BMW 740i has over 70 MEMS devices including anti-lock braking systems, active suspension, appliance and navigation control systems, vibration monitoring, fuel sensors, noise reduction, rollover detection, seatbelt restraint and tensioning etc., as shown in Fig. 1.3.

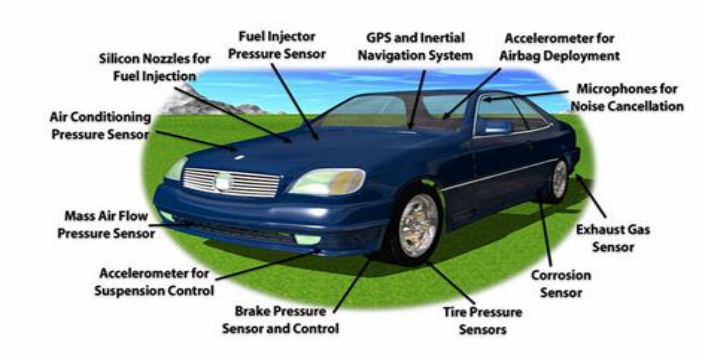

Fig.1.3 Automotive applications of Micro Electro Mechanical System

As a result, the automotive industry has become one of the main drivers for the development of MEMS for other equally demanding environments. Accelerometers are not just limited to automotive applications. Earthquake detection, virtual reality video games and joysticks, pacemakers, high performance disk drives and weapon systems arming are some of the many potential uses for accelerometers [4,7].

Another example of an extremely successful MEMS application is the miniature disposable pressure sensor [1] used in hospitals to monitor blood pressure. These sensors connect to a patient's intravenous (IV) line and monitor the blood pressure through the IV solution. For a fraction of their cost (₹635), they replace the early external blood pressure sensors that cost over ₹38235 and had to be sterilized and recalibrated for reuse. These expensive devices measure blood pressure with a saline-filled tube and diaphragm arrangement that has to be connected to an artery with a needle. The disposable sensor consists of a silicon substrate which is etched to produce a membrane and is bonded to a substrate as shown in Fig. 1.4.

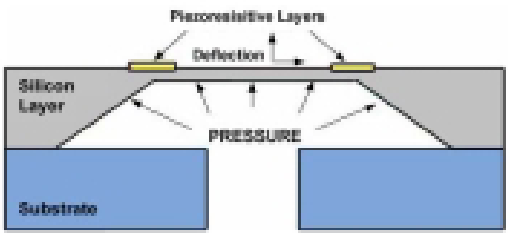

Fig.1.4 Schematic illustration of piezoresistive pressure sensor

A piezoresistive layer is applied on the membrane surface near the edges to convert the mechanical stress into an electrical voltage. Pressure corresponds to deflection of the membrane. The sensing element is mounted on a plastic or ceramic base with a plastic cap over it, designed to fit into a manufacturer's housing. A gel is used to separate the saline solution from the sensing element. More recently, the technology from the blood pressure sensor has been taken a step further in the development of the catheter-tip pressure sensor. This considerably smaller MEMS device is designed to fit on the tip of a catheter and measure intravascular pressure (its size being only 0.15 mm × 0.40 mm × 0.90 mm). Pressure sensors are the biggest medical MEMS application to date, than the MEMS accelerometer [4].

The next major application includes MEMS implantable pressure sensors which are used for continuous IOP monitoring in Glaucoma patients. Glaucoma is the second leading cause of blindness in the world after cataracts. A normal eye maintains a positive IOP in the range of 10-22 mm.Hg which is equivalent to 1.33kPa to 2.66kPa. Abnormal elevation (> 22 mm.Hg i.e., 2.66kPa) and fluctuation of IOP are considered the main risk factors for glaucoma. The implantable pressure sensor to measure intraocular pressure is shown in Fig. 1.5.

Fig.1.5. Implantable pressure sensor to measure Intraocular Pressure (IOP)

It consists of a disposable contact lens with a MEMS strain-gauge pressure sensor element, an embedded loop antenna (golden rings), and an ASIC microprocessor (2mm × 2mm chip). The MEMS sensor includes a circular active outer ring and passive strain gauges to measure corneal curvature changes in response to IOP [6]. The loop antenna in the lens receives power from the external monitoring system and sends information back to the system. In the applications listed above, the

MEMS sensor which is mostly used is the piezoresistive type rather than the capacitive and piezoelectric type.

1.3 MICRO SENSORS

A microsensor is an extremely small device capable of picking up and relaying environmental information. Such devices can measure biological, thermal, chemical, and other forms of data and send them to a processor, which then converts the information into a meaningful form to allow access to it for a variety of uses. Manufacturers of scientific equipment may produce microsensors as part of their lineup. The various Microsensor devices are accelerometers, gyroscope sensor, combo sensor, pressure sensor, proximity sensor, humidity sensor and magnetic sensor etc.,

1.3.1 Micro Pressure Sensors

Micro pressure sensors are small size sensors used for measurement of pressure. The first micro sensor was developed and used by industry piezoresistive pressure sensor to reduce fuel consumption by a tight control of the ratio between air and fuel and the other was disposable blood-pressure sensor to monitor the status of the patient during operation. Commercial products are usually either piezoresistive or capacitive. Micro pressure sensors work on the principle of mechanical bending of thin silicon diaphragm by the contact air or gas pressure. This physical movement is converted into electrical output by means of a suitable transduction mechanism [4] as shown in Fig.1.6.

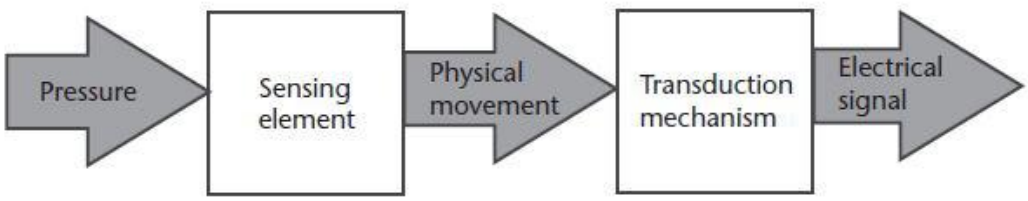

Fig.1.6 Basic elements and operating principle of pressure sensor

Pressure sensors are categorized as absolute, gauge and differential pressure sensors based on the reference pressure with respect to which the measurement is

carried out. Absolute pressure sensor measures the pressure relative to a reference vacuum encapsulated within the sensor. Such devices are used for atmospheric pressure measurement and as Manifold Absolute Pressure (MAP) sensors for automobile ignition and airflow control systems [1]. Pressure sensors used for cabin pressure control, launch vehicles, and satellites also belong to this category.

Gauge pressure sensor measures pressure relative to atmospheric pressure. One side of the diaphragm is vented to atmospheric pressure. Blood Pressure (BP), Intra-Cranial Pressure (ICP), gas cylinder pressure and most of ground-based pressure measurements are done by gauge pressure sensors. Vacuum sensors are gauge sensors designed to operate in the negative pressure region.

Differential pressure sensor measures accurately the difference ΔP between two pressures P_1 and P_2 across the diaphragm (with $\Delta P << P_1$ or P_2), and hence needs two pressure ports in top and bottom. It finds applications in aircrafts used in warfare. It is also used in high pressure oxidation systems where it is required to maintain an oxygen pressure ranging from 1 to 10 atmospheres inside a quartz tube during the oxidation of silicon. In this system, the outside of the quartz tube is maintained at a slightly higher gas pressure of nitrogen, and the pressure difference is monitored using a differential pressure sensor which ensures that the quartz tube does not experience a differential pressure greater than its rupture stress of 1 atmosphere (105 Pascal). The differential pressure sensor is also used in some applications where it is desirable to detect small differential pressures superimposed on large static pressures.

In almost all types of pressure sensors, the basic sensing element is the diaphragm, which deflects in response to the pressure. As the deflections in diaphragm-based sensors are small, they cannot be measured directly. This mechanical deflection or the resulting strain in the diaphragm is converted ultimately into electrical signals using suitable transduction mechanisms, namely, capacitive, piezoresistive or piezoelectric techniques, which are usually employed as adjectives for the pressure sensors [5].

1.3.2 Piezoresistive Type

In traditional metal diaphragm-based pressure sensors, the most common method has been to locate metal strain gauges (foil type) on the metal diaphragm, in positions of maximum stress to maximize the sensitivity. With the invention of piezoresistivity in Silicon, and silicon micromachining for diaphragm realization, boron-doped silicon piezoresistors have replaced the metal strain gauges. In this approach, much higher sensitivities have been achieved due to direct embedding of piezoresistors on the silicon diaphragm by implanting or diffusing boron in the selected regions of maximum stress as shown in Fig.1.7.

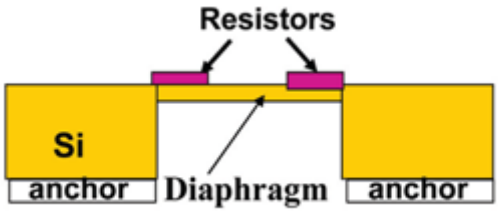

Fig.1.7 Piezoresistive pressure sensor

These resistors are connected in the form of a Whetstone Bridge which gives an output when the resistors are strained under the action of the pressure sensed by the diaphragm. Subsequent sections deal with the enabling of linear operation over a low range of pressure by piezoresistive type. They are also simple to fabricate. As a result, they have captured the major market of pressure sensors encompassing the automobile industry, defense, space as well as biomedical applications. Other transduction techniques are capacitance and piezoelectric approaches and they are identified as capacitive pressure sensor and piezoelectric pressure sensors respectively.

1.3.3 Capacitive Type

A schematic diagram of a silicon micro machined sensor of this type is shown in Fig. 1.8. This approach uses the diaphragm as one electrode of a parallel plate capacitor structure and diaphragm displacement causes a change in capacitance with respect to a fixed electrode. The merits of capacitive pressure sensors are their high

sensitivity, which is practically invariant with temperature. However, in this case, an electronic circuit is required to convert the capacitance change into an electrical output. An additional disadvantage of this approach is the nonlinear relationship between the capacitance and displacement and hence a force-balancing and linearizing electronic circuit is essential to capture a wide range of pressures.

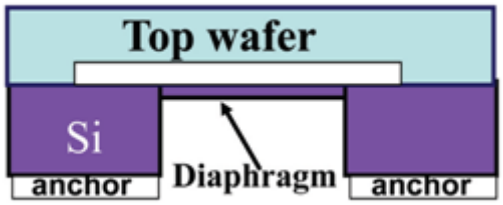

Fig.1.8 Capacitive pressure sensor

1.3.4 Piezoelectric Type

Silicon does not show a piezoelectric effect. Therefore, piezoelectric sensing elements, such as Lead Zirconate Titanate (PZT) or Zinc Oxide (ZnO) are placed/deposited on to the silicon diaphragm as shown in Fig.1.9.

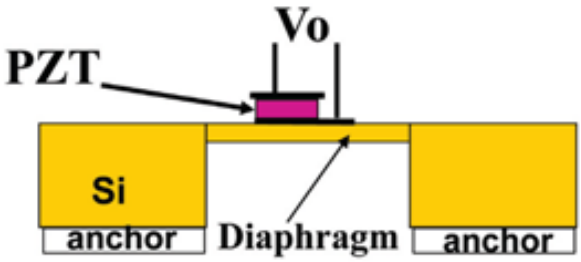

Fig.1.9 Piezoelectric pressure sensor

The deflection of the diaphragm induces strain in the piezoelectric material and hence a charge is generated. These sensors are suitable only for measuring dynamic pressure and are not suitable for static pressure sensing because piezoelectric materials respond only to changing strains. The major advantage of this approach is that an external power supply is not required.

1.4 CHALLENGES IN MEMS PRESSURE SENSORS

Pressure sensors are most primitive sensors required in all walks of life, irrespective of civilian, defense, aerospace, biomedical, automobile, oceanography or domestic applications. Among the various devices, pressure sensors using MEMS technology have received great attention because the pressure sensors find applications in everyday life involving sensing, monitoring and controlling pressure, and they therefore constitute 60 to 70 percent of the market amongst the various MEMS devices. Numerous applications have been reported by Sourabh Srivastav *et al.,* in fabrication sensing and application of both MEMS/NEMS technology [8]. MEMS technology provides the benefits of small size, low weight, high performance, easy mass production and low cost [9]. Several MEMS based biological sensors find application in physiological, medical and health applications such as triglyceride bio sensor, Bio-MEMS sensor for C-reactive protein detection, affinity sensor for glucose detection, MEMS capacitive force sensor in protein delivery, MEMS acoustic sensors for human hearing, ultra miniature MEMS capacitive pressure sensor to measure Intra Muscular Pressure (IMP) and blood cell counter [9]. MEMS flow sensors, concentration sensors, micro gas sensors and contact less temperature sensors are also some of modern day techniques revolutionized by advancements of micro machining. Recently, micro fabrication processes for retrievable complex MEMS components and the micro assembly processes for integrating those components into MEMS sensors and actuators are also reported [10]. Two dimensional human gesture tracking and recognition by the fusion of MEMS inertial and vision sensors are among the current research reported by Shengli Zhou *et al.,* [11]. Respiration detection chip with integrated temperature-insensitive MEMS sensors and CMOS signal processing circuits is also one of the emerging researches in Bio-MEMS [12]. As requirements widen, new challenges emerge and some of them are listed below [2, 3, 4, 5, 6, 7, 8, 9, 79]:

- Pressure sensor to reduce fuel consumption by a control of the ratio between air and fuel.

- Micro pressure sensors are used to monitor and measure minute gas pressure in environments or engineering systems, e.g. automobile intake pressure to the engine.
- Micro sized pressure sensors to measure the intraocular pressure in the eyes.
- Pressure sensors in various range of pressure from few Pascal to Mega Pascal.
- Very sensitive pressure sensors required in the field of biomedical application
- Pressure sensors to withstand harsh environment such as flash flood level measurement, chemical industries and automobile application etc.,
- Need of biocompatible pressure sensors
- Need for a rugged sensor which should with stand high temperatures
- Pressure sensors to survive in corrosive fluid such as ocean water applications
- Constraints on the pressure sensor chip design, fabrication and packaging.
- All these challenges have spurred the development of robust, reliable MEMS-based pressure sensor technologies involving silicon, Silicon on Insulator (SOI), Silicon on Sapphire (SOS), Silicon Carbide (SiC), Carbon Nanotubes (CNT) and Silicon Nano Wires (SiNWs).
- These constraints motivate the researcher to take up the design of micro pressure sensors.

1.5 PROBLEM IDENTIFICATION

Pressure is one of the critical parameters which requires measurement in different environmental conditions such as in aero space test, process control, biomedical, civil, agriculture and so on [4,5]. The range of pressure is classified as low pressure, medium pressure and high pressure. The medium pressure which is above 10 kPa and high pressure which is above MPa range can be easily measured. Pressure range below 10 kPa is considered as low pressure range. This pressure in low range is essentially to be measured for applications such as level measurement using hydrostatic head. Designing a suitable sensor for the low pressure range is more critical. The requirements of the low pressure sensor should be small size, high sensitivity and low cost. Silicon piezoresistive technology has been successful especially in addressing pressure sensing application for full scale pressure ranges of 5Psi (35kPa) and higher. Some flow measurements require pressures in the range

from 1Psi to 5Psi (7kPa to 35kPa). Level measurements require pressure range below 1Psi (less than 7kPa). The pressure ranges as low as 2 in. of water referred as 0.5kPa. Since water level measurement is detected by measuring the hydrostatic pressure [27] of the floodwater, the range is decided by the maximum water level height to be measured. This application is focussed on measuring the flash flood level in urban areas, when roads are flooded by sudden heavy rains, where the maximum flood level does not exceed 1m. The designed sensor should be able to sense the level from 1cm of water to 100cm of water. The 1cm is equivalent to 98Pa of pressure and 100cm is equivalent to 9.8kPa of pressure. The maximum pressure is considered as 1000Pa. 1kPa = 100cm of water = 0.01bar = 0.001N/mm^2. Similarly the intracranial pressure is also in the range of 1kPa [83, 99]. So, the pressure range chosen is 0-1000Pa. This low pressure is also necessary to be measured with high sensitivity and good linearity which is required for different application as mentioned above. Flat diaphragms are constructed with thick diaphragms greater than 5μm are used to sense pressure in range of MPa [99,101,102]. Perforated diaphragms are thin diaphragms with thickness greater than 3μm used to sense pressure in range of 10kPa and above [97, 98]. The proposed sculptured diaphragms are special geometry diaphragms with boss or rigid to withstand lower thickness of even less than 1μm to sense low pressure of 1000Pa. This is satisfied by the state of the art silicon of piezoresistive and micromachining technology.

1.6 OBJECTIVES OF THE WORK

The main objective of the present work is to develop a micro pressure sensor of high voltage sensitivity, acceptable linearity and improved stress with suitable transduction mechanism to sense the low pressure in range of 0-1000 Pa which is equivalent to a range of 1cm to 100cm of water level. As the diaphragm is the major key for any pressure sensor, it should be designed to withstand the maximum pressure and should not break. In order to realize the above said goal, the present work has been carried out with the following objectives;

- To analyze and compare the shape, size and choice of material for MEMS piezoresistive pressure sensor.

- To analyze the mathematical modelling of a flat diaphragm based MEMS piezoresistive pressure sensor.
- To design and analyze the performance of a single boss sculptured diaphragm based MEMS piezoresistive sensor.
- To design and analyze the performance of a double boss sculptured diaphragm based MEMS piezoresistive sensor.
- To design and analyze the performance of a single and double boss sculptured diaphragm based MEMS piezoresistive sensor with respect to square and rectangle shape incorporating the burst pressure analysis to find the diaphragm thickness.
- To validate the proposed structure with simulated and analytical results.
- To analyze the deflection, maximum longitudinal stress and maximum transverse stress.
- Proper placements of piezoresistors and sizing of piezoresistors were analyzed to enhance voltage sensitivity.
- To enhance sensitivity by using non-uniform thickness and Silicon-On-Insulator (SOI) technique.
- To compare the result with flat, sculptured and embossed diaphragm.

1.7 RESEARCH APPROACH

To achieve the goal with respect to above objectives: Initially, a suitable material and shape are analyzed to design the proposed diaphragm. The necessary mathematical equation of flat diaphragm is studied. The importance of aspect ratio h/L is to be studied to find the dimension and thickness for the diaphragm. The

proposed single boss diaphragm to measure low pressure is designed with uniform thickness 1μm and its center deflection, stress and piezoresistive analysis is to be carried out. The feasibility of positioning the boss to achieve the maximum deflection within the small scale deflection region is to be analyzed. The maximum longitudinal and transverse stress regions are to be identified for the placement of piezoresistors. The electrical output is to be estimated using a wheat stone bridge assembly. The square and rectangle shapes are analyzed for their performance. The proposed structure is to be validated with analytical and simulated results. To improve the performance, the double boss diaphragm with uniform thickness 1μm is to be designed and analyzed for the center deflection, stress and piezoresistive output. Similar to a single boss diaphragm, the feasibility of positioning the two bosses requires analysis to achieve the maximum deflection within the small scale deflection region. The maximum longitudinal and transverse stress regions are to be identified for the placement of piezoresistors. The electrical output is to be estimated using a wheat stone bridge assembly. The square and rectangle shapes are analyzed for their performance. The proposed structure is validated with analytical and simulated results. The performance is to be enhanced by reducing the thickness of the diaphragm is analyzed by burst pressure approach. This minimum range of thickness is used to maximize the output. The optimization of dimension for the proposed diaphragms is to be carried out to improve the stress. The position of piezoresistors, size of piezoresistors is to be analyzed to enhance the performance. The sensitivity is to be enhanced further by non uniform thickness technique and Silicon-On-Insulator (SOI) technique. The non uniform thickness is used for the diaphragm to concentrate the stress in the narrow regions where piezoresistors are to be placed to obtain the electrical output with wheat stone bridge assembly. The SOI is a silicon layer insulated by silicon dioxide layer to improve the electrical performance. The embossed diaphragm is a special case of bossed diaphragm is to be designed and its center deflection, stress and electrical output estimated for square and rectangular shapes. Finally the performance of flat diaphragm, sculptured diaphragm and embossed diaphragm is to be compared for their performance. This is achieved using Intellisuite MEMS CAD software tool.

1.8 ORGANISATION OF THESIS

This thesis has been organised as follows:

In Chapter 1, the introduction of Microfabrication technology, application of MEMS technology in various fields, micro pressure sensors and its types, different transduction mechanisms, challenges in MEMS pressure sensors, Problem identification, objectives of the proposed research and methodology for the proposed work are brought out.

In Chapter 2, a detailed review of the literature is carried out on design of MEMS pressure sensors.

In Chapter 3, a study of different materials, different shapes, h/L aspect ratio, modelling of piezoresistive pressure sensor with flat diaphragm, stress, performance characteristics, figures of merit, balloon effect and need for sculptured diaphragm are discussed.

In Chapter 4, the proposed diaphragm design for low pressure micro sensors is described and the results of the proposed structures are compared for their displacement, maximum stress and electrical output and validated by analytical equations using thickness 1μm.

In Chapter 5, the proposed diaphragm structure for low pressure micro sensor is optimised in terms of number of supports and their results are compared in terms of displacement, maximum stress and electrical output validated by analytical equations using thickness 1μm.

In Chapter 6, the proposed diaphragm for low pressure measurement is optimised in terms of number of supports and shape incorporated together with burst pressure approach validated by analytical method and the results were compared with the simulated output using thickness less than 1μm.

In Chapter 7, deals with the enhancement of voltage sensitivity by piezoresistors placement, piezoresistors length, embossed diaphragm, diaphragm with SOI and diaphragm with non-uniform thickness.

In Chapter 8, the conclusions arrived at from the results of all the proposed diaphragm design on measurement of low pressure with acceptable linearity and improved sensitivity is detailed.

CHAPTER 2

LITERATURE REVIEW

2.1 INTRODUCTION

Diaphragm design plays an important role in the design of any MEMS pressure sensor. Hence, it should be designed to ensure high sensitivity with minimum thickness, acceptable linearity, physical reliability and no breaking even at maximum pressure. The history of MEMS and materials used for its design, micromachining of silicon, types of micro pressure sensors, silicon micromachined pressure sensors, recent issues in piezoresistive micro pressure sensors and limitations of low pressure measurement and various constraints described in literature for the diaphragm design of MEMS pressure sensor are reviewed in this chapter.

2.2 HISTORY OF MEMS AND ITS MATERIAL

Piezoresistive sensors are among the earliest micromachined silicon devices. The need for smaller, less expensive, higher performance sensors helped drive early micromachining technology, a precursor to microsystems or Micro Electro Mechanical System (MEMS). In 1954, C.S. Smith, a researcher who reported the first measurements of the 'exceptionally large' piezoresistive shear coefficient in silicon and germanium [13]. This discovery showed that silicon and germanium could sense air or water pressure better than metal. Many MEMS devices such as strain gauges, pressure sensors, and accelerometers utilize the piezoresistive effect in silicon. In 1957, Mason *et al.,* first reported silicon strain gauges for measuring displacement, force and torque [14]. Due to this invention, semiconductor strain gauges, with sensitivity more than fifty times higher than conventional metal strain gauges were considered preferably in the sensing technology. In 1962, J.C. Sanchez *et al.,* proposed the first bonded semiconductor pressure sensors fabricated by sawing and

chemical etching [15]. W.G. Pfann *et al.*, proposed the integration of diffused piezoresistive elements with a silicon force collecting element [16]. The first integrated device, a diffused piezoresistive pressure sensing diaphragm was realized by Tufte *et al.*, at Honeywell Research in 1962 [17]. Piezoresistive sensors were the first commercial devices requiring three-dimensional micromachining of silicon. Consequently, this technology was a singularly important precursor to the MEMS technology that emerged in the 1980's. In 1982, Petersen's seminal paper "Silicon as a Mechanical Material" reviewed several micromachined silicon transducers, including piezoresistive devices, and the fabrication processes and techniques used to create them [18]. Petersen's paper helped drive the growth in innovation and design of micromachined silicon devices over the subsequent years. The MEMS field benefited, to a degree that no other sensor technology has, from developments in silicon processing and modeling for the integrated circuits (IC) industry. Technological advances in the fabrication of ICs including doping, etching and thin film deposition methods, have allowed significant improvements in piezoresistive device sensitivity, resolution, bandwidth and miniaturization [19]. The suitable material for construction of micro structures is reported by S.M. Spearing [20] and J.P. Sullivan *et al.*,[21]. Paul *et al.*, proposed the advanced silicon microstructures, sensors and systems [22] and Wise *et al.*, in his paper proposed about the integrated sensors, MEMS and microsystems [23].

2.3 MICROMACHINING OF SILICON

The fabrication techniques used in MEMS consist of the conventional techniques developed for integrated circuit processing and a variety of techniques developed specifically for MEMS. The three essential elements in conventional silicon processing are deposition, lithography, and etching. The common deposition processes, which include growth processes, are oxidation, chemical vapor deposition, epitaxy, physical vapor deposition, diffusion, and ion implantation. The types of lithography used are either optical or electron beam, and etching is done using either a wet or dry chemical etch process. Many of these conventional techniques have been modified for MEMS purposes, for example, the use of thick photo resists, grayscale lithography, or deep reactive ion etching. Some fabrication methods have been

developed specifically for MEMS using silicon, referred to as Silicon Micromachining and these include surface micromachining, wafer bonding, thick-film screen printing, electroplating, porous silicon, LIGA (the German acronym for Lithographie, Galvanoformung, Abformung), and focused ion beam etching and deposition [4].

2.3.1 Surface Micromachining

Harvey Nathanson from Westinghouse produced the first batch fabricated MEMS device. This device joined a mechanical component with electronic elements and was called a Resonant Gate Transistor (RGT). It was approximately one millimeter long and responded to a very narrow range of electrical input signals. It served as a frequency filter for ICs. The RGT was the earliest demonstration of micro electrostatic actuators. It was also the first demonstration of surface micromachining techniques. He got the patent for Resonant Gate Transistor by using surface micromachining of silicon in 1968. Surface micromachining does not shape bulk silicon but instead builds structures on the surface of the silicon by depositing thin films of “sacrificial layers” and “structural layers” and by removing eventually the sacrificial layers to release the mechanical structures [1, 3 and 4]. The fabrication steps were shown in Fig.2.1.

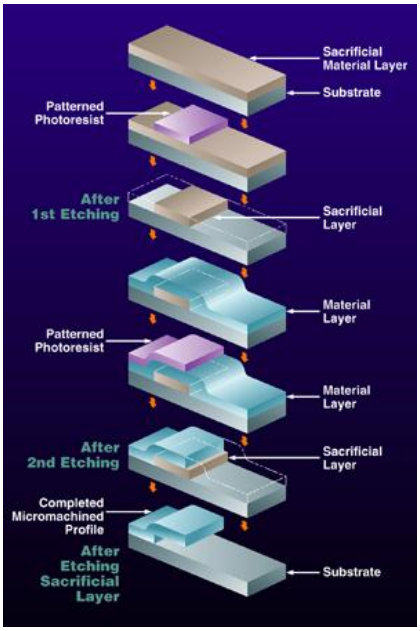

Fig.2.1 Steps of Surface Micromachining

The dimensions of these surface micromachined structures can be several orders of magnitude smaller than the bulk micromachined structures. The prime advantage of the surface-micromachined structure is their easy integration with IC components, as the wafer is also the working area for IC elements. It should be noted that as miniaturization is immensely increased by surface micromachining, the small mass structure involved may be insufficient for a number of mechanical sensing and actuation applications. In spite of its limitations, surface micromachining is used to fabricate many MEMS components such as comb drives, RF switch, gears and chains, Surface Acoustical Wave (SAW) sensors, inertial sensors and cantilevers.

2.3.2 Bulk Micromachining

"Electrochemically Controlled Thinning of Silicon" by H. A. Waggener illustrated anisotropic etching of silicon (removes silicon selectivity). This technique is the basis of the bulk micromachining process. It emerged in the early 1960s and has been in use since then in the fabrication of different microstructures. It is used in the manufacturing of a majority of commercial devices: such as pressure sensors, valves and 90% of silicon accelerometers. Fabricating these micromechanical elements requires selective etching techniques where it etches away the bulk of the silicon substrate leaving behind the desired geometries. The fabrication steps are shown in Fig.2.2.

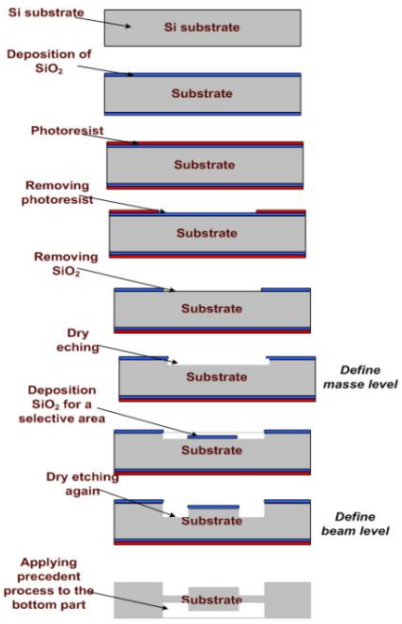

Fig.2.2 Steps of Bulk Micromachining

The microstructures fabricated using bulk micromachining [1, 3, 4] covers the thickness range from submicron to full wafer thickness (200 - 500μm) and the lateral size range from submicron to the lateral dimensions of a full wafer. Bulk micromachining [24, 25] can be divided into wet etching and dry etching of silicon according to the phase of etchants. This selectivity is possible due to the knowledge of faster etching in certain plane orientations than other planes (e.g., the <100> plane etches approximately 400 times faster than the <111> plane). In the 1970's, a micromachined pressure sensor using a silicon diaphragm was developed by Kurt Peterson from IBM research laboratory. Thin diaphragm pressure sensors were proliferated in blood pressure monitoring devices. This is considered to be one of the earliest commercial successes of microsystems devices. The following components such as cantilever arrays, nozzles, micro fluidic channels, needle arrays, AFM probes, membranes and chambers are MEMS structures that are possible only through the use of bulk micromachining processes.

2.3.3 LIGA (Lithographie (Lithography), Galvanoformung (galvanoforming), and Abformung (molding))

Another popular high aspect ratio micromachining technology is LIGA, which is a German acronym for “Lithographie Galvanoformung Abformung”. This is primarily a non-silicon based technology and requires the use of synchrotron generated x-ray radiation. The basic process defined in Fig.2.3 starts with the cast of an x-ray radiation sensitive PMMA (Poly Methyl MethAcrylate) onto a suitable substrate. A special x-ray mask is used for the selective exposure of the PMMA layer using x-rays. The PMMA is then developed and defined with extremely smooth and nearly perfectly vertical sidewalls. Also, the penetration depth of the x-ray radiation into the PMMA layer is quite deep and allows exposure through very thick PMMA layers, up to and exceeding 1 mm. After the development, the patterned PMMA acts as a polymer mold and is placed into an electroplating bath and Nickel is plated into the open areas of the PMMA. The PMMA is then removed, thereby leaving the metallic microstructure. As LIGA requires a special mask and a synchrotron (X-ray) radiation source for the exposure, the cost of this process is relatively expensive. A variation of the process which reduces the cost of the micromachined parts made with

this process is the reuse of the fabricated metal part (step 5) as a tool insert to imprint the shape of the tool into a polymer layer (step 3), followed by electroplating of metal into the polymer mold (step 4) and removal of the polymer mold (step 5).

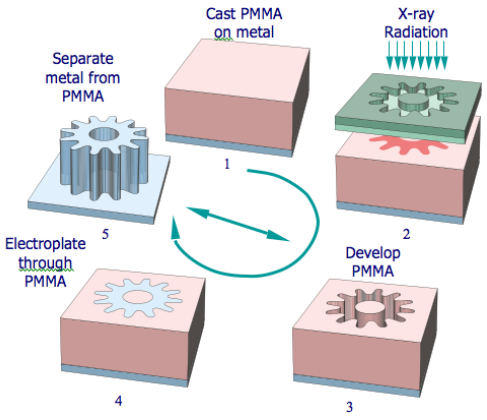

Fig. 2.3 An illustration of steps involved in the LIGA process to fabricate high aspect ratio MEMS devices

Obviously this sequence of steps eliminates the need for a synchrotron radiation source each time a part is made and thereby significantly lowers the cost of the process. The dimensional control of this process is quite good and the tool insert can be used many times before it is worn out [3, 4].

2.4 TYPES OF MICRO PRESSURE SENSORS

In the past years extensive research work has been carried out on diaphragm - type pressure sensors using advancements in silicon micro machining technology. These micro sensors are fabricated by using bulk micromachining, surface micromachining or combination of both techniques. French *et al.*, in the year 1989, invented the piezoresistance in ploysilicon and applications to strain gauges which advance pressure sensing technology [26]. The successful design of silicon micromachined pressure sensors address basic issues, including specialized geometry for enhanced linearity, suitable diaphragm thickness, boss dimensions, and resistor geometry were discussed by Mallon *et al.*, for the minimum pressure of 7kPa [27]. He proposed high precision etching including electro chemical and chemical etch-stop employing both high concentrations layers and P-N junction isolation results in low

pressure thin diaphragms referred as bossed diaphragms. B. Folkmer *et al.,* proposed the nitride material for diaphragm membrane using single crystalline piezoresistors for the pressure sensor. These sensors work on the principle of change in resistance with the deflection on the diaphragm due to applied pressure [28]. Esashi *et al.,* reviewed micromachined pressure sensors with various transduction mechanisms and principles [29].

The diaphragm type pressure sensors using change in capacitance with silicon diaphragms have non linear effects with partial improvement through variation of the reference capacitance for a parasitic insensitive capacitance measurement scheme using interdigitated electrode structure and a compensation of the linearity of the sensor achieved by Hyeoncheol Kim *et al.*,[30]. This high pressure sensor was designed with dimensions of 1600μm×1600μm×33μm with center electrode thickness 226μm for maximum pressure of 1000mm.Hg which is equivalent to 0.1 MPa. By this method, sensitivity is 0.74fF/mm. Hg and non-linearity 1.6% FSO (Full Scale Output) compared with conventional pressure sensor of sensitivity 2.1fF/mm.Hg and non-linearity 11% FSO. Since this method degrades the sensor sensitivity, a trade-off between sensitivity and non-linearity should be considered. The diaphragm type pressure sensors using change in capacitance with silicon diaphragm for flow measurement proposed by R.E.Oosterbroek *et al.*,[31]. Beeby S.P *et al.,* designed a micro engineered silicon pressure sensor with linear output and this low cost device is fabricated and validated [32]. With a view to improve the sensitivity, reliability and biocompatibility, a new Silicon-On- Insulator (SOI) monolithic capacitance sensor for absolute and differential pressure measurements of high pressure was introduced by P.D Dimitropoulos *et al.*,[33]. The SOI design achieved by CMOS switched capacitor ASIC with sensitivity of 2mV/kPa, within a span of 180kPa. The silicon material was replaced by silicon carbide in a capacitive pressure sensor for in-cylinder pressure measurement proposed by Li Chen *et al.*,[34]. The methods of bonding such as direct bonding and adhesive bonding for capacitive type pressure sensors influence the performance of the sensor were discussed by Fang He *et al.*,[35] and Cheng Pang *et al.*,[36].

The first micromachined fabry-perot cavity pressure transducer was reported in 1995 by Youngmin Kim *et al.,*[37]. The diaphragm design guidelines for optical pressure sensor were discussed by Xiaodang Wang *et al.,*[24]. A CMOS compatible ultrasonic transducer fabricated by Deep Reactive Ion Etching (DRIE) with integrated sensor and actuator for improving sensitivity which results in a simple multilayer structure was introduced by Libor Rufer *et al.,*[38]. The size of the integrated sensor is 1.3mm×1.3mm×5.2μm results in the sensitivity of 35mV/Pa at its resonance frequency of 40kHz with the maximum acoustic pressure generated by the transducer at 10mm is 5 mPa. Then a silicon based micro pressure sensitive element has been applied in the fiber optical pressure sensors. It is a highly integrated pressure sensor with improved performance proposed by F.Ceyssans *et al.,*[39], an optical pressure sensor using demodulation method proposed by Yixian Ge *et al.,*[40]. The MEMS accelerometers and pressure transducers are being used in different applications such as high resolution wall pressure measurements, low frequency noise measurements, thin film MEMS tactile sensors, ocean depth measurements employing silicon for diaphragm and silicon or polycrystalline silicon as sensing mechanism [41-45].

This review shows the different types of micro pressure sensors such as capacitive, piezoresistive and piezoelectric, fiber optic pressure sensor, types of bonding techniques, interdigitated electrode structure to improve the linearity of capacitance type sensor and SOI layer to improve the performance of pressure sensor were discussed.

2.5 REVIEW OF SILICON MICROMACHINED PRESSURE SENSORS

Tufte *et al.,*[17] reported the first silicon pressure sensors with piezoresistors integrated with the diaphragm using dopant diffusion. These diffused piezoresistive pressure sensors eliminated epoxy bonding and replaced the metal diaphragm with single crystal silicon, improved the performance of the sensors significantly. Following this, Peake *et al.,*[46] developed an integrated circuit digital, diffused silicon, piezoresistive pressure sensor for air data applications in the year 1969. In the late 1960s and early 1970s, three Microfabrication techniques, viz., anisotropic chemical etching of silicon, ion implantation and anodic bonding were developed.

These techniques played a major role in improving the performance of micromachined pressure sensors by reducing the cost of production, enabled miniaturization, increased sensitivity and precise placement of piezoresistors. In 1967, Stedman [47] pioneered bossed diaphragm pressure sensors, in 1971, Samaun *et al.*,[48] used anisotropic etching to form silicon diaphragm and increased sensitivity, L.B. Wilner [49,50] further improved the sensitivity by placing piezoresistors in the transverse direction at the concentrated stress locations and improve linearity by introducing sculptured diaphragms. In 1977, J.F. Marshall [51] at Honeywell patented the first silicon-based pressure sensors using ion implantation. In 1978, Kurtz *et al.,* [52] invented a low pressure, bossed-diaphragm, pressure transducer with good sensitivity and linearity. Clark and Wise [53] enabled refined designs with derivations of the governing electromechanical equations of thin diaphragm silicon pressure sensors using finite difference methods. From the 1980s to the present, continued improvements in fabrication technologies, such as anisotropic etching, photolithography, dopant diffusion, ion implantation, wafer bonding and thin film deposition, have enabled further reduction in size, increased sensitivity, higher yield and better performance. Several Microfabrication techniques have been developed and employed for precise control of the thickness of the diaphragm. Among those, precision etch stop used by Jackson *et al.,* Kim *et al.*,[54,55], silicon diffusion bonding by Peterson *et al.*,[56], electro chemical etch stop to have high precision control over thickness of the diaphragms by Kloeck B. *et al.*,[57], to produce a number of piezoresistive sensors includes, high pressure and high temperature sensors and accelerometers. In 1988, Spencer *et al.,* [58] compared the noise limits for piezoresistive and capacitive pressure sensors integrated with typical signal conditioning for varying diaphragm thickness, diameter and gap. F. Pourahmadi *et al*., [59] proposed the analytical modelling of thermal and mechanical stresses present in silicon microstructures. This is useful in estimating the change in resistance to bring out the electrical output of simple structures. The non linear analytical modelling of sculptured diaphragms of pressure sensors are proposed by H.Sandmaier *et al*., [60]. Kanda *et al.,* [61] considered several factors in their optimization of piezoresistive pressure sensors including: the shape of diaphragm (square or circular); the thickness uniformity of the diaphragm (with or without a center boss); anisotropy of the piezoresistivity and elasticity; and large deflection of

diaphragms. They found that a square diaphragm with a center boss on a <100> plane with four piezoresistors aligned along the <111> direction was the optimum design. The design criteria for surface micromachined pressure sensors with square and circular diaphragms have been reported in the literature [62, 63]. Piezoresistive pressure sensor designed using polycrystalline silicon has been investigated by Mosser *et al.,* [64] which in turn give the improved performance. Sun *et al.,* [65] presented a theoretical model of the reverse current and its effect on thermal drift of the bridge offset voltage, Bae *et al.,* [66] reported a design optimization of a piezoresistive pressure sensor considering the piezoresistors lengths and number of turns. Regardless of sensor dimension, piezoresistive sensors configured in a wheat stone bridge configuration achieved the best resolution. This review shows the development of Microfabrication methods, optimization of shapes, polycrystalline silicon for performance improvement, optimization of piezoresistor length, and <111> alignment for the optimum design are considered for the performance enhancement of proposed sculptured diaphragms.

2.6 ADVANCEMENTS IN PIEZORESISTIVE MICRO PRESSURE SENSORS

Morin *et al.,* [67] discuss the temperature dependence of piezoresistance of high-purity silicon and germanium, temperature dependence of the large coefficients (π_{44} for p-type and π_{11} for n-type) was measured by Tufte *et al.,* [68,69] as a function of impurity concentration. The optimum design consideration for silicon piezoresistive pressure sensing by employing square diaphragm has been recommended as it can provide 60% improvement in sensitivity compared with circular diaphragm proposed by Y.Kanda *et al.,* [61]. The piezoresistive pressure sensing is simple in design, linear over a wide range but the temperature dependence of piezoresistive coefficients of silicon is more important and to be analyzed and characterized in order to avoid stresses arising from assembly and packaging operations. The piezoresistive coefficients of silicon have been discussed by Y.Kanda [70]. Gniazdowski *et al.,* [71] has measured the longitudinal and transverse components of piezoresistance coefficient in p-type <110> silicon over the temperature range 25° C to 105° C. With a view to enhance the designers and

researchers, a set of simple equations which predicts the sensitivity of piezoresistive pressure microsensors in terms of diaphragm thickness, diaphragm length, Poisson's ratio, (piezoresistive coefficients) π_{44}, σ_{max} (maximum stress) and burst pressure were analyzed by Shih-Chin Gong *et al.,* [72,73]. The burst pressure is decided by a number of factors including diaphragm shape, thickness, lateral dimensions, diaphragm surface roughness and rupture stress of the material are reported by Henning *et al.,* [74]. The square diaphragms are better than the circular diaphragms with larger deflection sensitivity proposed by Zhao Linlin *et al.,* [75]. The voltage sensitivity is improved by using polycrystalline silicon material for piezoresistor and diaphragm is reported by M.S.Raman *et al.,* K.Sivakumar *et al.,* and Ingelin Clausen *et al.,* [76, 77, 78].

A detailed review of silicon micromachined pressure sensors was presented by K.N.Bhat [79] helped researchers to invent new designs of pressure sensors. The paper discussed silicon as a suitable material for MEMS, design criterion for flat type and sculptured diaphragms and their merits, pressure sensors using single crystal silicon, polysilicon piezoresistors with Silicon-On-Insulator (SOI) approach, MOSFET differential amplifiers integrated with pressure sensor by proper packaging using TO39 headers. The sensitivity of high pressure sensor varies from 5.81, 10.3 and 1.8 mV/Volt/Bar for the dimension 500μm×750μm×10μm, 500μm×1125μm×10μm and 500μm×875μm×15μm up to a maximum pressure of 10Bar which is equivalent to 1MPa. The result shows improvement in sensitivity in a rectangular diaphragm with reduced thickness. Some of the comparison studies reported in the literature [80] on the effect of the three diaphragm shapes with respect to deflection, stress and vibration frequency suggest that square diaphragms are useful for tactile sensors whereas rectangular diaphragms are suitable where packaging constraints limit the width versus the length and circular diaphragms is optimal in case of microphones where it gives large center deflection. The output offset induced by packaging due to thermomechanical stress is minimized by measuring material properties at different temperatures and package warpage for high resolution accelerometers were discussed Xin Zhang *et al.,* [81]. The temperature dependence of piezoresistive coefficients of p-type and n-type <001> silicon from temperature -150°C to +125°C using stress sensing chips investigated by Chun-Hyung Cho *et al.,*

[82]. This review reveals that, p-type piezoresistors must be oriented along the <110> directions to measure stress where piezoresistive coefficients are maximum. The advancements in MEMS technology spurred the author Usmah Kawoos *et al.,* [83] to propose a wireless completely implantable intracranial pressure monitoring device, operating at an ISM (Industrial-Scientific-Medical) band of 2.4GHz for the pressure range of 0-100mm.Hg (0 – 13.3kPa) with a capacitive MEMS sensor of size 2.5μm thick sealed cavity. The results illustrate a maximum pressure reading of 0.8 mm.Hg (106Pa) obtained for a sub-dural device with a capacitive type compared to 2 mm.Hg (266Pa) obtained for an epidural device with a piezoresistive sensor. Above all, the review shows common use of piezoresistive type sensor due to its linear operation and ease of fabrication, square and rectangular shape give better sensitivity than circular, rectangular type with reduced thickness improve the sensitivity, SOI layer to improve sensitivity, higher thickness of 10μm used for high pressure in the range of MPa, 2.5 μm used for sensing 10kPa and above and piezoresistive type recommended for biomedical application. The sculptured diaphragms reported above were not tested for burst pressure analysis which results in minimum thickness to achieve maximum sensitivity.

Jong M.Park *et al.,* [84] have developed a piezoelectrically actuated micro valve with a integrated piezoresistive pressure sensor and a temperature sensor for space application in a cryogenic environment. The integrated sensor monitor inlet pressure and coolant temperature and enabled the closed loop control of distributed cooling systems. In addition, the results of the temperature sensor can be used to compensate for the temperature coefficients of pressure sensor, in a compact from. The overall dimension of the sensor is 1.5×1.5×1.1 cm^3. This is achieved by a SOI wafer with anodic bonding. A novel design of application specific MEMS pressure sensor for harsh environment using touch mode capacitive sensor in range of 0 to 10 bar, for distributed system using optical MEMS sensor in range of 0 to 350 bar (0 to 35MPa) and for medical environment using wireless pressure sensor in range of 0-330 mm. Hg (0 – 44kPa) were discussed by Giulio Fragiacomo *et al.,* [85] and classified as high pressure sensor. A strain sensor employing a circular diaphragm with 1.35cm diameter having piezoelectric thickness of 300μm sandwiched between two silicon dices sense the strain produced by pressure less than 500kPa with

electrical output of 6.6mV for civil engineering applications presented by Joel Soman *et al.,* [86]. The strain sensor is made of lead zirconate titanate (PZT) for soil mechanics applications for efficient and precise dynamic measurement. Ivan padron *et al.,* [87] fabricated an integrated optical and electronic pressure sensor in one unit where the sensing element for both integrated part is an embossed silicon diaphragm that deflects under differential pressure. The optical part of the sensor is based on fabry-perot cavity interferometer with a laser source and detector; electronic part of the sensor based on the piezoresistive effects in silicon with embossed diaphragm of square shape is designed. This optical technique provides capabilities for small sizes, immunity to harsh environments, remote operation and ease of integration with other devices. The sensitivity is 2.6mV/kPa for the maximum pressure range of 0 to 35kPa. This also provides immunity to electromagnetic interference, chemical attack and high performance. The compensation models for hysteresis of silicon piezoresistive pressure sensor in order to improve the sensor accuracy reported by Yang Chuan *et al.,* [88]. The review reveals the method of anisotropic wet etching for square diaphragm, silicon as mechanical material, piezoresistive type with wheat stone bridge for temperature compensation, thick diaphragms to detect high pressures, embossed diaphragms for differential pressure are defined for high pressures measurement.

2.7 RECENT ISSUES IN PIEZORESISTIVE MICRO PRESSURE SENSORS

The applications and advancements of MEMS technology are not limited to any specific applications. The MEMS devices are widely used in the area of sensors, for example, pressure sensors, optical sensors, acoustic sensors, microphones, actuators, resonant sensors, micro valves, integrated sensors, temperature sensor, gas sensor, strain sensor. Etc. Pressure sensing is done by the primary sensing mechanism named as diaphragm which deflects due to applied pressure. In recent issues discussed by Vidhya Balaji *et al.,* [89] about the piezoresistive type pressure sensor, linearity of pressure sensor having thin diaphragms thickness 10μm were taken up with respect to their shapes and burst pressure. The surface areas of three different shapes were identical and the stress component at the corner, center and edge of diaphragms

analyzed for burst pressure conditions. The author concludes that circular types can be considered most useful at high applied pressures. Nitin R.Panse *et al.,* [90] has developed an analytical model of large deflection analysis of Flat and corrugated stainless steel diaphragms. Rigid circular diaphragms and their load deflection analysis compared with FEA and ANSYS by S.S. Gawade *et al.,* [91]. A new MEMS pressure sensor for measuring intraocular pressure sensor with clamped and slotted diaphragms using capacitive transduction has been discussed by M.Shahiri-Tabarestani *et al.,* [92]. In this approach, a slotted diaphragm gives a higher sensitivity than a clamped diaphragm. Moinuddin Ahmed *et al.,* [93] discussed MEMS absolute pressure sensors sandwiched between a flexible polyimide applied for structural health monitoring in aerospace applications. A sensitive silicon based piezoresistive pressure sensor for high pressure measurement has been discussed by Suja K.J *et al.,* [94] by using the SOI approach. Finite Element Analysis for piezoresistive pressure sensor were discussed by K.Y Madhavi *et al.,* [95] and Sarath S *et al.,* [96] proposed AC bridges in MEMS pressure sensors with full scale pressure of 150kPa results in a sensitivity of 9.3×10^{-3}mV/V/kPa.

An oxygen flow sensor using a differential pressure method in a pediatric ventilators proposed by Rajavelu *et al.,* [97,98] shows that thick diaphragms with perforations produce results with good linearity rather than thin nonlinear diaphragms. The diaphragms with 40% perforations of size 50μm×50μm are used. The diaphragm 500μm×500μm×7μm detected the pressure in the range of 0-20kPa with the voltage sensitivity of 0.079mV/V/kPa. The diaphragm 500μm×500μm×5μm detected the pressure in the range of 0-5kPa with the voltage sensitivity of 0.152mV/V/kPa. The diaphragm 500μm×500μm×7μm detected the pressure in the range of 0-20kPa with the voltage sensitivity of 0.079mV/V/kPa. The diaphragm 500μm×500μm×3μm detected the pressure in the range of 0-1kPa with the voltage sensitivity of 0.406mV/V/kPa. The diaphragm 700μm×700μm×5μm detected the pressure in the range of 0-1kPa with the voltage sensitivity of 0.402mV/V/kPa. In this literature, the improvement in voltage sensitivity with 40% perforated area irrespective of the thickness of the diaphragm is reported and the modified analytical models were developed to validate the results from simulation using COMSOL Multiphysics and Intellisuite. An overview of pressure sensors including their design of thin and thick

diaphragms, engineering, technology and packaging challenges have been discussed by K.N.Bhat *et al.,* [99]. The different material for harsh environments, high temperatures, CNT based sensors single walled CNT and Multi-walled CNT, reliable packaging constraints for medical applications to reduce the cost of production, packaging related with safe environment, proper electrical interface were presented in this article encouraged the researchers to know about the constraints in designing. The placement of piezoresistors and their size were discussed to enhance the sensitivity with SOI approach for high pressures in the range of 0 to 5MPa given by M.Narayanaswamy *et al.,* [100, 101]. The modelling of diaphragm design and SOI pressure sensors with thick diaphragms was reported in the article. Sensitivity enhanced by using minimum thickness from burst pressure approach also presented. SOI structure consists of a top single-crystal silicon layer, either separated from the bulk substrate by an insulating layer (for instance SiO_2) or directly supported by an insulating substrate [33, 99, 100, 101]. Technologies based on the use of a buried layer, SiO_2, as an insulator in SOI wafers have been widely developed in microelectronics because of their advantages compared to silicon bulk substrates. Attempts were made to form BOX layers by oxygen implantation in silicon wafers. Specific techniques have been developed to achieve very thin layers through bonding and thinning processes. First developed in order to obtain SOI wafers with very thin top silicon layers, these techniques are referred to as Bond and Etch-back Silicon - On - Insulator processes (BESOI) [102, 103, 104, 105].

Further downscaling of strain gauge based MEMS devices referred to as Carbon Nano Tubes (CNTs) are ideal candidates due to large gauge factors, low power operation and nanometer dimension proposed by Thomas Helbling *et al.,* [106]. This can be used as long term stable and tunable transducers for measuring membrane deflection in ultra miniaturized pressure sensors. The sensor size as small as 50μm diameter prove that sensor downscaling to a size similar to the living micrometer cosmos is made possible by the use of CNTFET strain gauges. The development of MEMS technology moves towards the goal of a micromachined acoustic proximity sensor for real time cavity monitoring of underwater high speed super cavitating vehicles. Low resistance silicon based Through Silicon Vias (TSVs) has been integrated with the device to enable backside contacts for drive and sense

circuitry. The CMOS compatible process using DRIE produces 1mm diameter with 20μm thickness results with a sensitivity of 0.98μV/V/Pa. The magnetic field densities were detected by resonant magnetic field sensor based on MEMS technology including a signal conditioning circuit with 4-20mA output presented by Saul M.D.Nicolas *et al.*, [107]. Multilayered MEMS pressure sensor using piezoresistive Silicon Nano Wires (SiNWs) are characterized using center displacement loading approach discussed by Liang Lou *et al.*, [108]. The dimensions of the device are 2mm×2mm with thickness varies from 2μm to 5μm. The different material applied for the design of pressure sensor to ensure the stable output by Carbon Nano Tubes (CNTs) and Silicon Nano Wires (SiNWs) are emerging research methods in piezoresistive type. The Acoustic sensors with improved sensitivity are presented by Mahanth Prasad *et al.*, [104] using 25μm thick silicon diaphragm with SOI wafers and ZnO piezoelectric film sandwiched between two aluminium electrodes provides the sensitivity of 382μV/Pa in the frequency range of 30 Hz to 8kHz under varying acoustic pressures.

The review of recent issues with respect to a piezoresistive pressure sensor reveals that thick diaphragms or perforated diaphragms for high pressure measurement, burst pressure analysis to find minimum thickness to achieve maximum sensitivity, SOI wafers to improve performance, large gauge factor with CNTs for nano devices stable output by multilayered SiNWs are applied in biomedical application and acoustic applications.

2.8 SUMMARY

The review of all the above literature reveals that, pressure measurement using MEMS pressure sensor is accurate, high sensitive and realizable for high pressure in the range from 10kPa to 10MPa range. The flat diaphragms designed with large thickness of 10μm measures the pressure in the range of MPa. Burst pressure analysis is carried out to find the minimum thickness to achieve maximum sensitivity. The flat diaphragms are analyzed with respect to square shape is reported in literature [99,100,101]. The perforated diaphragms with thickness 3μm measure the pressure up to a range of 20kPa. These perforated thick diaphragms are an alternative to non

perforated thin diaphragms analyzed with square shape for the 3μm and 5μm thickness with sensitivity 0.406mV/kPa and 0.387mV/kPa [97, 98]. But they were not reported with respect to burst pressure which is required to find minimum thickness to achieve maximum sensitivity. But, the performance improvement by polycrystalline silicon material for the diaphragm design is reported [77,78]. It shows that diaphragm thickness is not a constraint for high pressure measurement. But neither a flat nor a perforated diaphragm is reported to sense the low pressure with thickness less than or equal to 1μm to improve sensitivity. The sculptured diaphragm [27,59] for sensing low pressure is reported with thickness 2μm to 12μm, but not tested with burst pressure condition. So, for low pressure range from 0-1000Pa, a diaphragm is sensitive only if thickness is reduced. The thickness of the diaphragm is to be reduced below 1μm. At the same time it is not possible to make perforations in the diaphragm with thickness less than or equal to 1μm which may tend to break. Even, when the thickness reduced beyond 1μm, the diaphragm deflection is nonlinear and produces nonlinear stress component due to stretching which creates balloon effect. These limitations are to be minimized and sensitivity should be maximized by reducing the diaphragm thickness below 1μm by using the proposed sculptured diaphragm. Reduction of diaphragm thickness for the proposed sculptured diaphragm is achieved by burst pressure analysis where sensitivity can be improved. The proper positioning of the piezoresistors, sizing of piezoresistors and SOI technique reported by M.Narayanaswamy *et al.*, [101] is used to enhance the sensitivity. The stress component is improved by using the proposed non uniform thickness technique. As diaphragm design is the key part of any MEMS pressure sensor, it should be designed in such a way as to prevent bursting for maximum pressure, physically realizable in micro scale range, better sensitivity and acceptable linearity.

CHAPTER 3

SELECTION OF MATERIAL, SHAPE AND MODELLING OF PIEZORESISTIVE PRESSURE SENSOR

3.1 INTRODUCTION

The ability to use MEMS fabrication methods in mass production of high performance sensors at low cost has opened up a wide range of applications for pressure sensors which include automotive, aerospace, marine, instrumentation and industrial process control, hydraulic systems, microphones, bioscience and medical applications. Since the introduction of MEMS, piezoresistive pressure transducers have become the dominant types, owing to their high performance, stability and repeatability. Recent trends indicate increased need for pressure sensors suitable for low pressures, hazardous environments, high temperatures and biomedical applications. Advanced applications involve requirements of small volume, high performance characteristics, environmental restrictions and materials compatibility [87]. This chapter discusses the software used, material selection and suitable shape, importance of h/L aspect ratio and basic modelling of piezoresistive pressure sensor.

3.2 SIMULATION TOOL

Intellisense Corning commercialized the MEMS CAD package IntelliSuite, current version 7.1 [4]. It is also a FEM-based simulation and design tool specifically developed for MEMS and runs on a standard PC under Windows. The user starts by drawing the masks in IntelliMask, which is a standard drawing package with typical features for mask designs such as multiple translations copy, layer control, and hierarchical cells. Each mask is drawn on a separate layer and saved in a different file. It is also possible to import and export the masks in GDS II of DXF file format. The next step is to define the fabrication process in a tool called IntelliFab. It contains a

large database of silicon base materials, deposition steps of various materials, and etching steps for all commonly used materials in MEMS. The previously defined masks are used to define areas in which material is removed or added. Once the user has created the full process flow (referred to as Process Table) IntelliFab visualizes the fabricated device in an easy-to-use viewer that allows zooming, panning, and three-dimensional rotation of the virtual prototype. Templates are available for standard MEMS processes. The properties of a material used in any process step can be defined and altered in a powerful tool called MEMS Material. If, for example, one process step is to deposit silicon nitride (Si_3N_4) in a PECVD furnace, material properties include stress, density, thermal expansion coefficient, Young's modulus, and Poisson's ratio. If the material property is not a constant but depends on one or several fabrication conditions, their relationship may be displayed graphically. Stress of silicon nitride, for instance, depends on the deposition temperature, and their relationship is shown in the graph in the top-right window. In the lower window the data points are given together with the literature source from which the information was taken.

The various simulation solvers which are mechanical, electromagnetic, electromechanical, and electrostatic, can be run either from IntelliFab or directly. The mechanical solver meshes the device to be analyzed. The meshing process can be controlled by defining global or localized limits for the mesh of the certain areas of interest. Then it computes the natural mechanical resonant modes, which can be visualized in an animation. Furthermore, it allows the application of mechanical loads such as forces and moments to the different surfaces of the structure, but also thermal loads in form of heat convection. Thermal distribution generated by flow or current through materials with varying resistivity and their mechanical deformation caused by thermal strain can be simulated. Any analysis can be performed as a response to a static load or dynamically as a result of a time varying load. The electrostatic solver uses a very similar meshing process and computes a capacitance matrix for the various layers and surfaces. Furthermore, it allows an analysis of the resulting charge density, electrostatic forces and pressures.

The electromechanical solver allows application various loads to the user to the device under consideration such as electrostatic loads through applying voltages, temperature, pressure, acceleration, and displacements, and subsequently calculate the resulting mechanical reactions (such as stress distributions, deformations, and displacements) and electrical properties (such as capacitance, charge density and electric field). Another solver is the micro fluidic analysis module. This tool allows analysis of thermal effects to the user, concentration, and flow within a fluid. It also simulates velocity and electric field distributions as a result of electro kinetic phenomena. Another very useful tool is AnisE, an anisotropic etch process simulator. With AnisE, the user can use the layout of the microstructure to be prototyped to view a three-dimensional representation of it, access information about the etch rates of different etchants, and then simulate the etching under different time, temperature, and concentration parameters.

Finally, Intellisense contains a module called 3-D Builder, which can be called from any of the solvers or separately as a standalone application. This tool allows for building and meshing the three-dimensional geometry of MEMS structures with a graphical interface. The screen is divided into two areas: on the left is the two dimensional layer window where the outline of different layers can be drawn; and on the right is the three-dimensional viewing window, which allows the user to visualize the device in three dimensions and includes zooming, rotating, and panning functions. Furthermore, the thickness of any layer can be changed. In this way, a MEMS device can be created without having to define the full fabrication process flow. The module produces a file that can be used for analysis in any of the solvers or, alternatively, a mask file that can be processed further by IntelliMask.

3.3 MATERIAL SELECTION

Silicon micromachining offers several advantages over the conventional machining techniques, the most important among them being the ability to batch process silicon wafers for fabricating mechanical devices such as sensors, actuators, and microstructures having size in the range of 1 to 10 microns. This also gives the added ability to integrate electronics with the micromachined devices. Silicon also

happens to be an ideal material for mechanical sensors because of its excellent mechanical properties required for reproducible elastic deformations under identical mechanical load. Table 3.1 gives the mechanical properties of the silicon [18, 21] and several other materials for comparison.

Table 3.1 Mechanical properties of MEMS materials

Material	**Yield strength (GPa)**	**Hardness (Kg/mm^2)**	**Young's modulus (GPa)**	**Density (g/cm^3)**
Diamond*	53	7000	1035	3.5
SiC*	21	2480	700	3.2
TiC*	20	2470	497	4.9
Al_2O_3*	15.4	2100	530	4.0
Si_3N_4*	14	3486	385	3.1
Iron*	12.6	400	196	7.8
SiO_2 (fibers)	8.4	820	73	2.5
Si*	**7.0**	**850**	**190**	**2.3**
Steel	4.2	1500	210	7.9
Stainless Steel	2.1	660	200	7.9
Mo	2.1	275	343	10.3
Al	0.17	130	70	2.7

*These metals exists in single crystal form

It can be seen that diamond has the highest hardness ($7000Kg/mm^2$) and elastic modulus (1035 GPa). The extreme wear resistance is 10,000 times greater than Silicon. However, the primary challenge with diamond lies in integrating the mechanical devices with electronics. This is further complicated by the chemical inertness of diamond making it a difficult material to machine. Similarly, silicon carbide has drawn attention for MEMS as it offers much higher stiffness, hardness, toughness and wear-resistance than the core CMOS material. However it is also a difficult material to process due to its relatively low chemical reactivity, extremely high melting point (2300°C). In spite of these difficulties, silicon carbide based MEMS pressure sensor has been successfully fabricated and reported [20]. The

deflection sensitivity of different materials such as Sicz (single crystal silicon), Polysilicon, SiO_2, Si_3N_4, Al_2O_3, Molybdenum, Gold, Aluminium and Diamond are investigated for the square diaphragm of dimensions 700µm×700µm×0.21µm which is presented in Fig.3.1.

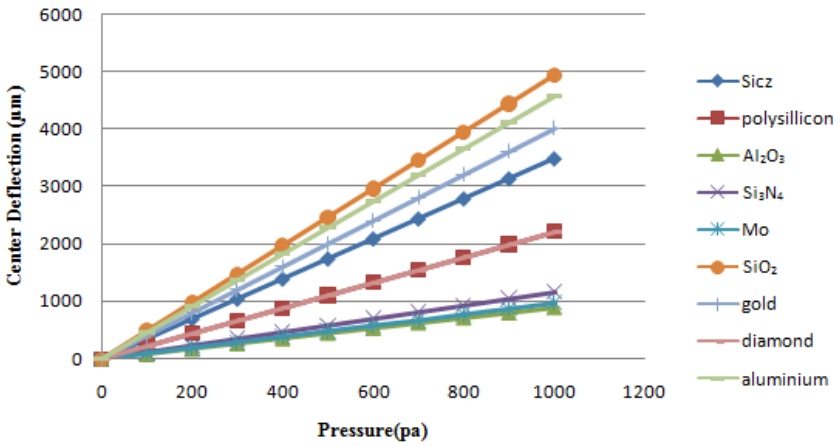

Fig.3.1 Pressure versus center deflection of different MEMS materials

The graph shows that silicon (single crystal), silicon-di-oxide and ploysilicon give a higher deflection sensitivity than aluminium, Gold, Silicon carbide, Silicon Nitride, Molybdenum and aluminium Oxide. Single crystal silicon is free from hysteresis and creep. Silicon is harder than most metals and has higher elastic limits in both tension and compression. It has the added advantage that it is used as an electronic material in an already advanced VLSI technology [79, 99]. Therefore miniaturized mechanical devices can be realized on silicon with high precision and they can be easily integrated with electronics.

3.4 SHAPE OF DIAPHRAGM

The choice of a diaphragm shape is mainly based on the fabrication process used for realizing. In addition it depends upon several other factors such as applications and distribution of the required stress field. Three most common diaphragm shapes are square, rectangular and circular. In most cases, square and rectangular shapes are preferred due to ease of fabrication by the anisotropic wet etching of silicon. Employment of square diaphragm for pressure sensing is recommended since that can provide 60% improvement in sensitivity compared with

circular diaphragms [61, 42 and 89]. On the other hand, the fabrication of circular diaphragms with silicon is possible by Deep Reactive Ion Etching (DRIE) [38]. The required shape for low pressure application is selected by analyzing the deflection sensitivity in the pressure range from 0 to 1000Pa. Wet etching used for creating the square and rectangular models and deep reactive ion etching used for circular diaphragm with clamping. The surface area is considered identical to help comparison of the performance of the three shapes. The three structures were created using silicon with the following material properties given in Table 3.2.

Table 3.2 Material properties of silicon

Material property	Value
Yield Strength	7 Gpa
Hardness	850 Kg/mm^2
Young's Modulus	170 GPa
Melting point	1410°C
Gauge Factor	100-200
Poisson's ratio	0.3
Temperature	20°C

The dimensions chosen for shape analysis are presented in the Table 3.3 below. In all the cases, the thickness h of the diaphragm is 1μm.

Table 3.3 Dimensions of different shapes of diaphragm

Diaphragm shape	Dimensions of diaphragm
Square	700μm×700μm×1μm
Rectangular	1000μm×500μm×1μm
Circular	Radius 125 μm×1μm

The analytical equations to find the center deflection of the square, rectangular and circular diaphragms were given below in Table 3.4.

Table 3.4 Center deflection, stress and coefficients of different shapes of diaphragm

Shape of diaphragm	Center deflection or Displacement (y)	Stress (σ)	Coefficients α, β_1 and β_2
Square	$\frac{(\alpha \times P \times b^4)}{(Eh^3)}$	$\frac{(\beta \times P \times b^2)}{h^2}$	for L/b=1, α=0.0138
Rectangle	$\frac{(\alpha \times P \times b^4)}{(Eh^3)}$	$\sigma_{xx} = \frac{(\beta_2 \times P \times b^2)}{h^2}$ $\sigma_{yy} = \frac{(\beta_1 \times P \times b^2)}{h^2}$	for L/b = 2, α=0.0277 for L/b=2, β_2=0.2472 for L/b=2 , β_1=0.4974
Circle	$-\frac{3w(m^2-1)r^2}{(16\pi Em^2h^3)}$	$\sigma_{rr} = \sigma_{\theta\theta} = \frac{(3vw)}{(4\pi h^2)}$	Nil

The abbreviations of various parameters are

- P - Pressure Applied in Pascal (Pa),
- L - Length of diaphragm in µm,
- b - Width of diaphragm in µm,
- h - Thickness of diaphragm in µm
- y - Center deflection or Displacement in µm
- σ_{xx} (σ_l) - Stress along x axis or Longitudinal Stress in MegaPascal (MPa)
- σ_{yy} (σ_t) - Stress along y axis or Transverse Stress in MegaPascal (MPa)
- σ_{rr} ($\sigma_{\theta\theta}$) - Stress at the center for circular diaphragm in MegaPascal (MPa)
- E - Young's Modulus in GigaPascal (Gpa)
- ν - Poisson's ratio
- r- Radius of the diaphragm in µm,
- w - Total force acting on the plate ($w = \pi r^2 P$)
- m - Constant ($m = 1/\nu$)

The coefficients α, β_1 and β_2 are given in Table 3.5. These can be selected based on length to width ratio.

Table 3.5 Coefficients α, β_1 and β_2 based on length to width ratio

a/b	1	1.2	1.4	1.6	1.8	2.0	∞
α	0.0138	0.0188	0.0226	0.0251	0.0267	0.0277	0.0284
β_1	0.3078	0.3834	0.4356	0.4680	0.4872	0.4974	0.5000
β_2	0.1386	0.1794	0.2094	0.2286	0.2406	0.2472	0.25

The center deflection sensitivity of three shapes with respect to applied pressure is shown in Fig. 3.2.

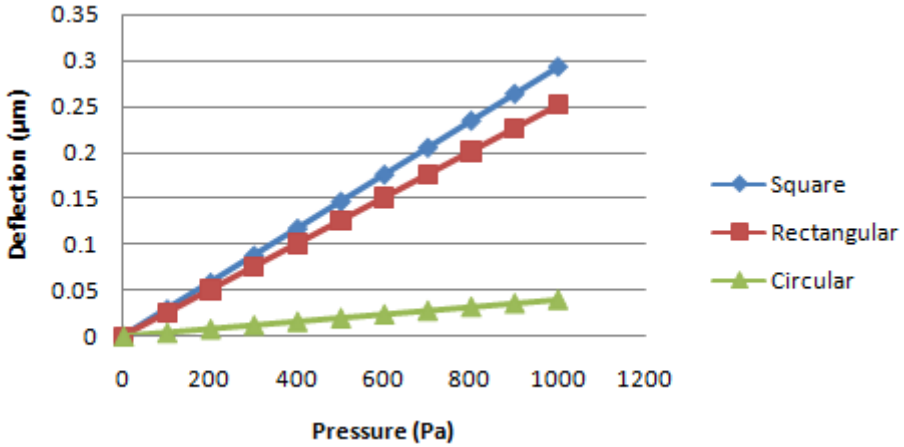

Fig.3.2 Comparison of deflection sensitivity for square, rectangular and circular diaphragm

From Fig. 3.2, the square and rectangular shapes yield a higher deflection sensitivity than circular diaphragm for range of 0-1000Pa. The stress obtained for square, rectangular and circular at a maximum pressure of 1000Pa were presented in Table 3.6.

Table 3.6 Comparison of longitudinal stress and transverse stress

Shape of diaphragm	Longitudinal stress(MPa)	Transverse stress(MPa)
Square	111.076	111.076
Rectangular	50.9806	98.9308
Circular	9.1967	9.1967

The result reveals that, the square shape flat diaphragm yields the maximum stress which is equal both in longitudinal and transverse direction. The highest stress

obtained for rectangular shape but obviously the longitudinal and transverse stresses are not equal. The circular shape yields the lowest stress and longitudinal and transverse stresses are equal. On comparing both deflection and stress, square and rectangular shape is better than circular shape.

3.5 MODELLING OF DIAPHRAGM IN LINEAR REGION OPERATION

The diaphragm design is the most crucial step among the various stages of pressure sensor realization. The dimensions of the diaphragm need to be chosen to ensure linear output over the entire pressure range of operation of the sensor. The diaphragms of the pressure sensors turn out to be square (when a=b) in the lateral direction while being rigidly anchored at the edges as shown in Fig.3.3.

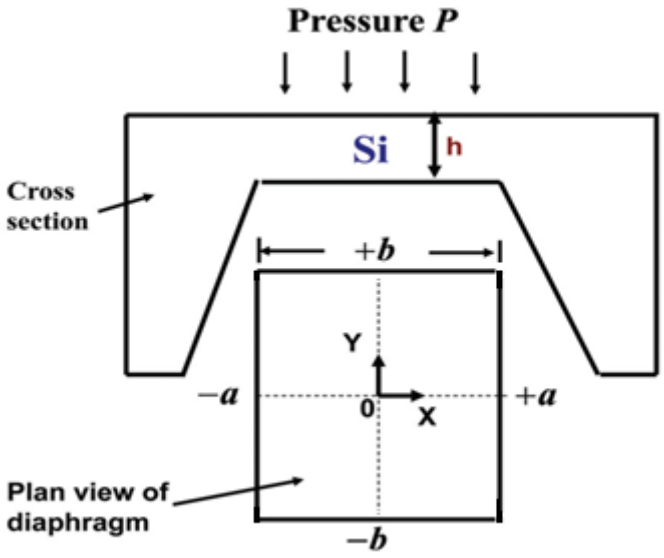

Fig.3.3 Micromachined square diaphragm of silicon showing the cross section and the diaphragm plan view [79]

3.5.1 Deflection

Consider a square diaphragm of thickness h and length 2a, subjected to a uniform pressure P. From the theory of plates [109, 110], the maximum deflection at the center of the diaphragm is given by the equation [73, 79]

$$P = E\frac{h^4}{a^4}\left(g_1\frac{w_0}{h} + g_2\frac{w_0}{h}\right) \quad (3.1)$$

where E is Young's modulus and g_1 and g_2 are constants related to Poisson's ratio ν, by the relation

$g_1 = 4.13/1-\nu^2$ and $g_2 = 1.98(1-0.585)/1-\nu$ (3.2)

Substituting ν=0.3 for silicon, g_1 and g_2 turn out to be 4.54 and 2.33 respectively. Thus the maximum deflection w_0 is linearly related to pressure P till $w_0 << h$. The second term inside the bracket is about 0.5% of the first term when $w_0 = 0.1h$. So the first term is defined as Small Scale Deflection (SSD) region and second term is defined as Large Scale Deflection (LSD) region. The deflection w_0 in the linear region of operation can be expressed as follows for a square diaphragm.

$$\frac{w_0}{h} = \frac{pa^4}{E\,h^4\,g_1} \tag{3.3}$$

Using equation (3.3) for a square diaphragm, of silicon (E=170GPa), with length 2a=500μm and thickness h=10μm, the maximum deflection is estimated to be 0.5μm when $P=10^5$ Pascal=1bar.

3.5.2 Maximum Stress

The maximum stress σ_{max}, which occurs at the center of the edge of the square diaphragm (i.e., at x=±a in Fig.3.3) can be expressed by the analytical expression for a square diaphragm [79] as,

$$\sigma_{max} = P\left[\frac{a}{h}\right]^2 \tag{3.4}$$

where 'P' is the pressure applied, '2a' the length of the diaphragm and 'h' the diaphragm thickness.

3.5.3 Importance of Aspect Ratio (h/L)

The thickness and length i.e., (h/L) ratio is a prime design parameter to improve the linearity and sensitivity. Further, while designing a pressure sensor attention is paid to the level of stress generated at burst pressure and that should be kept within the fracture limit of silicon. Further, the stress generated near the center of diaphragm

edge is normally higher than other regions; however, it was observed that with increasing aspect ratio (h/L) the stress generated at diaphragm center exceeds the stress developed near the diaphragm edge.

The theoretical center deflection and stress calculated for a square diaphragm by using equation from Table 3.4 and the comparison of simulated versus analytical center deflection is shown in the Fig.3.4 for the dimensions of 500µm×500µm×2.21µm in the low pressure range of 0 to 1000Pa. The thickness chosen is based on the small scale deflection lesser than 40% of h.

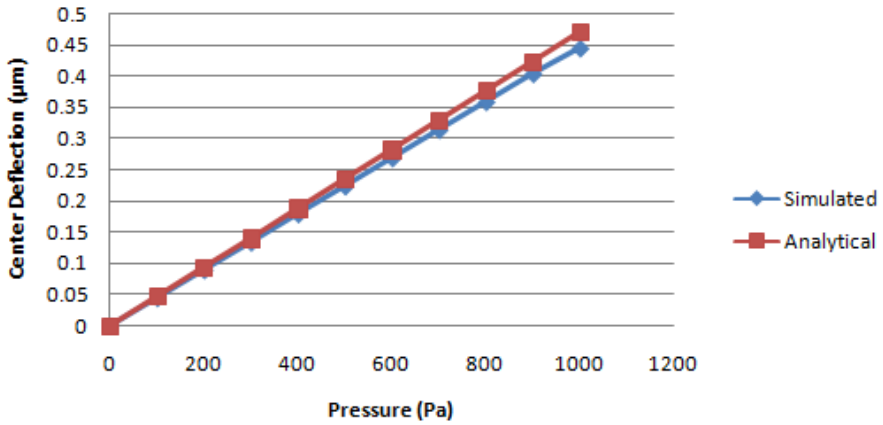

Fig.3.4. Comparison of analytical and simulated center deflection for a square diaphragm

To optimize the h/L ratio, the square diaphragm is simulated by varying h/L ratio and graph is plotted for the center deflection of the diaphragm. All the dimensions are in µm. The deflection sensitivity analyzed for various aspect ratios is shown in Fig.3.5 and Fig.3.6.

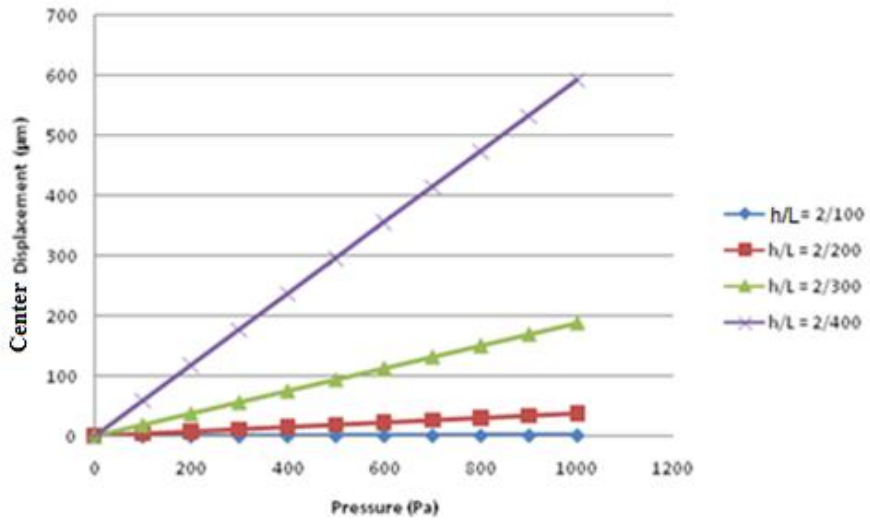

Fig.3.5 Comparison of aspect ratio (h/L) with center deflection keeping h constant and L varying

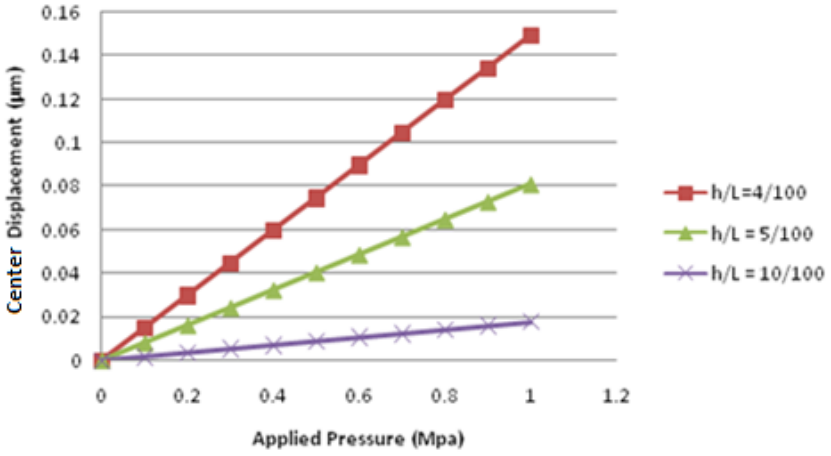

Fig. 3.6 Comparison of aspect ratio (h/L) with center deflection keeping L constant and h varying

The result reveals achievement of the maximum deflection sensitivity when the thickness is kept as small as possible when compared with the length of the diaphragm. But the thickness of a diaphragm is fixed by satisfying small scale deflection of thin plates as well as burst pressure will be discussed in chapter 6.

.

3.5.4 The Proof Pressure and Burst Pressure

The proof pressure is generally defined as 1.5 times the nominal pressure of the sensor. The sensor is required to operate up to this pressure while maintaining the

overall specifications. Burst pressure [79] is another important design consideration for the diaphragm dimensions, as this limits the ultimate stress to which the diaphragm can be subjected. This is the pressure at which the maximum stress σ_{max} on the diaphragm becomes equal to the critical stress σ_c which is actually the yield strength of the material. For the case of the single crystal silicon=7GPa. Thus, for a square diaphragm having side length 2*a* and thickness h, the burst pressure P_B is determined by substituting $\sigma_{max}=\sigma_c$ in equation (3.4) and can be written as [79]

$$P_B \left(\frac{a}{h}\right)^2 = \sigma_c \tag{3.5}$$

As the applied pressure on the diaphragm increases, the stress on the diaphragm increases correspondingly. As a result, when the maximum stress on any portion of the diaphragm exceeds the yield strength of the diaphragm material, the diaphragm will burst. While this burst pressure governs the maximum operating pressure of a pressure sensor, the linearity of operation determines the maximum pressure up to which the sensor can be used within the limits of the specified accuracy. The burst pressure is decided by a number of factors including diaphragm shape, thickness, lateral dimensions and rupture stress of the material and diaphragm surface roughness [74].

3.5.5 The Gauge Factor and the Piezoresistive Effect

The piezoresistive effect can be quantified using the gauge factor which is defined as the ratio of the relative change in resistance (ΔR/R) when the resistor is subjected to a strain €, and is expressed by the relation [79],

$$G=\frac{\Delta R}{R\,€} \tag{3.6}$$

The resistance R of a rectangular resistor of length L, width W, thickness h and the resistivity ρ, is expressed by the relation ,

$$R=\frac{\rho L}{Wh} \tag{3.7}$$

When the resistor is subjected to strain, the following relation gives the relative change in resistance (ΔR\R)

$$\frac{\Delta R}{R} = \frac{\Delta L}{L} - \frac{\Delta W}{W} = \frac{\Delta h}{h} + \frac{\Delta \rho}{\rho} \tag{3.8}$$

Here ΔL, ΔW, Δh, and $\Delta \rho$ are the changes in the respective parameters due to strain. If the resistor experience tensile stress along the length, the thickness and width of the resistor will decrease whereas the length will increase. Using Poisson's ratio ν, the change ΔL, in length is correlated to the change, ΔW in width, and the change, Δh in thickness of the piezoresistors by the following equation [79]

$$\frac{\Delta W}{W} = \frac{\Delta h}{h} - \nu \frac{\Delta L}{L} \tag{3.9}$$

The gauge factor G is obtained as

$$G = \frac{\Delta R}{R \epsilon} = 1 + 2\nu + \frac{\Delta \rho}{\rho \epsilon} \tag{3.10}$$

Where $\epsilon = \frac{\Delta L}{L}$ is the strain. The first two terms in equation represent the change in resistance due to dimensional changes and are dominant in metal gages while the last term is due to change in resistivity.

Thus the gauge factor of different types of strain gauges will be vastly different. This is mainly due to difference in an extent in the resistivity, ρ, changes under the influence of strain. For metals ρ does not vary with strain and Poisson's ratio and ν, is typically in the range of 0.3 to 0.5, leading to gauge factors of only about 2 to 5 in metal strain gauges. In semiconductor strain gauges, the piezoresistive effect, which causes a large change in ρ is dominant and hence the gauge factor is considerably high. Gauge factor up to 200 for p–type silicon and up to 140 for n- type silicon have been reported.

A small gauge factor is reported in metal strain gauges and they are in the range of 1 to 5 as the change in resistance in metals is due to strain mainly attributed to a change in physical dimensions. On the other hand, a gauge factor in the range of 80 to 200 has been observed in the diffused semiconductor resistors. This is attributed to the piezoresistive effect, which results in a large change in resistivity (ρ) in semiconductors, whereas in metal foils and thin film metals change in resistivity is very small [79].

3.5.6 Piezoresistive Coefficient

The resistance change can be calculated as a function of stress using the concept of the piezoresistive coefficient [13]. Contributions to the resistance change come from the longitudinal stress (σ_l) and transverse stress (σ_t) with respect to the current flow. Assuming that mechanical stresses are constant over the resistors, the resistance changes ΔR with respect to the resistance R is given by [79],

$$\frac{\Delta R}{R} = \sigma_l \pi_l + \sigma_t \pi_t \tag{3.11}$$

Where π_L and π_t are the longitudinal and transverse piezoresistive coefficient, calculated by given equations respectively.

$$\pi_l = \frac{\pi_{11}+\pi_{12}+\pi_{44}}{2} \tag{3.12}$$

$$\pi_t = \frac{\pi_{11}+\pi_{12}-\pi_{44}}{2} \tag{3.13}$$

3.5.7 Wheat Stone Bridge Assembly

The wheat stone bridge assembly shown in Fig.3.7 is the next important step to convert the small displacement into an electrical output by means of piezoresistive transduction mechanism. The four piezoresistors are placed on top of the diaphragm in which two resistors are placed to experience tensile stress in order to give increase in resistance, and other two other resistors are placed to experience compressive stress so as to give decrease in resistance.

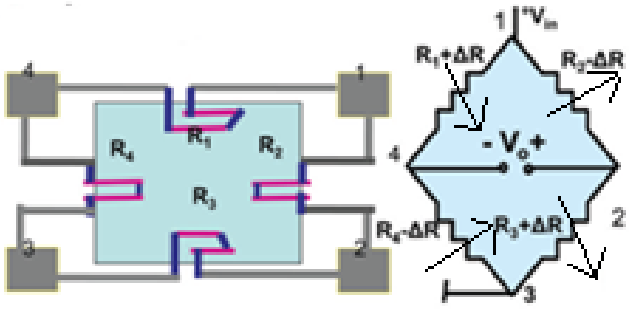

Fig.3.7 Wheat Stone bridge assembly

The output voltage is calculated by the equation [79]

$$\frac{V_o}{V_b} = \frac{R_4}{R_4+R_1} - \frac{R_3}{R_3+R_2} \tag{3.14}$$

where V_b is the bridge excitation voltage.

3.6 PERFORMANCE CHARACTERISTICS

The main parameters and specifications of the pressure sensor are sensitivity in the linear range of operation, offset voltage, ballooning effect and hysteresis.

3.6.1 Offset Voltage

The offset voltage is defined as output voltage of the pressure sensor at zero input pressure. This is due mainly to two reasons. The first one is some residual stress on the membrane. The second is the variability in the four resistors. Even though the resistors are processed by diffusion simultaneously, there are some variations due to non-uniformity in the starting polysilicon layer or due to non-uniformity in dopant diffusion in the polysilicon resistor. Therefore, piezoresistive pressure sensors invariably show offset voltage. One of the approaches used for offset voltage compensation has been to connect the external resistors. This involves the use of an open bridge configuration and the use of external precision resistors to complete the bridge during the packaging stage. Over the years, more elegant and efficient techniques of compensating for the offset voltage using electronics have evolved [79].

3.6.2 Sensitivity

The sensitivity of a pressure sensor is defined as

$$S = \frac{\Delta V}{\Delta P} \tag{3.15}$$

at a particular input voltage. The sensitivity is low when resistors are fabricated using polycrystalline silicon whose gauge factor is low compared to that of single crystal diffused resistors. Higher sensitivities and lower noise levels are typically achieved with diffused or ion implanted single crystal silicon strain gauges [79].

3.6.3 Ballooning Effect

Ballooning effect is one of the nonlinear parameter of pressure sensors. This nonlinearity in the piezoresistive pressure sensors is caused mainly by the following factors:

(i) The nonlinear relationship applied between the stress and the pressure. If the deflection of the diaphragm is large compared to its thickness, the central plane of the diaphragm stretches like a balloon. Due to this balloon effect, the diaphragm is subjected to a stretching stress component, σ_s, in addition to the stress, σ_b caused by the bending of the diaphragm. The stress, σ_b, caused by bending, is reduced in magnitude as the stretch of the diaphragm takes a part of the pressure load and this result in nonlinearity. The nonlinearity caused by the balloon effect (ie the stretch) is smaller when the sensor is subjected to pressure from the front side where the resistors are located. This is because σ_s is always positive irrespective of its position in the diaphragm and the direction of the applied pressure, whereas the polarity of σ_b can be either positive or negative depending on its position in the diaphragm and the sign of the applied pressure. Thus, both σ_s and σ_b are positive at the diaphragm edge when the pressure is applied from the front whereas σ_b is negative and σ_s is positive when the pressure is applied from the rear. Hence when the pressure is applied from the front side the stresses add up and the total stress tends to be closer to the linear theory which assumes that the stress distribution is a result of pure bending.

(ii) The piezoresistive coefficient of silicon is generally considered to be independent of stress. But, this is not really true in practice when examined with high accuracy. The nonlinear relationship between the piezoresistive coefficient and the stress is thus another source of nonlinearity in piezoresistive pressure sensors.

(iii) The third cause of the nonlinear output voltage is the difference in piezoresistive sensitivity between the resistors of the Wheatstone bridge. For low- pressure sensors, linearity becomes an issue. Bossed diaphragms

or sculptured diaphragms, as will be discussed in subsequent sections, are used to overcome this problem.

3.6.4 Hysteresis

Hysteresis is yet another parameter of pressure sensors and this is also specified as a percentage of the full-scale output voltage of the sensor. This parameter is a matter of concern in pressure sensors, which employ metal diaphragms, due to the non-elastic characteristics of ductile metals, even with very good spring materials. However, the single crystal silicon is an excellent spring material. At temperatures below 600°C, the silicon stress versus strain curve has no plastic zone and the material has essentially no creep. Pressure sensors employing a silicon diaphragm as a sensing element has hysteresis below 0.1%, which is very low [79].

3.7 FIGURES OF MERIT

The following parameters were considered as key to analyze the performance of the proposed diaphragms in the forth coming chapters. The center deflection sensitivity with respect to applied pressure, Longitudinal Stress (S_{xx}), Transverse Stress (S_{yy}), Thickness of diaphragm, Percentage of deflection with respect to thickness and Output Voltage Sensitivity.

3.8 HIGH PRESSURE AND LOW PRESSURE DIAPHRAGMS

Measurement of very high pressure range in the order of MPa is easier and diaphragm structure is simple and can be constructed with flat diaphragm with thickness greater than 10μm is sensitive and give good output. For measurement of high pressures in the range of 20 kPa, diaphragms of thickness less than 10μm are used with perforations on the diaphragm to ensure sensitivity. Low pressure in the order of 1000Pa and below also require measurement and used in level measuring technique in flash flood level measurement and intracranial pressure measuring in biomedical application. To measure this pressure range, thin diaphragms required to be sensitive. But the thin diaphragms bend and stretch and produce balloon effect

which shows a nonlinear effect and not a suitable operation. Stress produced is due to bending effect is linear in output and stress produced due to stretching effect is nonlinear and should be avoided. So a special diaphragm is needed to tackle this problem.

3.8.1 Thickness and Stress Contradictions

As the maximum stress in a flat diaphragm with length of 2a and thickness is proportional to P $(a/h)^2$, the sensitivity of a piezoresistive pressure sensor fabricated on a flat diaphragm can be increased by making the (a/h) ratio larger. However, equation (3.3) shows that the deflection w_o to thickness h ratio is proportional to P $(a/h)^4$. Therefore, in a low pressure range (e.g. a full-scale pressure of about 1000Pa), flat-diaphragm pressure sensors are not suitable as the sensitivity requires considerable increase by making the (a/h) ratio extremely large and this would lead to large deflections resulting in a high degree of nonlinearity [27, 59, 79,89]. As discussed in 3.6.3, non-linearity is the result of the stretching of the middle plane, which becomes significant when the deflection becomes comparable to the thickness of the diaphragm.

If the deflection of the diaphragm is large when compared to its thickness, the central plane of the diaphragm stretches like a balloon [79] as shown in Fig.3.8.

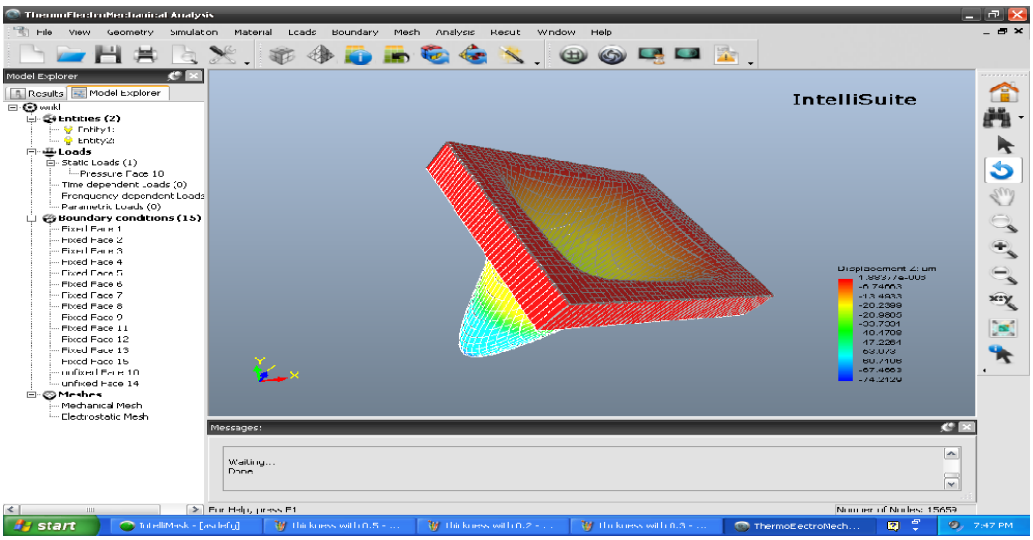

Fig.3.8 Ballooning Effect

The center deflection of the flat square diaphragm with dimensions 500μm ×500μm at 1000Pa with respect to different thickness varying from 0.1μm to 5μm is given in Table 3.7.

Table 3.7 Thickness versus center deflection and percentage of center deflection

Thickness of the diaphragm (μm)	Center deflection (μm)	Percentage of center deflection (%)
5 μm	0.03908 μm	0.78%
4 μm	0.07584 μm	1.896%
3 μm	0.17957 μm	5.98%
2 μm	0.5936 μm	29.68%
1 μm	4.7609 μm	476%

The results show that, when thickness is decreased from 5 μm to 1 μm to sense low pressure of 1000 Pa, the diaphragm either exhibits balloon effect as in Fig.3.8 or poor deflection sensitivity which is not allowable in SSD to ensure linearity. To overcome these contradictions, a special geometry diaphragm proposed where thickness is reduced without the balloon effect.

3.8.2 Need for Sculptured Diaphragm

To sense low pressure the diaphragm thickness is to be reduced to the minimum. But this leads to the balloon effect and make a nonlinear effect in the output. So, for low- pressure sensors, linearity becomes an issue. Perforated Diaphragms [97,98] can also be designed to reduce the diaphragm thickness and this will sense pressure up to 10 kPa. But the thickness cannot be reduced below 3μm as it is difficult to make perforations in order to sense low pressure. Design of bossed diaphragms or sculptured diaphragms [27] will be discussed in subsequent chapters to overcome this issue.

3.9 SUMMARY

The introduction to simulation tool Intellisuite has been briefed out. The mechanical properties of different metals have been compared and the significance of silicon as mechanical material briefed out. The performance of three most common shapes square, rectangular and circular has been obtained with equal surface area and thickness has been compared. Out of these, square yields the higher stress than the rectangular and circular shape. For further analysis square and rectangular shapes have been considered. As piezoresistive type is the linear transduction mechanism, simple and easy to fabricate, the modelling behind the piezoresistive type have been analyzed in detail. The necessities of wheat stone bridge assembly to extract electrical output, importance of burst pressure to design minimum thickness have also been discussed. The importance of piezoresistive coefficients has also been discussed. The performance parameters such as offset voltage, sensitivity, ballooning effect and hysteresis were discussed. The figures of merit to analyze the proposed design in forth coming chapters have been listed out. The thickness versus stress contradictions and the need for sculptured diaphragm in low pressure range have been discussed.

CHAPTER 4

DESIGN AND ANALYSIS OF SINGLE BOSS SCULPTURED DIAPHRAGM

4.1 INTRODUCTION

The sculptured diaphragm is a specialized geometry with a rigid center or boss. The sculptured diaphragms are designed with minimum thickness, compensating the large (a/h) ratio with local stiffening by means of rigid center and better linearity. In order to improve sensitivity and linearity simultaneously, specialized geometries, such as diaphragms with a rigid center or boss [27, 60] have been introduced for increasing the stiffness to limit the maximum deflection of the diaphragm, and for enhancing linearity. Such a structure is also known as the sculptured diaphragm or the bossed diaphragm. In this approach, the structure is locally stiffened to limit the overall deflection, while maintaining a relatively thin section where the piezoresistors are placed. Thus the total nonlinear deflection due to membrane stress is reduced. Since the deflection and resulting stress occur at a localized area, and also because the stress is concentrated in relatively localized thin areas of the diaphragm, this technique is sometimes referred to as the stress concentration technique.

4.2 DIAPHRAGM DESIGN

The diaphragm is designed with a single rigid or support at the bottom in the center. The dimensions of the diaphragm are (Lμm× Wμm× hμm) 500μm× 500μm ×1μm where L is the length, W is the width and h is the thickness of the diaphragm respectively. The shape of the diaphragm is selected as square shape. The structure is created by bulk micromachining [24] with single crystal silicon by the czochrolski process. Despite the preference to use circular diaphragms to prevent unwanted stress

concentration, silicon diaphragms of square shape can be easily fabricated using anisotropic wet chemical etching on silicon wafers of <100> orientation. [61, 62, 63, 80] It is also easier to align the resistors parallel and perpendicular to the edges of the diaphragm which are in the <110> direction, thus ensuring that the piezoresistive coefficients π_l and π_t are maximum along this direction. The following steps are used to create the structure using IntelliFab and IntelliMask software.

a. The silicon substrate with required die size to be mentioned with the thickness of the 50µm. This is a czochrolski <111> orientation process as shown in Fig.4.1.

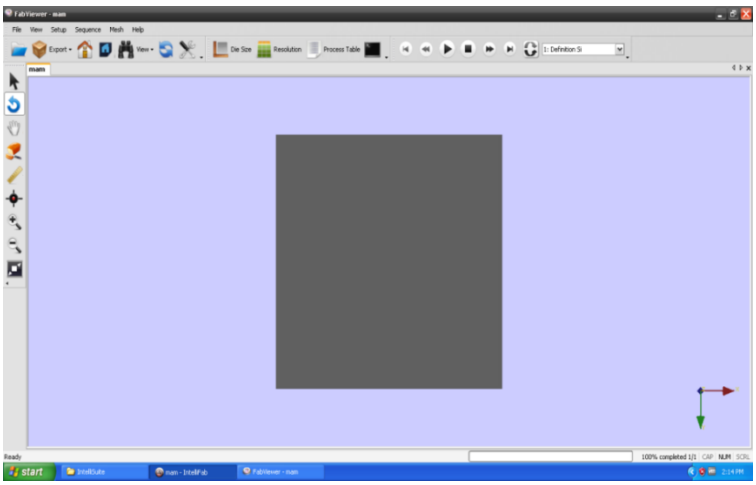

Fig.4.1 Silicon substrate

b. The photo resist to make single sculpture is made with the thickness 3µm using PRS 1800 – spin – S1805 as shown in Fig.4.2.

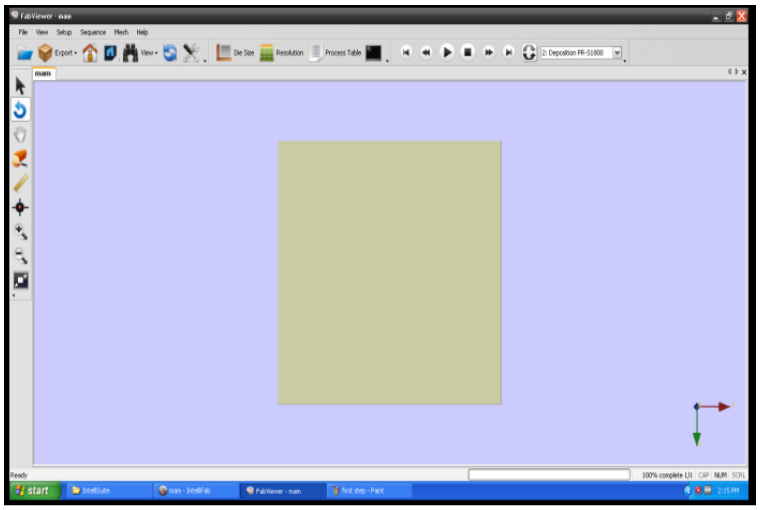

Fig.4.2 Photo resist

c. The UV light exposed on the top of the photo resist to make the pattern on the silicon diaphragm as shown in Fig.4.3.

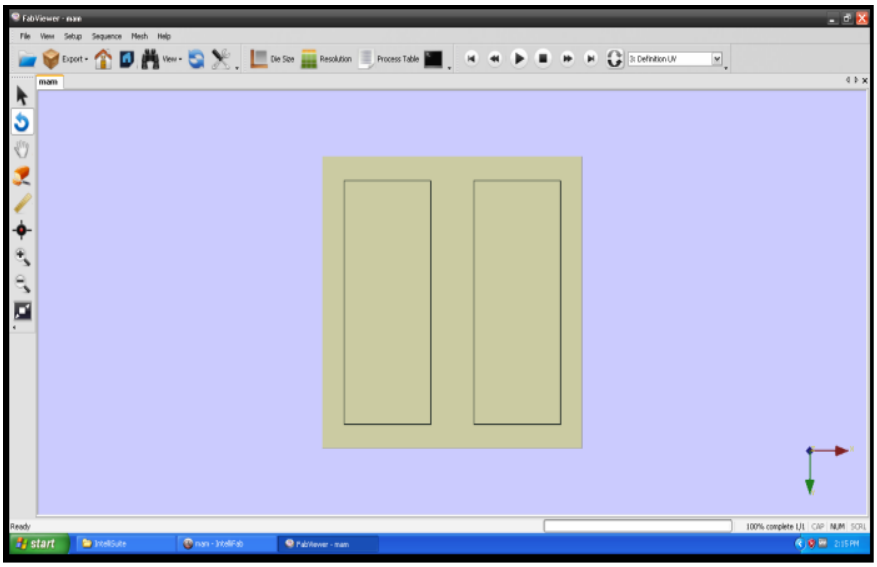

Fig.4.3 UV exposure for single boss sculptured diaphragm

d. The wet chemical etching is used to make the diaphragm with support at the bottom. The process PRS1800 – wet – 1112A where partial etching is processed as shown in Fig.4.4.

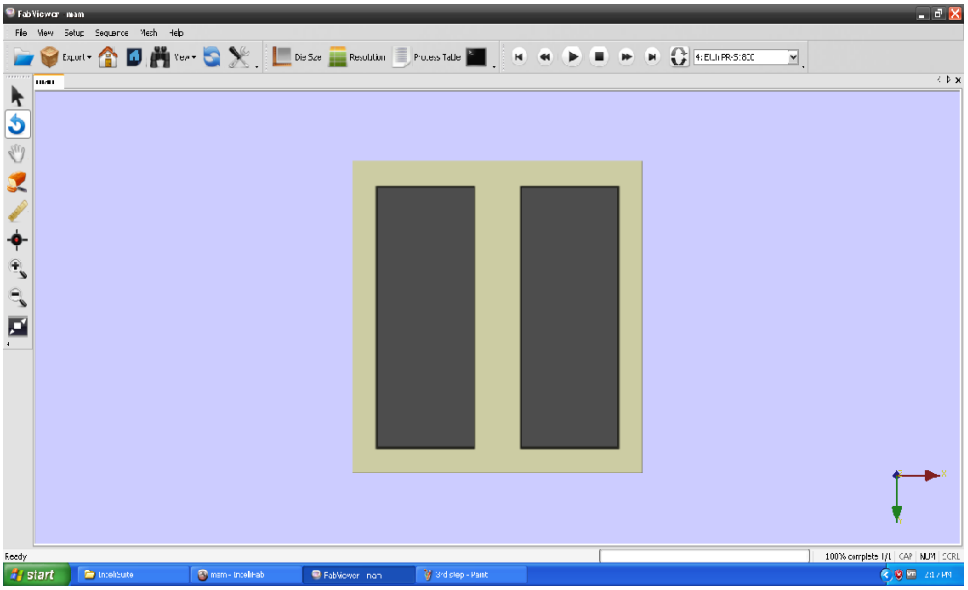

Fig.4.4 Wet chemical etching

e. The Reactive Ion Etching (Etch-Si –RIE –LAM490 – Partial Etching) is made for the clamping to remain on all four sides of diaphragm as shown in Fig.4.5.

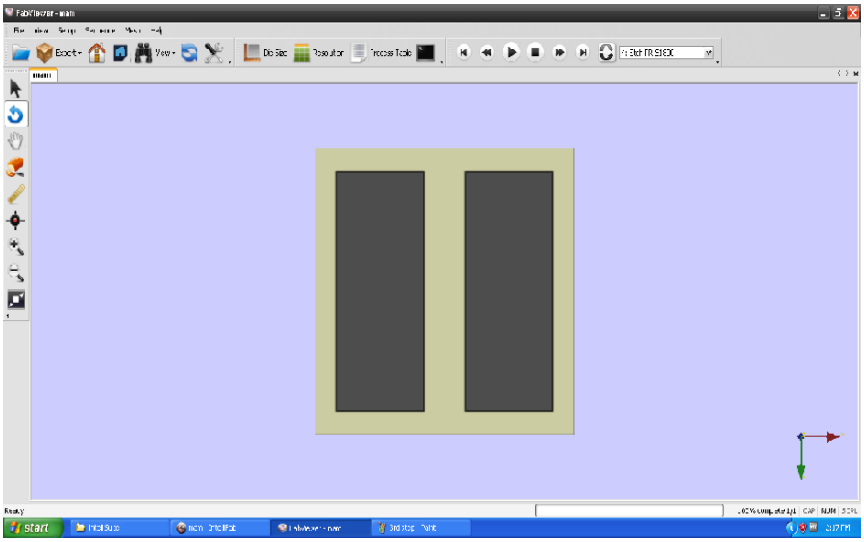

Fig.4.5 Reactive ion etching

f. The remaining resist is to be removed by wet chemical etching (Etch – PR1800 – Wet – 1112A) as shown in Fig.4.6.

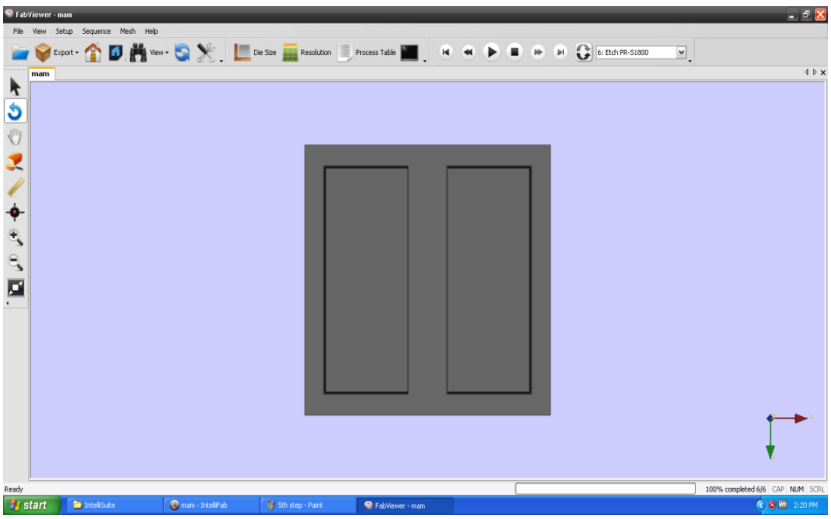

Fig.4.6 Wet chemical etching

g. This final structure in Fig.4.6 is transferred from IntelliFab to TEM tool to carry out the deflection, stress and piezoresistive analysis.

4.3 MODELLING OF SINGLE BOSS SCULPTURED DIAPHRAGM

The pressure-deflection model of a flat square diaphragm [100] is given as

$$\frac{Pa^4}{Eh^4} = \frac{4.2}{(1-\nu^2)}\left[\frac{y}{h}\right] + \frac{1.58}{(1-\nu)}\left[\frac{y}{h}\right]^3 \quad (4.1)$$

where 'P' is the applied pressure in Pa, 'y' is the center deflection of the diaphragm in μm, '$a = L/2$ ' is the half side length of the diaphragm in μm, 'E' is the young's modulus in GPa, 'h' is the thickness of the diaphragm in μm and 'ν' is the poisson's ratio of the diaphragm material.

The first term in the RHS of equation (4.1) represents the Small Scale Deflection (SSD) that is very small compared to the diaphragm thickness (deflection is less than 40% of the diaphragm thickness). Whereas the second term of equation (4.1) gives Large Scale Deflection (LSD), in which deflection is 40% larger than the diaphragm thickness [75].

The assumptions of thin plate deflection theory [109,110] considered for acheivement of SSD are:

- The maximum membrane deflection is less than 40% of the membrane thickness.
- Membrane thickness doesnot exceed 10% of the diaphragm length.
- There is no initial stress in the membrane.

The deflection *y* in the linear region of operation with respect to thickness 'h' is expressed as follows for a square diaphragm,

$$y = \frac{\alpha\, pL^4}{h^3 E} \quad \text{and} \quad \alpha = \frac{(1-\nu^2)}{4.2\times 2^4} \text{ is a constant} \quad (4.2)$$

where 'p' pressure applied, 'L' length of the diaphragm, 'h' thickness of the diaphragm, E young's modulus and α=0.0138 for L/W=1(square). However, it cannot be used for characterizing the load deflection model of single sculptured diaphragms. Hence, development of a new model becomes necessary to describe the load deflection response of these sculptured diaphragms. Equation (4.2) is suitably

modified to describe the equations for sculptured diaphragms. When the diaphragm is added with supports in the center, two important changes happen. First the active force loading area decreases. Second the rigidity of the diaphragm is reduced. So incorporation of these factors in the modelling is essential to obtain the correct load deflection response. The length 'L' decides the loading area and the thickness "h" of the diaphragm decides the rigidity in equation (4.2). Therefore, the correctness or validity of the modified analytical model depends on the ability to define the effective side length L_{eff} and effective diaphragm thickness h_{eff} that replace 'L' and 'h' in equation (4.2). In a sculptured diaphragm, one support of required dimension is added to a square diaphragm of 500μm×500μm in the bottom which tends to change the effective 'L_{eff}'. After the introduction of one support, the square diaphragm is modified into two rectangle diaphragms on the two sides of the support as shown in Fig.4.7 where the center deflection takes place on the centers of the shaded regions.

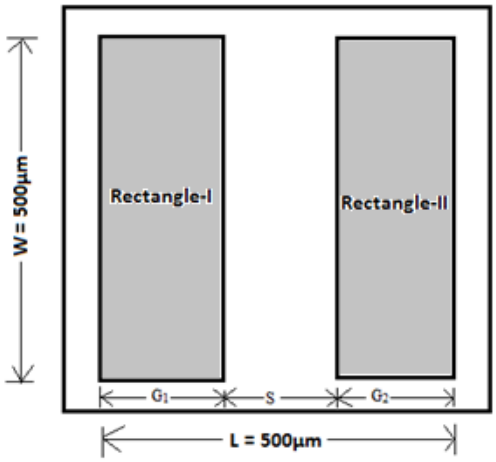

Fig.4.7 Top view of single boss sculptured diaphragm after addition of single support

In the Fig.4.7, S – Support length (μm), G_1 length of new rectangle-I formed in the left side by addition of support(μm), and G_2 is the length of the new rectangle-II formed in the right side by addition of support(μm), L-total length of the diaphragm and W- total width of diaphragm. Now the change in effective length on the two sides given in the following equation:

$$L_{eff} = Total\ Length - Support\ length = L - S \quad (4.3)$$

Based on effective length, L_{eff} /W ratio , coefficients α and β are to be selected from the Table 4.1.

Table 4.1 Coefficients α, β_1 and β_2 with respect to L_{eff} /W ratio

L_{eff} /W	1	1.2	1.4	1.6	1.8	2.0	∞
α	0.0138	0.0188	0.0226	0.0251	0.0267	0.0277	0.0284
β_1	0.3078	0.3834	0.4356	0.4680	0.4872	0.4974	0.5000
β_2	0.1386	0.1794	0.2094	0.2286	0.2406	0.2472	0.25

Now the center deflection given by equation (4.2) is modified as

$$y = \frac{\alpha P G_1^4}{Eh^3} = \frac{\alpha P G^4}{Eh^3} \tag{4.4}$$

Where G_1 and G_2 are the length of shaded region where maximum deflection occurs (μm). Therefore $G=G_1=G_2$ (μm)

Similarly the effective diaphragm thickness 'h_{eff}' obtained from the new structure after addition of single support can be written as given in the following equation,

$$h_{eff} = h \tag{4.5}$$

There is no change in the thickness, and remains the same. Now the modified deflection equation for the diaphragm with support can be written as given in the following equation:

$$y_{eff} = \frac{\alpha P G^4}{Eh^3} \tag{4.6}$$

The stress developed in the YY and XX direction in the diaphragm under different applied pressure in the SSD region is given by the equation (4.7),

$$\sigma_{yy} = \beta_1 P \left[\frac{G}{h}\right]^2 \quad and \qquad \sigma_{xx} = \beta_2 P \left[\frac{G}{h}\right]^2 \tag{4.7}$$

where 'P' pressure applied in Pa, 'G' the length of the new rectangle in μm and 'h' the thickness of the diaphragm in μm.

The equation for the wheatstone bridge output voltage (V_o) is given [79] as,

$$\frac{V_o}{V_b} = \frac{R_4}{R_4+R_1} - \frac{R_3}{R_2+R_3} \tag{4.8}$$

where V_b is the bridge excitation voltage. Intially resiatance $R_1 = R_2 = R_3 = R_4 = R_o$ which is the resistance of piezoresistor at zero pressure. When pressure is applied, change in resistance with respect to R_o is changed as [79] follows,

$$\frac{\Delta R}{R_o} = \frac{(\pi_{11}+\pi_{12}+\pi_{44})\sigma_l+(\pi_{11}+\pi_{12}-\pi_{44})\sigma_t}{2} \tag{4.9}$$

where σ_l and σ_t are the longitudinal and tensile stress along the diaphragm. In longitudinal orientation, for R_2 and R_4: $\sigma_l=\sigma_1$ MPa and $\sigma_t=\sigma_2$ MPa. In transverse orientation, for R_1 and R_3: $\sigma_l=\sigma_2$MPa and $\sigma_t=\sigma_1$MPa.

When pressure is applied, the new change in resistance are obtained by the following equations,

$$R_1 = R_3 = R_o(1 + 0.5 \times (1.436 \times \sigma_l - 1.326 \times \sigma_t) \times 10^{-3}) \quad (4.10)$$

$$R_2 = R_4 = R_o(1 + 0.5 \times (1.436 \times \sigma_t - 1.326 \times \sigma_l) \times 10^{-3}) \quad (4.11)$$

Where R_2 and R_4 are in longitudinal direction and R_1 and R_3 are in transverse direction. Substituting (4.10) and (4.11) in (4.8), the voltage sensitivity is obtained as in equation (4.12),

$$\frac{V_o}{V_b} = \frac{2.762\times10^{-3}(\sigma_l - \sigma_t)}{4+0.11\times10^{-3}(\sigma_l+\sigma_t)} \quad (4.12)$$

4.4 LOAD DEFLECTION ANALYSIS

The structure shown in Fig.4.8 is a planar silicon diaphragm formed by bulk micromachining [3, 4, 24,]. The single boss sculptured diaphragm created has three regions at the bottom of the substrate namely G_1, G_2 and S as shown in Fig.4.8. The main objective of this work is to analyze the positioning of the boss by varying these regions to achieve the maximum deflection sensitivity within the SSD region for square diaphragms. The sensor is subjected to pressure on the front side as in Fig.4.8 where the piezoresistors are to be placed. The pressure range varied from 0 to 1000Pa.

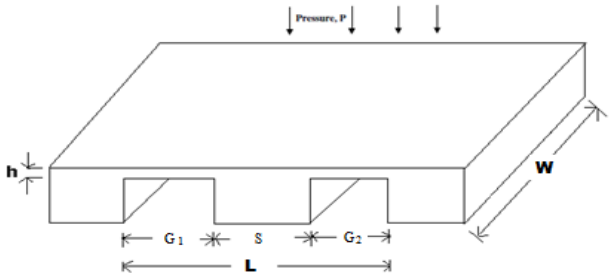

Fig.4.8 Cross sectional view of single boss sculptured diaphragm

All the dimensions are in μm. The thickness of the diaphragm h = 1 μm. The simulated single boss sculptured diaphragm is shown in Fig.4.9 where the center deflection occurs in the two rectangle portions formed on the two sides of support.

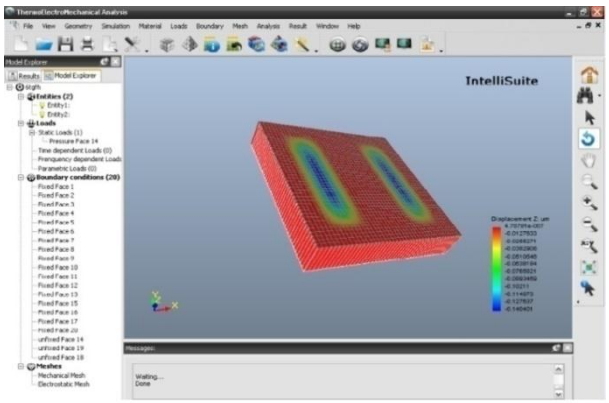

Fig.4.9 Simulated single boss sculptured diaphragm with center deflection at 1000Pa

The optimized dimensions 'G_1', 'G_2' and 'S' of a single boss sculptured diaphragm with thickness, center deflection and percentage of center deflection were given in Table 4.2a for different structures namely 'C_1', 'C_2', 'C_3', 'C_4' , 'C_5' , 'C_6' and 'C_7'.

Table 4.2a Pressure versus center deflection for single boss square sculptured diaphragm

	Center deflection (μm)						
	C_1	**C_2**	**C_3**	**C_4**	**C_5**	**C_6**	**C_7**
Pressure	**G_1=G_2 =230μm**	**G_1=G_2 =220μm**	**G_1=G_2 =210μm**	**G_1=G_2 =200μm**	**G_1=G_2 =190μm**	**G_1=G_2 =180μm**	**G_1=G_2 =170μm**
(Pa)	**S=40μm**	**S=60μm**	**S=80μm**	**S=100μm**	**S=120μm**	**S=140μm**	**S=160μm**
0	0	0	0	0	0	0	0
100	0.046756	0.0360411	0.02768	0.02768	0.0203226	0.014877	0.0102597
200	0.0935137	0.0720822	0.055362	0.055362	0.040647	0.0297541	0.0205194
300	0.140271	0.108123	0.083043	0.083043	0.0609707	0.0446311	0.0307791
400	0.187027	0.144164	0.110724	0.110724	0.0812943	0.0595081	0.0410388
500	0.233784	0.180206	0.138405	0.138405	0.101618	0.0743852	0.0512985
600	0.280541	0.216247	0.166086	0.166086	0.121941	0.0892622	0.0615582
700	0.327298	0.252288	0.193767	0.193767	0.142265	0.104139	0.0718179
800	0.374055	0.288329	0.221448	0.221448	0.162589	0.119016	0.0820776
900	0.420812	0.32437	0.249129	0.249129	0.182912	0.133893	0.0923373
1000	0.467568	0.360411	0.27681	0.27681	0.203236	0.14877	0.102597
% deflection	47%	36%	28%	28%	20%	15%	10%

The feasibility of G_1, G_2 and S are varied to achieve the center deflection of the sculptured diaphragm within the SSD region. At small deflections (<~10% diaphragm thickness) the pressure-deflection relationship is linear. As the pressure increases, the rate of deflection decreases and the pressure-deflection relationship becomes nonlinear. As a rule of thumb, a deflection of 12% of diaphragm thickness produces a terminal nonlinearity of 0.2%; a deflection of 30% produces a nonlinearity of 2% [4]. The suitability of the deflection range depends on the desired specification of the sensor and the acceptable degree of compensation. Due to these constraints to ensure linearity, the SSD is analyzed for less than 20% with respect to diaphragm thickness to ensure linearity within 0.5%. The deflection sensitivity is plotted as shown in Fig.4.10.

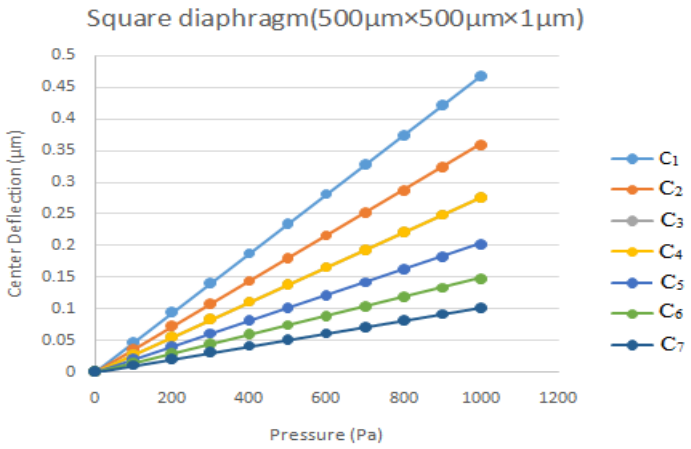

Fig.4.10 Pressure versus center deflection

The load deflection analysis shows that the diaphragms ‘C_1’, ‘C_2’, ‘C_3’ and ‘C_4’ yields more than 20% deflection where ‘C_5’ gives 20% deflection, ‘C_6’ gives 15% deflection and ‘C_7’ gives 10% deflection and satisfying the SSD of less than 20%, i.e within 20% of h. ‘C_5’, ‘C_6’ and ‘C_7’ satisfies the SSD condition. It also shows that the gap width G_1 and G_2 are varied between 170µm to 190µm and the support width S is varied from 120µm to 160µm yield the small scale deflection for a square diaphragm of dimensions 500µm×500µm×1µm. Similarly the diaphragm is created with rectangular dimensions of 500µm×300µm×1µm and analyzed for the

deflection sensitivity at a pressure of 1000Pa for different structures namely 'C_1', 'C_2', 'C_3', 'C_4' , 'C_5' and 'C_6' which is presented in Table 4.2b.

Table 4.2b Pressure versus center deflection for single boss rectangular sculptured diaphragm

	Center deflection (μm)					
	C_1	**C_2**	**C_3**	**C_4**	**C_5**	**C_6**
Pressure at 1000 (Pa)	**G_1=G_2 =230μm**	**G_1=G_2 =210μm**	**G_1=G_2 =200μm**	**G_1=G_2 =190μm**	**G_1=G_2 =180μm**	**G_1=G_2 =170μm**
	S=40μm	**S=80μm**	**S=100μm**	**S=120μm**	**S=140μm**	**S=160μm**
	0.3599	0.2370	0.2370	0.18233	0.1388	0.0988
% deflection	35%	24%	24%	18%	14%	9%

The result shows reduction in deflection when the width is reduced from 500 μm to 300 μm compared with the square diaphragm. The permissible SSD is up to 40%. Due to constraints, the maximum SSD is analyzed within 20% of h. The structure 'C_4', 'C_5' and 'C_6' satisfies the SSD less than 20% and 'C_1', 'C_2' and 'C_3' are greater than 20% deflection.

4.5 STRESS ANALYSIS

The next important step is to analyze the maximum stress regions in the longitudinal and transverse directions which are essential for placing the piezoresistors on top of the diaphragm. The longitudinal stress (S_{xx}) and transverse stress (S_{yy}) plot of the single boss sculptured diaphragm are shown in Fig.4.11 and Fig.4.12.

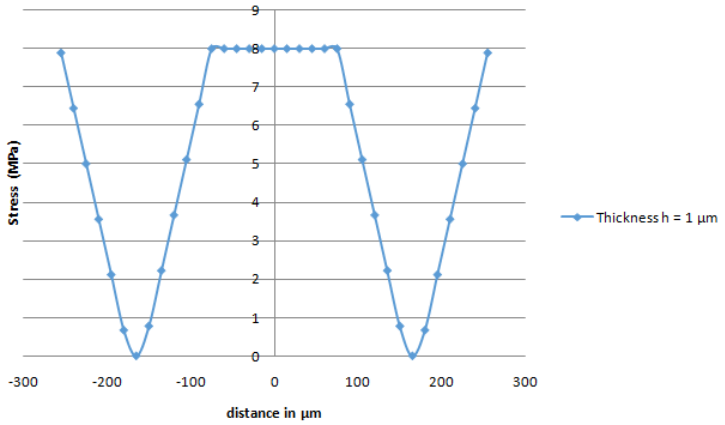

Fig.4.11 Longitudinal stress of single boss sculptured diaphragm at 1000Pa

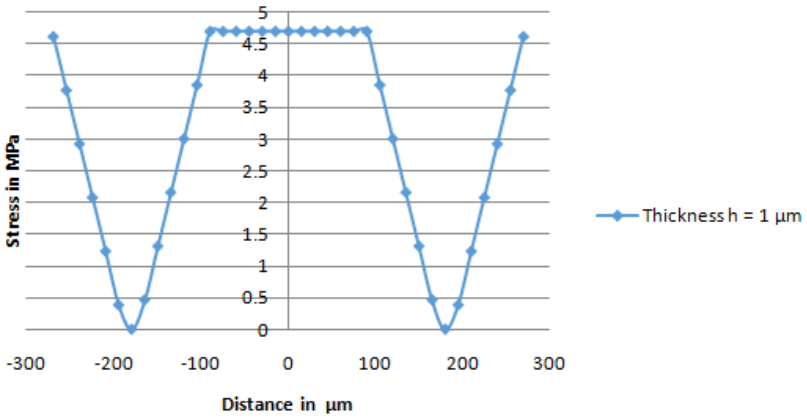

Fig.4.12 Transverse stress of single boss sculptured diaphragm at 1000Pa

A closer look at Fig.4.11, clearly shows that the longitudinal stress S_{xx} is tensile (+ve) in nature developed at and around 80µm from the center of the diaphragm and compressive (-ve) in nature developed at 150µm from the center of the diaphragm. Fig.4.12 shows that the transverse stress S_{yy} is tensile (+ve) in nature developed at and around 90µm from the center of the diaphragm and compressive (-ve) in nature at and around 220µm from the center of the diaphragm. The maximum longitudinal and transverse stress values for the different single boss sculptured diaphragms 'C_1', 'C_2', 'C_3', 'C_4', 'C_5', 'C_6' and 'C_7' of square type at 1000Pa are given in Table 4.3a.

Table 4.3a Comparison of maximum longitudinal stress and transverse stress of the different single boss square sculptured diaphragms

Pressure at 1000 (Pa)	C_1	C_2	C_3	C_4	C_5	C_6	C_7
	$G_1=G_2$ =230µm	$G_1=G_2$ =220µm	$G_1=G_2$ =210µm	$G_1=G_2$ =200µm	$G_1=G_2$ =190µm	$G_1=G_2$ =180µm	$G_1=G_2$ =170µm
	S=40µm	S=60µm	S=80µm	S=100µm	S=120µm	S=140µm	S=160µm
S_{xx}(MPa)	16.539	14.125	11.8802	11.8802	9.796	7.891	6.1808
S_{yy}(MPa)	10.1046	8.4543	7.0839	7.083	5.7184	4.6164	3.529

The stress results in Table 4.3a show that the optimized structure 'C_5' gives the highest stress and highest deflection (20%) within SSD than 'C_6' and 'C_7'. Though, structures 'C_1', 'C_2', 'C_3' and 'C_4' yield the higher stress than 'C_5', 'C_6' and 'C_7', it is not satisfying the required SSD condition. Since support is added in the diaphragm, the longitudinal and transverse stress is not equal in magnitude as similar to the flat rectangular diaphragm in Table 3.6. To estimate the electrical output, the square diaphragm 'C_5' is selected for further analysis as it is within the limits of SSD and safe to realize. The maximum longitudinal stress regions of the simulated single boss sculptured diaphragm are highlighted in red colour as shown in Fig.4.13.

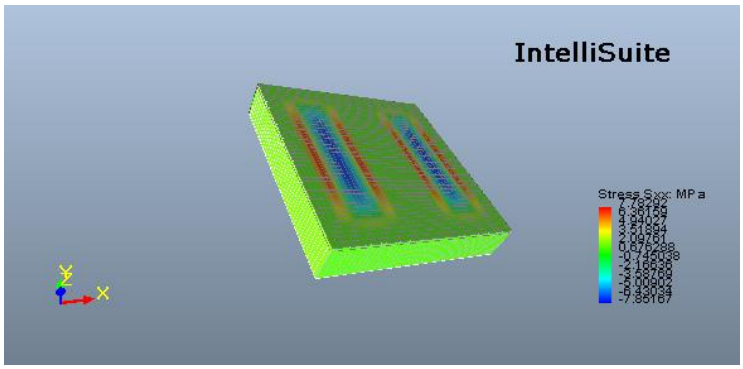

Fig.4.13 Simulated single boss sculptured diaphragm with longitudinal stress distribution at 1000Pa

The maximum transverse stress regions of the simulated single boss sculptured diaphragm are highlighted in red colour as shown in Fig.4.14.

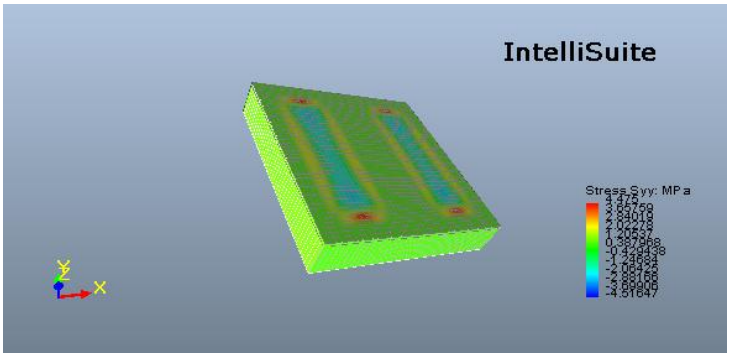

Fig.4.14 Simulated single boss sculptured diaphragm with transverse stress distribution at 1000Pa

The maximum longitudinal and transverse stress values for the different single sculptured diaphragms 'C_1', 'C_2', 'C_3', 'C_4', 'C_5' and 'C_6' of rectangular type at 1000Pa are given in Table 4.3b.

Table 4.3b Comparison of maximum longitudinal stress and transverse stress of the different single boss rectangular sculptured diaphragms

At Pressure 1000 Pa	C_1	C_2	C_3	C_4	C_5	C_6
	$G_1= G_2$ =230µm	$G_1=G_2$ =210µm	$G_1= G_2$ =200µm	$G_1=G_2$ =190µm	$G_1= G_2$ =180µm	$G_1= G_2$ =170µm
	S=40µm	S=80µm	S=100µm	S=120µm	S=140µm	S=160µm
S_{xx}(MPa)	13.079	10.302	10.302	8.84	7.38	5.95
S_{yy}(MPa)	11.9922	8.7667	8.766	7.22	5.95	4.67

The comparison of stress values for 'C_1', 'C_2', 'C_3', 'C_4', 'C_5' and 'C_6' diaphragms reveals that 'C_4', 'C_5' and 'C_6' satisfies both SSD and stress. But 'C_1', 'C_2' and 'C_3' give a very high deflection of greater than 20% and its stress values are also high. On comparing Table 4.3a and 4.3b, the square diaphragm is seen to give good stress sensitivity than a rectangular diaphragm with single support. The longitudinal stress values of the square diaphragm are higher than rectangular diaphragm with single support. Though S_{xx} value reduces, S_{yy} value has been increased for rectangular type diaphragm it satisfies the SSD condition.

4.6 POSITIONING THE PIEZORESISTORS FOR ESTIMATION OF ELECTRICAL OUTPUT

The polysilicon with suitable properties [43,44,45,78] has been considered in this work to realize the piezoresistors using surface micromachining on the top of the diaphragm. Improvement of the voltage sensitivity, requires placing the four piezoresistors in such a way that two resistors (R_2, R_4) experience tensile stress and exihibit increase in their resistance and the remaining two resistors (R_1, R_3) experience compressive stress and exihibit decrease in their resistance from the resistance value measured at no stress condition [77].

Hence resistors (R_2, R_4) are palced at 80µm from the center of the diaphragm in the XX direction and resistors (R_1, R_3) are placed at 220µm from the center of the diaphragm in the YY direction as shown in Fig.4.15.

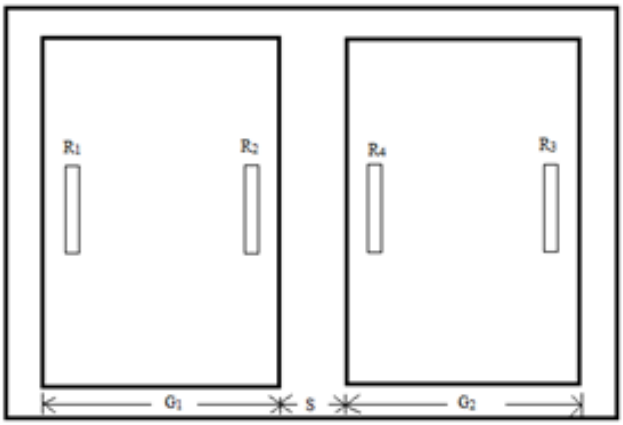

Fig.4.15 Piezoresistor placement on the optimized diaphragm 'C_6'

The smith piezoresistive coefficients [13] used in the simulation are as follows: $\pi_{11} = 6.6\times10^{-11}$ Pa^{-1}; $\pi_{12} = 1.1\times10^{-11}$ Pa^{-1}; $\pi_{44} = 138\times10^{-11}$ Pa^{-1}, sheet resitance of the p-type silicon resistor is 1000 Ω per square cm and temperature = 20°C. The size of polysilicon piezoresistor is 40µm×20µm×1µm. The voltage sensitivity has been estimated using wheat stone bridge assembly for the C_6 type sculptured diaphragm. The bridge excitation voltage 'V_b' is 5V. The estimated electrical output is in the range of 64.99 µV/Pa.

4.7 COMPARISON OF ANALYTICAL AND SIMULATED RESULTS

The modified analytical equation obtained in section 4.3 is used to obtain analytical results, which are used to compare and validate the simulated results for a square type single boss sculptured diaphragm. The comparison of center deflection, longitudinal stress and transverse stress is given in Table 4.4.

Table 4.4 Comparison of analytical and simulated center deflection, longitudinal stress, transverse stress, output voltage

	Analytical results				Simulated results			
Pressure (Pa)	**Center deflection (μm)**	**S_{xx} (MPa)**	**S_{yy} (MPa)**	**V_o (μV/Pa)**	**Center deflection (μm)**	**S_{xx} (MPa)**	**S_{yy} (MPa)**	**V_o (μV/Pa)**
0	0	0	0	0	0	0	0	0
100	0.0139	0.806	0.479	6.87	0.014877	0.789	0.461	6.499
200	0.0278	1.612	0.812	13.74	0.0297541	1.578	0.922	12.998
300	0.0417	2.45	1.24	20.61	0.0446311	2.367	1.383	19.497
400	0.0556	3.27	1.67	27.48	0.0595081	3.156	1.844	25.996
500	0.0695	4.06	2.05	34.35	0.0743852	3.945	2.305	32.495
600	0.0834	4.87	2.42	41.22	0.0892622	4.734	2.766	38.994
700	0.0973	5.697	2.87	48.09	0.104139	5.523	3.227	45.493
800	0.1112	6.43	3.26	54.96	0.119016	6.312	3.688	51.992
900	0.1251	7.215	3.69	61.83	0.133893	7.101	4.149	58.491
1000	0.139	8.067	4.88	68.7	0.14877	7.89	4.61	64.99

On comparing the analytical and simulated results of output voltage from Table 4.4, analytical values at 1000Pa are in terms of 68.7μV/Pa and the simulated output is 64.99μV/Pa. The sensitivity is improved by proper placement of piezoresistors, size of piezoresistors and thickness of diaphragm is reported in the next chapters.

4.8 SUMMARY

The single support diaphragm with dimensions 500μm×500μm×1μm is constructed with reactive ion etching. The structure is analysed for deflection

sensitivity through variation of the support width in the range from 120μm to 160μm to achieve small scale deflection within 20% of h. Similarly the rectangular diaphragm with 500μm×300μm×1μm is created and analyzed for the deflection and stress. Deflection and stress are found to be comparatively low for a rectangular diaphragm which, however, ensures linearity. But the rectangular diaphragm ensures linearity. The square sculptured diaphragm is analyzed for the maximum stress regions to place two resistors (R_1, R_3) to undergo increase in resistance and two resistors (R_2, R_4) to undergo decrease in resistance in the longitudinal and transverse directions respectively. The four piezoresistors are wired by wheatstone bridge arrangement which estimates the electrical output. The output is in the order of 64.99μV/Pa at 1000Pa. The analytical results show that, the output is 68.7μV/Pa at 1000 Pa. Square diaphragm with S_{xx} 7.89MPa which is higher than the rectangular diaphragm with S_{xx} 7.38MPa. The output is to be enhanced by increasing the number of supports to sense this range of pressure which is discussed in the next chapter.

CHAPTER 5

DESIGN AND ANALYSIS OF DOUBLE BOSS SCULPTURED DIAPHRAGM

5.1 INTRODUCTION

In the previous chapter, single support diaphragm is used to a sense low pressure range using a square shape diaphragm gives the sensitivity of about 64.99μV. The feasibility of maximizing the output is explored in this chapter by using the double support diaphragm in which two supports are added which in turn increase the linearity of output and also the sensitivity by concentrating stress in the narrow region. In this approach, the structure is locally stiffened to limit the overall deflection, while maintaining a relatively thin section where the piezoresistors are placed. The thin regions are the major stressed regions of the diaphragm where piezoresistors are placed and sensitivity improved. Also in this chapter, improvement of sensitivity is explored by reducing the thickness of the diaphragm using SOI layer.

5.2 DIAPHRAGM DESIGN

The diaphragm is designed with two rigid or two support at the bottom of the diaphragm. The dimensions of the diaphragm is (Lμm× Wμm× hμm) 500μm× 500μm ×1μm where 'L' is the length, 'W' is the width and 'h' is the thickness of the diaphragm. The square has been selected for the diaphragm shape. The choice is based mainly on the fabrication process used for realizing it. In addition, it depends upon several other factors such as the applications and distribution of the required stress field. The square and rectangular shapes are preferred in most cases due to the ease of fabrication by the anisotropic wet chemical etching of silicon. On the other hand, the fabrication of circular diaphragms in silicon is possible by Deep Reactive Ion Etching (DRIE). Some of the comparison studies reported in the literature [61, 62] on the effect of the three diaphragm shapes with respect to deflection, stress and

vibration frequency suggest that square diaphragms are useful for tactile sensors whereas rectangular diaphragms are suitable where packaging constraints limit the width vis-à-vis the length. Optimal nature of the diaphragm is reported [63] in the case of structures like microphones because of the largest center deflection for a given area.

The structure is created with single crystal silicon by the czochrolski process using a proper mask with reactive ion etching. Though it would be preferable to use circular diaphragms to prevent unwanted stress concentration, silicon diaphragms turn out to be square or rectangular when they are fabricated using anisotropic wet chemical etching on silicon wafers of <100> orientation. It is also easier to align the resistors parallel and perpendicular to the edges of the diaphragm which are in the <110> direction, thus ensuring maximum values for the piezoresistive coefficients π_l and π_t along this direction. The following steps are used to create the structure using IntelliFab and IntelliMask software. All the fabrication steps of double boss sculptured diaphragm are similar to single boss sculptured diaphragm, except step (b) in creating the mask with photo resist, which is shown in Fig.5.1.

a. The silicon substrate with required die size to be mentioned with the thickness of the 50µm. This is a czochrolski <111> orientation process.
b. The photo resist to make double sculpture is made with the thickness 3µm using PRS 1800 – spin – S1805 as shown in Fig.5.1.

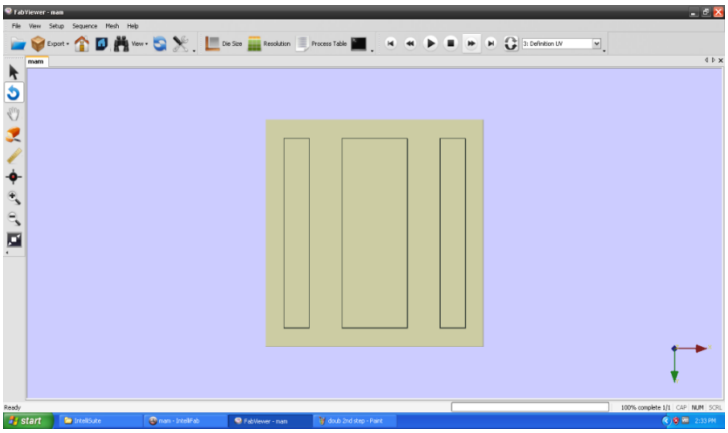

Fig.5.1 Mask with photo resist for double boss sculptured diaphragm

c. The UV light exposed on the top of the photo resist to make the pattern on the silicon diaphragm.
d. The wet chemical etching used to make the diaphragm with support at the bottom. The process PRS1800 – wet – 1112A where partial etching is processed.
e. The Reactive Ion Etching (Etch-Si –RIE –LAM490 – Partial Etching) for the clamping to remain on all four sides of diaphragm is processed.
f. The remaining resist is to be removed by wet chemical etching (Etch – PR1800 – Wet – 1112A) is processed.
g. The final structure is transferred from IntelliFab to TEM analysis to carry out the deflection, stress and piezoresistive analysis.

5.3 MODELLING OF DOUBLE BOSS SCULPTURED DIAPHRAGM

The pressure-deflection model of a flat square diaphragm [100] is given as

$$\frac{Pa^4}{Eh^4} = \frac{4.2}{(1-\nu^2)}\left[\frac{y}{h}\right] + \frac{1.58}{(1-\nu)}\left[\frac{y}{h}\right]^3 \quad (5.1)$$

where ‘P’ is the applied pressure in Pa, ‘y’ is the center deflection of the diaphragm in μm, ‘$a = L/2$ ’ is the half side length of the diaphragm in μm, ‘E’ is the young’s modulus in GPa, ‘h’ is the thickness of the diaphragm in μm and ‘ν’ is the poisson’s ratio of the diaphragm material.

The first term in the RHS of equation (5.1), represents the SSD that is very small compared to the diaphragm thickness (deflection is less than 40% of the diaphragm thickness). Whereas the second term of equation (5.1) gives LSD, in which deflection is larger than the diaphragm thickness [75]. The assumptions of thin plate deflection theory made for the achievement of SSD [109,110] are:

- The maximum membrane deflection is less than 40% of the membrane thickness.
- Membrane thickness doesnot exceed 10% of the diaphragm length.
- There is no initial stress in the membrane.

The deflection *y* in the linear region of operation with respect to thickness 'h' is expressed as follows for a square diaphragm,

$$y = \frac{\alpha\, p L^4}{h^3 E} \quad \text{and} \quad \alpha = \frac{(1-\nu^2)}{4.2\times 2^4} \text{ is a constant} \tag{5.2}$$

where 'p' pressure applied, 'L' length of the diaphragm, 'h' thickness of the diaphragm, E young's modulus and α=0.0138 for L/W=1(square). For rectangle diaphragm, α value change with respect to length/width ratio as given in Table 5.1.

Table 5.1 Coefficients α, β_1 and β_2 with respect to L_{eff}/ W ratio

L_{eff}/W	1	1.2	1.4	1.6	1.8	2.0	∞
α	0.0138	0.0188	0.0226	0.0251	0.0267	0.0277	0.0284
β_1	0.3078	0.3834	0.4356	0.4680	0.4872	0.4974	0.5000
β_2	0.1386	0.1794	0.2094	0.2286	0.2406	0.2472	0.25

However, it cannot be used for characterizing the load deflection response of double sculptured diaphragms. Hence, development of a new model to describe the load deflection response of these sculptured diaphragms becomes necessary. Equation (5.2) is suitably modified to describe the equations for double sculptured diaphragms. When the diaphragm is added with two supports, two important changes happen. First the active force loading area decreases. Second the rigidity of the diaphragm is reduced. So incorporation of these factors in the modelling is essential to obtain the correct load deflection model. The length decides the loading area and the thickness 'h' of the diaphragm decides the rigidity in the equation (5.2). Therefore, the correctness or validity of the modified analytical model depends on the ability to define the effective length 'L_{eff}' and effective diaphragm thickness 'h_{eff}' that replace 'L' and 'h' in (5.2). In double sculptured diaphragm, two supports of required dimension are added to a square diaphragm of 500μm×500μm in the bottom which tends to change the effective length 'L_{eff}'. After the introduction of two supports, the square diaphragm is modified with three rectangle portions on the two sides of the support as shown in Fig.5.2.

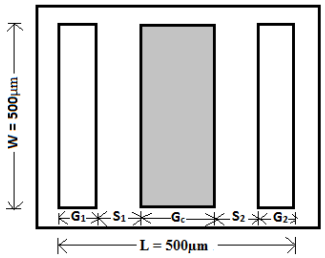

Fig.5.2 Top view of double boss sculptured diaphragm after addition of two supports

The center deflection takes place on the shaded region of the double boss diaphragm as in Fig.5.2.Here, S_1, S_2 – support length, G_c – Gap length where deflection occurs (μm), G_1 - length of rectangle formed in the left side by addition of support S_1(μm), and G_2 is the length of the rectangle formed in the right side by addition of support S_2(μm), L-total length of the diaphragm and W- total width of diaphragm. Now the change in effective length on the two sides given in the following equation:

$$L_{eff} = L - S_1 - S_2 \tag{5.3}$$

Based on effective length, L_{eff}/W ratio, coefficients α and β are to be selected from the Table 5.1.

Now the center deflection given by equation (5.2) is modified as

$$y = \frac{\alpha P G_c^4}{Eh^3} \tag{5.4}$$

Where G_c –length of the shaded region where maximum deflection occurs (μm).

Similarly the effective diaphragm thickness 'h_{eff}' obtained from the new structure after addition of support can be written as given in the following equation,

$$h_{eff} = h \tag{5.5}$$

As there is no change in the thickness, it remains the same. Now the modified deflection equation 'y_{eff}' for the sculptured diaphragm can be written as given in the following equation:

$$y_{eff} = \frac{\alpha P G_c^4}{Eh^3} \tag{5.6}$$

The stress developed in the YY and XX direction in the diaphragm under different applied pressure in the SSD region is given by the equation,

$$\sigma_{yy} = \beta_1 P \left[\frac{G_c}{h}\right]^2 \quad and \qquad \sigma_{xx} = \beta_2 P \left[\frac{G_c}{h}\right]^2 \tag{5.7}$$

where 'σ' is the maximum stress in Pa, 'P' pressure applied in Pa, 'G_c' the length of the shaded region in μm and 'h_{eff}' the thickness of the diaphragm in μm.

The equation for the wheatstone bridge output voltage (V_o) is given [79] as,

$$\frac{V_o}{V_b} = \frac{R_3}{R_2+R_3} - \frac{R_4}{R_1+R_4} \tag{5.8}$$

where V_b is the bridge excitation voltage. Intially the resistancee are $R_1 = R_2 = R_3 = R_4 = R_o$ which is the resistance at zero pressure. When pressure is applied, change in resistance with respect to R_o is [79] as follows,

$$\frac{\Delta R}{R_o} = \frac{(\pi 11+\pi 12+\pi 44)\sigma_l+(\pi 11+\pi 12-\pi 44)\sigma_t}{2} \tag{5.9}$$

where σ_l and σ_t are the longitudinal and tensile stress along the diaphragm. In longitudinal orientation, for R_2 and R_4: $\sigma_l=\sigma_1$ MPa and $\sigma_t=\sigma_2$ MPa. In transverse orientation, for R_1 and R_3: $\sigma_l=\sigma_2$MPa and $\sigma_t=\sigma_1$MPa.

When pressure is applied, the new change in resistance are obtained by the following equations,

$$R_1 = R_3 = R_o(1 + 0.5 \times (1.436 \times \sigma_l - 1.326 \times \sigma_t) \times 10^{-3}) \tag{5.10}$$

$$R_2 = R_4 = R_o(1 + 0.5 \times (1.436 \times \sigma_t - 1.326 \times \sigma_l) \times 10^{-3}) \tag{5.11}$$

Where R_2 and R_4 are in longitudinal direction and R_1 and R_3 are in transverse direction. Substituting (5.10) and (5.11) in (5.8), the voltage sensitivity is obtained as

$$\frac{V_o}{V_b} = \frac{2.762\times 10^{-3}(\sigma_l - \sigma_t)}{4+0.11\times 10^{-3}(\sigma_l+\sigma_t)} \tag{5.12}$$

5.4 LOAD DEFLECTION ANALYSIS

The structure shown in Fig.5.3 is a planar silicon diaphragm formed by bulk micromachining [3, 4, 24]. The double boss sculptured diaphragm created has five regions namely G_1, G_2, S_1, S_2 and G_c as in Fig.5.3. The main objective of this work is to analyze the positioning of the boss by varying these regions to achieve the maximum deflection sensitivity within the SSD region for square diaphragm within 20% of h. The sensor is subjected to pressure on the front side as in Fig.5.3 where the piezoresistors are to be placed. The pressure range is varied from 0 to 1000Pa.

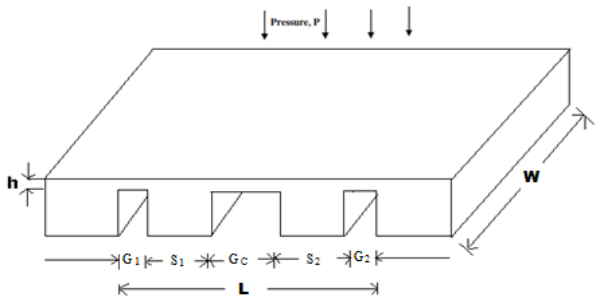

Fig.5.3 Cross sectional view of double boss sculptured diaphragm

The feasibility of varying the five different parameters G_1, G_2, S_1, S_2 and G_c of double boss sculptured diaphragm with center deflection for different structures namely T_1, T_2, T_3, T_4, T_5 and T_6 were given in Table 5.2, 5.3, 5.4, 5.5 and 5.6. All the dimensions are in μm. The simulated double boss sculptured diaphragm is shown in Fig.5.4 where the center deflection occurs in the G_c region as marked in the Fig.5.2. i.e., in between the two supports.

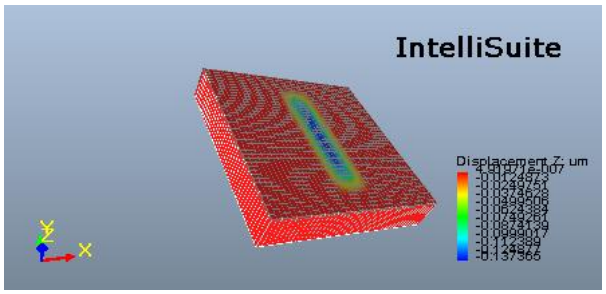

Fig.5.4 Simulated double boss sculptured diaphragm with center deflection at 1000Pa

The thickness of the diaphragm h = 1 μm. To optimize the structure to satisfy the deflection lesser than 40% of h, the center width **(G_c)** is varied from 140μm to 360μm; the supports (**S_1, S_2)** on two sides varied from 50μm to 160μm; side gap (**G_1**, **G_2)** is fixed at 20μm.

Table 5.2 Pressure versus center deflection for double boss sculptured diaphragm by varying S_1,S_2 from 50 μm to 60μm ; G_c from 140μm to 360μm ; G_1,G_2 = 20μm (fixed)

	Center deflection(μm)					
	T_1	T_2	T_3	T_4	T_5	T_6
Pressure	G_1=G_2 =20μm	G_1 =G_2=20μm	G_1=G_2=20μm	G_1 =G_2 =20μm	G_1=G_2 =20μm	G_1=G_2=20μm
(Pa)	G_c =360μm	G_c =300μm	G_c =240μm	G_c =200μm	G_c =180μm	G_c =140μm
	S_1=S_2=50μm	S_1=S_2=80μm	S_1=S_2=110μm	S_1=S_2=130μm	S_1=S_2=140μm	S_1=S_2=160μm
0	0	0	0	0	0	0
100	0.194807	0.106633	0.0467458	0.027681	0.014877	0.0078
200	0.389613	0.213266	0.0934918	0.055362	0.029754	0.0156
300	0.584421	0.319899	0.1402374	0.083043	0.044631	0.0234
400	0.779228	0.426531	0.1869832	0.110724	0.059508	0.0312
500	0.974033	0.533164	0.233729	0.138405	0.074385	0.039
600	1.168842	0.639797	0.2804748	0.166086	0.089262	0.0468
700	1.363649	0.746431	0.3272206	0.193767	0.10413	0.0546
800	1.558456	0.853063	0.3739664	0.221448	0.119016	0.0624
900	1.753263	0.959696	0.420712	0.249129	0.133874	0.0702
1000	1.94807	1.06633	0.467458	0.27681	0.14877	0.078
% age of deflection	194%	106%	47%	28%	15%	8%

The pressure-deflection relationship is linear at small deflections (<~10% diaphragm thickness). As the pressure increases, the rate of deflection decreases and the pressure-deflection relationship becomes nonlinear. As a rule of thumb, a deflection of 12% of diaphragm thickness produces a terminal nonlinearity of 0.2%; a deflection of 30% produces a nonlinearity of 2% [4]. The suitability of the deflection range depends on the desired specification of the sensor and the acceptable degree of compensation. Due to these constraints to ensure linearity, the SSD is analyzed for less than 20% with respect to diaphragm thickness to ensure linearity within 0.5%.

The percentage of deflection within the SSD region is compared for different structures namely T_1, T_2, T_3, T_4, T_5 and T_6. The structure 'T_5' is close to 20% of deflection and this is the optimized structure from this category. The 'T_5' structure

gives 28% deflection which is very high in deflection and 'T_6' structure gives 8% which is very small in deflection.

Similarly the structure is further optimized by varying the center width **(G_c)** from 140µm to 300µm; the supports **(S_1, S_2)** on two sides varied from 60µm to 140µm; side gap **(G_1 , G_2)** is fixed at 40µm.

Table 5.3 Pressure versus center deflection for double boss sculptured diaphragm by varying S_1,S_2 from 60 µm to140µm; G_c from 140 µm to 300µm; G_1,G_2 =40 µm (fixed)

	Center deflection (µm)					
	T_1	**T_2**	**T_3**	**T_4**	**T_5**	**T_6**
Pressure	**G_1 = G_2 =40µm**	**G_1 = G_2= 40µm**	**G_1 = G_2 =40µm**	**G_1 = G_2 =40µm**	**G_1 = G_2 =40µm**	**G_1 = G_2 =40µm**
in Pa	**G_c =300µm**	**G_c =260µm**	**G_c =220µm**	**G_c =200µm**	**G_c =180µm**	**G_c =140µm**
	S_1=S_2=60µm	**S_1=S_2=80µm**	**S_1=S_2=100µm**	**S_1=S_2=110µm**	**S_1=S_2=120µm**	**S_1=S_2=140µm**
0	0	0	0	0	0	0
100	0.106633	0.0729573	0.0467458	0.027681	0.014877	0.00706494
200	0.213266	0.145903	0.0934917	0.055362	0.0297541	0.014129
300	0.319899	0.2188543	0.1402374	0.083043	0.044631	0.0211941
400	0.426531	0.291805	0.1869832	0.110724	0.059508	0.0282593
500	0.533164	0.3647569	0.233729	0.138405	0.074385	0.0353224
600	0.639797	0.437708	0.2804748	0.166086	0.089262	0.042389
700	0.74643	0.5106595	0.3272206	0.193767	0.10413	0.049454
800	0.853063	0.58361	0.3739664	0.221448	0.119016	0.05651952
900	0.959696	0.659051	0.420712	0.249129	0.133874	0.06358446
1000	1.06633	0.729513	0.467458	0.27681	0.14877	0.0706494
% age of deflection	107%	73%	47%	28%	15%	7%

The percentage of center deflection within the SSD region (i.e., lesser than 20% of h) is achieved by varying the G_1, G_2, S_1, S_2 and G_c. To ensure higher linearity, 20% of h is analyzed in SSD. Among the different structures 'T_5' is close to 20% of deflection and this is the optimized structure from this category. The other structures are result with either very high deflection or very small deflection.

Similarly the structure is further optimized by varying the center width **(G_c)** from 220µm to 320µm; the supports **(S_1,S_2)** on two sides varied from 30µm to 120µm; side gap **(G_1,G_2)** is fixed at 60µm.

Table 5.4 Pressure versus center deflection for double boss sculptured diaphragm by varying S_1,S_2 from 60 µm to 140µm; G_c from 140 µm to 300µm ; G_1,G_2 = 60µm (fixed)

	Center deflection in µm					
	T_1	**T_2**	**T_3**	**T_4**	**T_5**	**T_6**
Pressure	**G_1=G_2=60µm**	**G_1=G_2 =60µm**	**G_1=G_2 =60µm**	**G_1=G_2=60µm**	**G_1=G_2=60µm**	**G_1=G_2 =60µm**
in Pa	**G_c =320µm**	**G_c =300µm**	**G_c =280µm**	**G_c =260µm**	**G_c =240µm**	**G_c =220µm**
	S_1=S_2=30µm	**S_1=S_2=40µm**	**S_1=S_2=70µm**	**S_1=S_2=90µm**	**S_1=S_2=100µm**	**S_1=S_2=120µm**
0	0	0	0	0	0	0
100	0.147528	0.106632	0.0467458	0.027681	0.014877	0.00706494
200	0.295056	0.213265	0.093498	0.055362	0.0297541	0.0141299
300	0.442584	0.319896	0.1402374	0.083043	0.044631	0.0211948
400	0.590113	0.42653	0.1869832	0.110724	0.059508	0.0228593
500	0.73764	0.53316	0.233729	0.138405	0.0743852	0.0353247
600	0.885169	0.639795	0.280474	0.166086	0.089262	0.042389
700	1.032696	0.746427	0.3272206	0.193767	0.10413	0.04945458
800	1.18023	0.85306	0.3739664	0.221448	0.119016	0.05651952
900	1.327758	0.959692	0.420712	0.249129	0.133873	0.06358446
1000	1.47528	1.06632	0.467458	0.27681	0.14877	0.0706494
% age of deflection	148%	107%	47%	28%	15%	7%

The percentage of center deflection within the SSD region (i.e., lesser 20% of h) is achieved by varying the G_1, G_2, S_1, S_2 and G_c. To ensure high linearity in output, the structure with SSD lesser than 20% of h is considered and analyzed. 'T_5' is close to 20% of deflection and this is the optimized structure from this category.

Similarly the structure is further optimized by varying the center width **(G_c)** from 220µm to 320µm; the supports **(S_1, S_2)** on two sides varied from 30µm to 120µm; side gap **(G_1 , G_2)** is fixed at 60µm.

Table 5.5 Pressure versus center deflection for double boss sculptured diaphragm by varying S_1,S_2 from 20 µm to 90µm; G_c from 140 µm to 300µm ; G_1,G_2 = 80µm (fixed)

	Center deflection in µm					
	T_1	**T_2**	**T_3**	**T_4**	**T_5**	**T_6**
Pressure	**G_1=G_2 =80µm**	**G_1=G_2 =80µm**	**G_1=G_2 =80µm**	**G_1=G_2 =80µm**	**G_1=G_2 =80µm**	**G_1=G_2 =80µm**
in Pa	**G_c =300µm**	**G_c =260µm**	**G_c =240µm**	**G_c =200µm**	**G_c =180µm**	**G_c =140µm**
	S_1=S_2 = 20µm	**S_1=S_2 = 40µm**	**S_1=S_2 = 50µm**	**S_1=S_2 =70µm**	**S_1=S_2 = 80µm**	**S_1=S_2= 90µm**
0	0	0	0	0	0	0
100	0.106635	0.07295	0.046746	0.0276809	0.014877	0.0070649
200	0.21327	0.145901	0.093492	0.050553618	0.029754	0.0141299
300	0.319905	0.2188521	0.140238	0.083043	0.044631	0.0211948
400	0.426539	0.291805	0.186984	0.110724	0.059508	0.0282593
500	0.533175	0.364754	0.23373	0.138405	0.074385	0.0353247
600	0.639809	0.437704	0.280476	0.166186	0.089682	0.0423899
700	0.746445	0.510655	0.327222	0.193767	0.10413	0.04945438
800	0.853097	0.583605	0.373968	0.221448	0.119016	0.05651952
900	0.959715	0.656556	0.420714	0.249129	0.133873	0.06358446
1000	1.06635	0.729507	0.47646	0.276809	0.14877	0.0706494
% age of deflection	106%	73%	48%	28%	15%	7%

The percentage of center deflection within the SSD region (i.e., lesser than 20% of h) is achieved by varying the G_1, G_2, S_1, S_2 and G_c to ensure good linearity. The structure 'T_5' is close to 20% of deflection and this is the optimized structure from this category.

Similarly the structure is further optimized by varying the center width **(G_c)** from 220µm to 320µm; the supports **(S_1, S_2)** on two sides varied from 30µm to 120µm; side gap **(G_1 , G_2)** is fixed at 60µm.

Table 5.6 Pressure versus center deflection for double boss sculptured diaphragm by varying S_1,S_2 from 10 µm to 60µm; G_c from180 µm to 280µm; G_1,G_2 =100µm(fixed)

	Center deflection in µm			
	T_1	T_2	T_3	T_4
Pressure	$G_1 = G_2$ =100µm	$G_1 = G_2$ =100µm	$G_1 = G_2$ =100µm	$G_1 = G_2$ =100µm
in Pa	G_c =280µm	G_c =240µm	G_c =200µm	G_c =180µm
	S_1=S_2 =10µm	S_1=S_2 =30µm	S_1=S_2 =50µm	S_1=S_2 =60µm
0	0	0	0	0
100	0.046796	0.0276809	0.014877	0.00706494
200	0.093492	0.0553618	0.029754	0.0141299
300	0.140238	0.083043	0.044631	0.0211948
400	0.186984	0.1107244	0.059508	0.0282593
500	0.233748	0.138399	0.074385	0.0353245
600	0.280476	0.166086	0.089262	0.0423897
700	0.327222	0.193767	0.10413	0.04945458
800	0.373968	0.221448	0.119016	0.05651952
900	0.420714	0.249129	0.133873	0.06358446
1000	0.467496	0.276798	0.148773	0.0706489
% age of deflection	47%	28%	15%	7%

In this category, G_1, G_2 fixed at 100 µm, G_c = 200µm and S_1= S_2 =50µm, produce the center deflection within 15%. But the stress produced by this is very low in value. Since the support length is very small, this restricts the diaphragm to deflect and so stress is also poor. The structure with large value of support gives the higher deflection i.e., 'T_5' from Table 5.2 is considered for further study in order to achieve maximum stress. The graph for load deflection analysis of square diaphragm for Table 5.2 is shown in the Fig.5.5. The graph shows linearity of pressure versus center deflection over the pressure range of 0-1000Pa. The optimized diaphragm 'T_5' from is selected for stress analysis and piezoresistive analysis to estimate the electrical output. The selected diaphragm satisfies the deflection within 20% of thickness of the diaphragm to ensure good linearity.

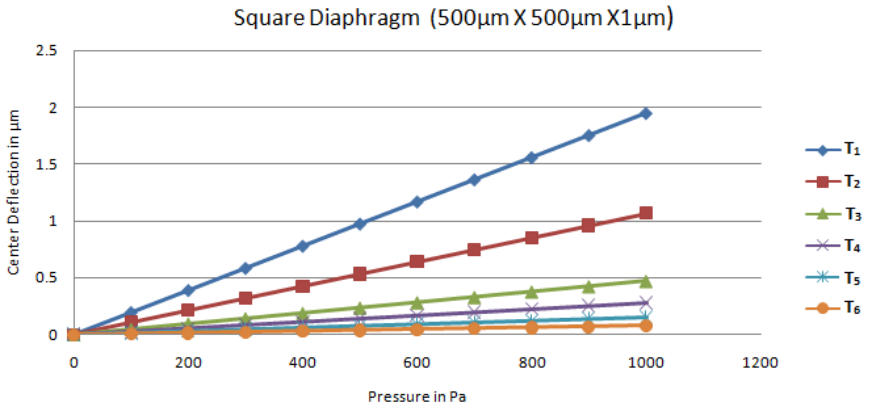

Fig.5.5 Pressure versus center deflection

The load deflection analysis carried out for the double support diaphragm reveals that center support width G_c = 180 µm, G_1 and G_2 = 20µm and S_1 and S_2 = 140 µm gives the center deflection 15% of h which ensures high linearity, and this structure is referred as " T_5" which is considered for further analysis. Similarly the diaphragm is created with rectangular dimensions of 500µm×300µm×1µm for different structures namely T_1, T_2, T_3, T_4, T_5 and T_6 and analyzed for the deflection sensitivity at a pressure of 1000Pa which is presented in Table 5.7.

Table 5.7 Pressure versus center deflection for double boss sculptured diaphragm by varying S_1 , S_2 =50 µm to 160µm and G_c = 140 µm to 360µm; fixed G_1 , G_2 =20µm; for rectangular diaphragm with dimensions 500µm×300µm×1µm

	Center deflection(µm)					
	T_1	**T_2**	**T_3**	**T_4**	**T_5**	**T_6**
At Pressure	**G_1 =G_2 =20µm**	**G_1 =G_2=20µm**	**G_1=G_2=20µm**	**G_1=G_2 =20µm**	**G_1=G_2 =20µm**	**G_1=G_2=20µm**
	G_c =360µm	**G_c =300µm**	**G_c =240µm**	**G_c =200µm**	**G_c =180µm**	**G_c =140µm**
1000 (Pa)	**S_1=S_2=50µm**	**S_1=S_2=80µm**	**S_1=S_2=110µm**	**S_1=S_2=130µm**	**S_1=S_2=140µm**	**S_1=S_2=160µm**
	0.91291	0.642454	0.359896	0.233708	0.138836	0.0696521
% age of deflection	91%	64%	36%	23%	14%	7%

It is found that, when the width reduced from 500µm to300µm, the deflection of the diaphragm is also reduced. The structures 'T_5' and 'T_4' close to 20% ensure high linearity, but all other structures give more than 20% deflection or less than 20%

deflection. The center deflection is similar to the single boss diaphragm both in the square and rectangular type. The dimension of the rectangular type should be properly selected such that the stress component increases in order to increase the sensitivity.

5.5 STRESS ANALYSIS

The next important step is to analyze the maximum stress regions in the longitudinal and transverse directions which are essential for placing the piezoresistors on top of the diaphragm. The longitudinal stress (S_{xx}) and transverse stress (S_{yy}) plot of the double support diaphragm is shown in Fig.5.6.

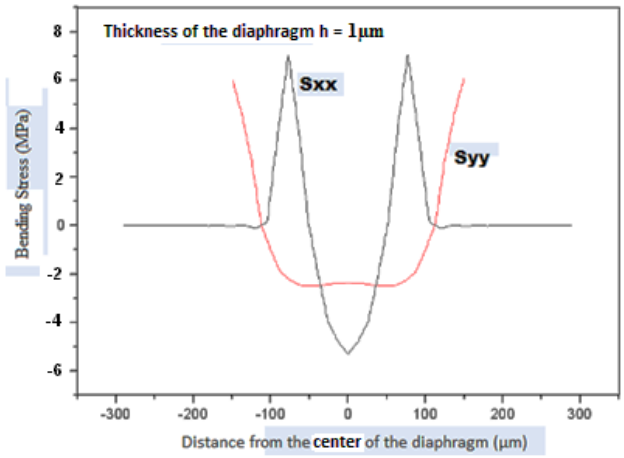

Fig.5.6 Longitudinal stress and transverse stress of double boss sculptured diaphragm at 1000Pa

A closer look at Fig.5.6, clearly shows that the longitudinal stress S_{xx} is tensile (+ve) in nature developed at and around 80µm from center of the diaphragm and compressive (-ve) in nature developed at the center of the diaphragm. The transverse stress S_{yy} is tensile (+ve) in nature developed at and around 150µm from the center of the diaphragm and compressive (-ve) in nature at and around 50µm from the center of the diaphragm.

The maximum longitudinal and transverse stress values for the different structures 'T_1', 'T_2', 'T_3', 'T_4', 'T_5' and 'T_6'of double boss sculptured diaphragm at 1000Pa are given in Table 5.8a for square type.

Table 5.8a Comparison of maximum longitudinal stress and transverse stress at 1000Pa for double boss sculptured diaphragm – square type

Stress estimated at 1000 Pa	Stress (MPa)					
	T_1	T_2	T_3	T_4	T_5	T_6
	$G_1=G_2=20\mu m$	$G_1=G_2=20\mu m$	$G_1=G_2=20\mu m$	$G_1=G_2=20\mu m$	$G_1=G_2=20\mu m$	$G_1=G_2=20\mu m$
	$G_c=360\mu m$	$G_c=300\mu m$	$G_c=240\mu m$	$G_c=200\mu m$	$G_c=180\mu m$	$G_c=140\mu m$
	$S_1=S_2=50\mu m$	$S_1=S_2=80\mu m$	$S_1=S_2=110\mu m$	$S_1=S_2=130\mu m$	$S_1=S_2=140\mu m$	$S_1=S_2=160\mu m$
S_{xx}	37.0411	28.8078	16.5012	11.98	7.891	4.9424
S_{yy}	27.5034	17.8073	10.1026	7.08397	4.6164	2.6975

The structures 'T_1', 'T_2', and 'T_3' that do not satisfy SSD though their stress values are very high and are not considered. The longitudinal stress and transverse stress are found higher for the 'T_4' structure, but it gives 28% percentage of deflection which is greater than the limits of small scale deflection. 'T_6' structure gives a very poor deflection of 8% which creates the balloon effect. Therefore, 'T_5' structure with 15% percentage deflection with the moderate stress value is considered for further analysis. The 'T_5' structure satisfies both SSD and ensures linearity. The maximum longitudinal and transverse stress values for the optimized 'T_5', double support diaphragm at 1000Pa are given in Table 5.8b for rectangular diaphragm.

Table 5.8b Comparison of maximum longitudinal stress and transverse stress at 1000Pa for double boss sculptured diaphragm – rectangular type

Stress estimated at 1000 Pa	Stress (MPa)					
	T_1	T_2	T_3	T_4	T_5	T_6
	$G_1=G_2=20\mu m$	$G_1=G_2=20\mu m$	$G_1=G_2=20\mu m$	$G_1=G_2=20\mu m$	$G_1=G_2=20\mu m$	$G_1=G_2=20\mu m$
	$G_c=360\mu m$	$G_c=300\mu m$	$G_c=240\mu m$	$G_c=200\mu m$	$G_c=180\mu m$	$G_c=140\mu m$
	$S_1=S_2=50\mu m$	$S_1=S_2=80\mu m$	$S_1=S_2=110\mu m$	$S_1=S_2=130\mu m$	$S_1=S_2=140\mu m$	$S_1=S_2=160\mu m$
S_{xx}	19.595	17.2709	13.0499	10.3024	7.39313	4.91704
S_{yy}	25.0776	18.8786	11.9904	8.7066	5.95586	3.67279

The structures 'T_1', 'T_2', 'T_3' and 'T_4' that do not satisfy SSD though their stress values are very high and are not considered. 'T_5' and 'T_6' satisfying the SSD less than 20% and their stress values are less than the square diaphragm. But the transverse stress of 'T_5' and 'T_6' are higher than square diaphragm. On comparing Table 5.8a and 5.8b, the square diaphragm gives a better stress sensitivity than a rectangular diaphragm with double support. The longitudinal stress values of the square diaphragm are higher than rectangular diaphragm with double support. Though

Sxx value reduces, S_{yy} value has been increased for rectangular type diaphragm. The stress obtained is to be converted into electrical output by piezoresistive analysis in the next section. The simulated diaphragm with longitudinal and transverse stress is shown in Fig.5.7 and 5.8.

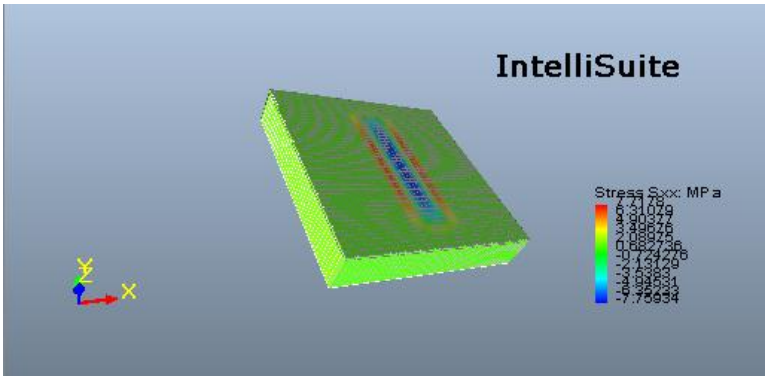

Fig.5.7 Simulated double boss sculptured diaphragm with longitudinal stress distribution at 1000Pa

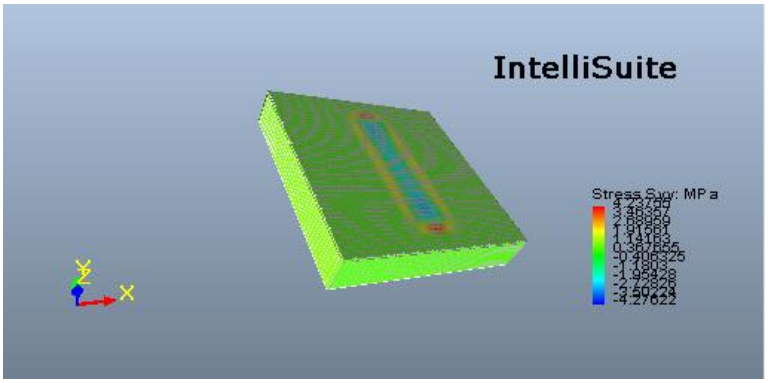

Fig.5.8 Simulated double boss sculptured diaphragm with transverse stress distribution at 1000Pa

The maximum regions of longitudinal and transverse stress are indicated in red colour in Fig.5.7 and 5.8. The blue colour indicates the minimum stress regions. The maximum longitudinal stress occurs at (90µm, 0µm) and (-90µm, 0µm) highlighted as red colour as in Fig.5.7. The maximum transverse stress occurs at (0 µm, 150 µm) and (0 µm, -150 µm) highlighted as red colour as in Fig.5.8.

5.6 POSITIONING THE PIEZORESISTOR FOR ESTIMATION OF ELECTRICAL OUTPUT

The polysilicon with suitable properties [43,44,45,78] has been considered in this work to realize the piezoresistors using surface micromachining on the top of the diaphragm. Improvement of the voltage sensitivity, requires placing the four piezoresistors in such a way that two resistors (R_2, R_4) experience tensile stress and exihibit increase in their resistance and the remaining two resistors (R_1, R_3) experience compressive stress and exihibit decrease in their resistance from the resistance value measured at no stress condition. Hence resistors (R_2, R_4) are palced at 80µm from the center of the diaphragm in the XX direction and resistors (R_1, R_3) are placed at 150µm from the center of the diaphragm in the YY direction as shown in Fig.5.9.

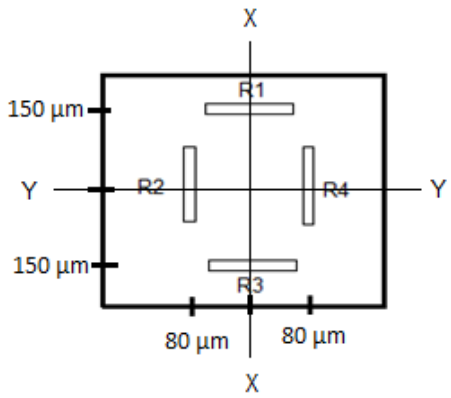

Fig.5.9 Piezoresistor placement on the optimized diaphragm in the G_c region

The smith piezoresistive coefficients [13] used in the simulation are as follows: $\pi_{11} = 6.6\times10^{-11}$ Pa^{-1}; $\pi_{12} = 1.1\times10^{-11}$ Pa^{-1}; $\pi_{44} = 138\times10^{-11}$ Pa^{-1}, sheet resitance of the p-type silicon resistor is 1000 Ω per square cm and temperature = 20°C. The size of polysilicon piezoresistor is 40µm×20µm×1µm. The voltage sensitivity has been estimated for the 'T_5' type sculptured diaphragm using the wheat stone bridge assembly. The bridge excitation voltage is 5V.

The simulated output is 64.99µVPa for the optimized 'T_5' double boss sculptured disphragm. Further reduction of thickness to 0.2µm with Silicon-On-Insulator (SOI) has been done to improve the voltage sensitivity. The SOI layer improves electrical performance and is helpful for the electrical integration of the

piezoresistor on the diaphragm. The SiO_2 layer also gives higher defletcion sensitivity, reduces the thickness of the diaphragm and improves the performance by reducing power consumption [33,100,101,102,103]. The optimized 'T_5' sensor with SOI gives a voltage sensitivity of 104.9 µV/Pa. The sensitivity further improves to 154 µV/Pa through the use of polycrystalline silicon both for diaphragm and piezoresistor with thickness of diaphragm reduced from 1µm to 0.5 µm which is as shown in Fig.5.10.

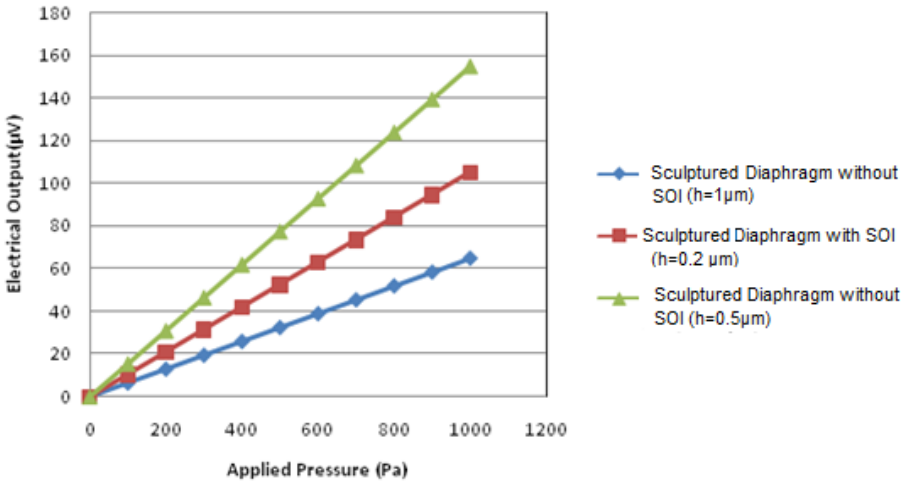

Fig.5.10 Applied pressure versus electrical output of sculptured diaphragm 'T_5'

The results indicate that the same material for diaphragm and piezoresistor gives output more than twice the conventional voltage sensitivity and diaphragm with SOI improves almost equal to twice the conventional voltage sensitivity. The sensitivity of the double boss sculptured diaphragm is enhanced through the reduction of diaphragm thickness.

5.7 COMPARISON OF ANALYTICAL AND SIMULATED RESULTS

The modified analytical equation obtained in section 5.3 is used to obtain analytical results which are used to compare and validate the simulated results for a square type single sculptured diaphragm. The comparison of center deflection, longitudinal stress and transverse stress is given in Table 5.9.

Table 5.9 Comparison of analytical and simulated center deflection, S_{xx}, S_{yy} and output voltage

	Analytical results				Simulated results			
Pressure (Pa)	**Center deflection (μm)**	**S_{xx} (MPa)**	**S_{yy} (MPa)**	**V_o (μV /Pa)**	**Center deflection (μm)**	**S_{xx} (MPa)**	**S_{yy} (MPa)**	**V_o (μV/Pa)**
0	0	0	0	0	0	0	0	0
100	0.01425	0.806	0.479	6.87	0.014877	0.789	0.461	6.499
200	0.0285	1.612	0.812	13.74	0.0297541	1.578	0.922	12.998
300	0.04275	2.45	1.24	20.61	0.0446311	2.367	1.383	19.497
400	0.057	3.27	1.67	27.48	0.0595081	3.156	1.844	25.996
500	0.07125	4.06	2.05	34.35	0.0743852	3.945	2.305	32.495
600	0.0855	4.87	2.42	41.22	0.0892622	4.734	2.766	38.994
700	0.09975	5.697	2.87	48.09	0.104139	5.523	3.227	45.493
800	0.114	6.43	3.26	54.96	0.119016	6.312	3.688	51.992
900	0.12825	7.215	3.69	61.83	0.133893	7.101	4.149	58.491
1000	0.1425	8.067	4.88	68.7	0.14877	7.89	4.61	64.99

The simulated output volatge is 64.99μV/Pa whereas the analytical output is in terms of 68.7μV/Pa. The proper position of piezoresistor and size of piezoresistor is to be analysed. Also the rectangular diaphragm dimension should be analysed based on the length to width aspect ratio to enhance the stress.

5.8 SUMMARY

The double support diaphragm with dimensions 500μm×500μm×1μm is constructed with reactive ion etching. The structure is analyzed for deflection sensitivity through variation of the G_1, G_2, S_1, S_2 and G_c to achieve small scale deflection within 20% of h. Similarly the rectangular diaphragm with 500μm×300μm×1μm is created and analyzed for the deflection and stress. It is found that deflection is comparatively low for rectangular diaphragm. The square with a double sculptured diaphragm is analyzed for the maximum stress regions to place two resistors (R_1, R_3) to undergo increase in resistance and two resistors (R_2, R_4) to undergo decrease in resistance in the longitudinal and transverse directions. The four piezoresistors are wired by Wheatstone bridge arrangement which estimates the electrical output. The output is in the order of 64.99μV at 1000Pa. The sensitivity is improved through use of silicon-on-insulator (SOI) technology by which integration

of piezoresistors is easily achieved. The output using SOI method is around 104.9μV at 1000Pa. The voltage sensitivity improves through use of polysilicon piezoresistors with thickness reduced from 1μm to 0.5μm is about 154μV at 1000Pa. The voltage sensitivity improves with smaller diaphragm thickness. It also reveals that, length to width aspect ratio to be analyzed to fix the dimension for the rectangular diaphragm as it ensures better linearity than square diaphragm which is reported in next chapter. The size and positioning of piezoresistors is also essential to enhance the sensitivity of sculptured diaphragms. To enhance the performance of double boss diaphragm, thickness is to be reduced below 1μm using the burst pressure approach is reported in next chapter.

CHAPTER 6

DESIGN OF SINGLE AND DOUBLE BOSS SCULPTURED DIAPHRAGM WITH THICKNESS LESS THAN 1µm INCORPORATING BURST PRESSURE ANALYSIS

6.1 INTRODUCTION

The single support and double sculptured diaphragms are used to improve sensitivity and linearity of the low pressure sensing. In the previous chapter, single and double sculptured diaphragms have been constructed with thickness of 1µm which gives the sensitivity in the range of µV. The square and rectangle shapes have been analyzed for the performance. The dimension of rectangular shape is to be analyzed on the basis of length to width aspect ratio. The thickness has to be further reduced for improvement of voltage sensitivity. At the same time, thickness cannot be reduced beyond certain limit as it tends to break. It means that diaphragm thickness should be as low as possible for high sensitivity. However, the thickness should be physically realizable, and should not lead to damage of the diaphragm on application of maximum pressure and should not induce any non-linear effects [100]. The permissible minimum thickness has to be analyzed by burst pressure approach. The piezoresistor size used in the previous chapter is of dimensions 40µm×20µm×1µm to estimate the electrical output. It is also considered that, the sensitivity is to be improved by decreasing the size of the piezoresistors. Since the thickness has to be reduced below 1µm, it is suitable to use rectangular shape in the design of the diaphragm. Therefore, both square and rectangle shapes were analyzed to achieve better sensitivity of low pressure sensing.

6.2 DIMENSIONS OF THE DIAPHRAGM

The dimensions of the square and rectangular diaphragm are chosen by analyzing the maximum longitudinal and transverse stress at maximum pressure. The width of the diaphragm is 500µm and thickness of the diaphragm is 1 µm, both are constant. The length is increased for the diaphragm from 500 µm to 1000 µm. The longitudinal and transverse stress results of single boss and double boss diaphragm at maximum pressure of 1000Pa is shown in Fig.6.1 and Fig.6.2.

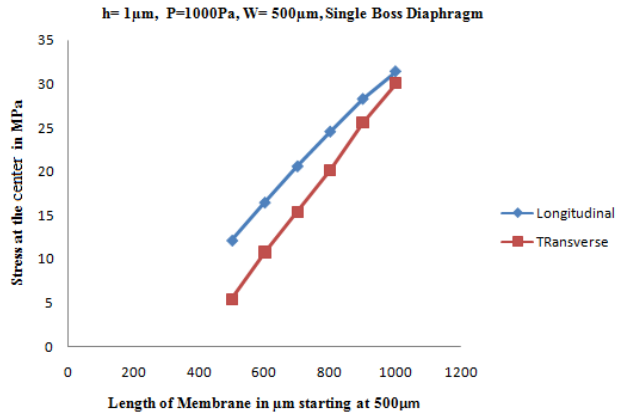

Fig.6.1 S_{xx} and S_{yy} at the longer edge of rectangular single boss sculptured diaphragm

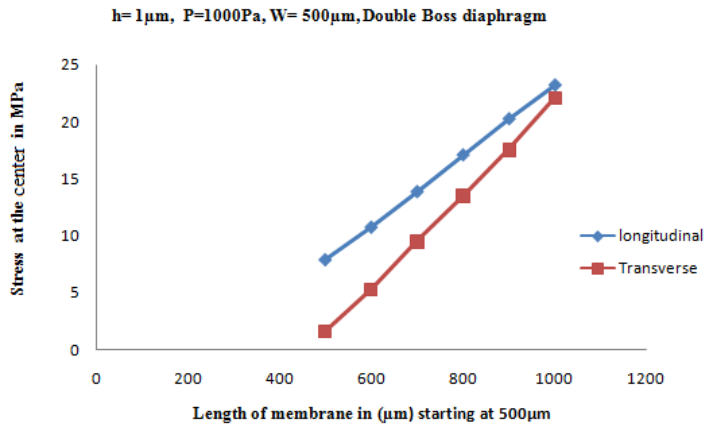

Fig.6.2 S_{xx} and S_{yy} at the longer edge of rectangular double boss sculptured diaphragm

The result obtained for single boss and double boss sculptured diaphragm in Fig.6.1 and 6.2 show that longitudinal and transverse stress increase when the length

increases from 500 µm and both the stress value reach the saturation when the length is twice the width. Therefore the dimensions of the rectangular diaphragm are fixed at 500µm×1000µm.

6.3 BURST PRESSURE ANALYSIS

The thickness of the sculptured diaphragm is reduced to increase the stress concentration as in equation (4.7). This reduced thickness for the square and rectangular sculptured diaphragm is analyzed by burst pressure condition as shown in Fig.6.3. Burst pressure P_B is defined as the pressure at which maximum stress σ_{max} on the diaphragm becomes equal to the critical stress σ_c which is actually the yield strength of material [89, 99]. Although theoretically the fracture or yield strength is 7Gpa for silicon, yet due to the influence of the diaphragm shape, thickness, lateral dimensions, rupture stress of the material and diaphragm surface roughness, the yield strength has been found considerably lower [89] and its value is equal to 1GPa. P_B is five times the maximum pressure i.e., $P_B = 5 \times P_{max} = 5 \times 1000 = 5000Pa$.

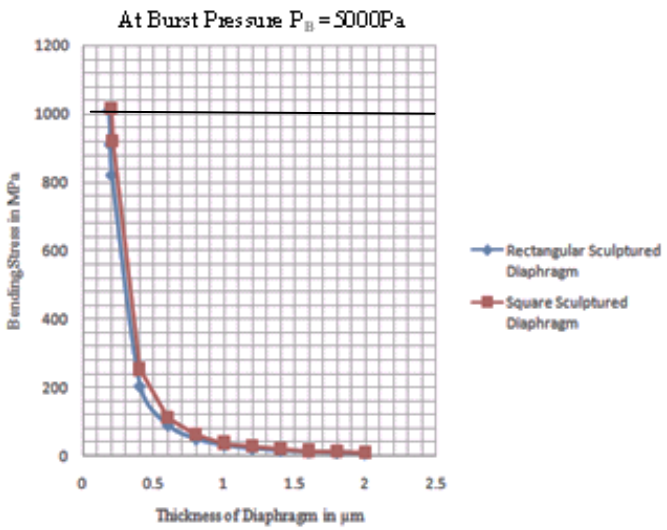

Fig.6.3 Burst pressure analysis for square and rectangular sculptured diaphragm

The graph shows that when thickness reduces from 1µm to 0.5µm, the stress increases gradually and when thickness reduces below 0.5µm stress increases very sharply to yield strength. So, during optimization, the thickness of the sculptured

diaphragm is selected in between 0.5µm to 1µm to avoid burst condition. The graph shows that the rectangular sculptured diaphragm yields a critical stress with lower thickness than the square sculptured diaphragm. The minimum thickness obtained from the graph were h_{min} = 0.18µm (for rectangular) and h_{min} = 0.21 µm (for square).

The exact value of the diaphragm thickness at which the maximum bending stress exceeds the yield strength of the material at burst pressure of 5000Pa is presented Table 6.1.

Table 6.1 Thickness versus maximum bending stress

Thickness of diaphragm (µm)	Shape of diaphragm	Maximum bending stress (MPa)
0.21	Square	1015MPa
0.18	Rectangular	1011MPa

6.4 LOAD DEFLECTION ANALYSIS OF SCULPTURED DIAPHRAGM WITH SQUARE AND RECTANGULAR SHAPES

The single boss sculptured diaphragm created has three regions at the bottom of the substrate namely G_1, G_2 and S as shown in Fig.6.4a. Similarly double boss sculptured diaphragm created has five regions namely G_1, G_2, S_1, S_2 and G_c as shown in Fig.6.4b.

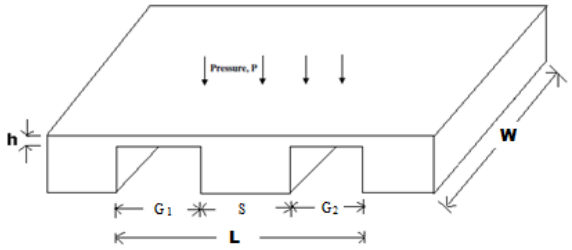

a. Single boss sculptured diaphragm

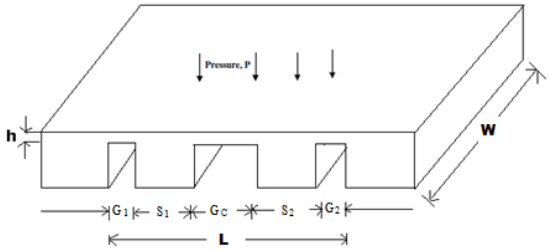

b. Double boss sculptured diaphragm

Fig.6.4 Cross sectional view of sculptured diaphragm

The abbreviations for the terms given in Fig.6.4 are as follows: L- Length, W - Width, h - Thickness, G_c-Center gap width, G_1,G_2- Support gap width, S, S_1,S_2 - Support width. All the dimensions are in µm.

The main objective of this work is to analyze the positioning of the boss by varying these regions to achieve the maximum deflection sensitivity within the small scale deflection region for square and rectangular diaphragms and also varying the thickness of the diaphragm from 0.5µm to 1 µm. The sensor is subjected to pressure on the front side as in Fig.6.4 where the piezoresistors are to be placed. The pressure range varies from 0 to 1000Pa. The feasibility of dimension optimization of single boss sculptured diaphragm is explored for square shape. The center deflection (y) and percentage of center deflection (y_p) with different thickness (h) at a maximum pressure of 1000Pa is given in Table 6.2.

Table 6.2 Load deflection analysis of single boss sculptured diaphragm (square)

Shape	h (µm)	G_1 (µm)	G_2 (µm)	S (µm)	y (µm)	y_p (%)
Square diaphragm (at a maximum pressure of 1000Pa)	1	180	180	140	0.14877	15
	1	190	190	120	0.203	20
	0.9	180	180	140	0.221	25
	0.9	170	170	160	0.1525	17
	0.9	**160**	**160**	**180**	**0.1525**	**17**
	0.8	180	180	140	0.314	39
	0.8	160	160	180	0.2168	27
	0.8	150	150	200	0.1492	19

The load deflection analysis shows that when diaphragm thickness is reduced, the percentage of deflection increases, but should be lesser than 20% of thickness of the diaphragm. The required percentage of deflection is achieved by varying the support width 'S' in respect to 'G_1' and 'G_2'. The thickness of the single boss diaphragm is reduced from 1µm to 0.8µm. The deflection estimated shows that when diaphragm thickness reduces, the deflection sensitivity increases and exceeds the small scale deflection percentage. The deflection sensitivity with in SSD range is optimized for the single boss square sculpture diaphragm with following dimension: thickness h=0.9µm and G_1= G_2 = 160µm, S = 180 µm is highlighted in the Table 6.2. This also reveals that, a square diaphragm thickness requires reduction in order to achieve a 17% deflection.

The feasibility of dimension optimization of single boss sculptured diaphragm is explored for a rectangular shape. The center deflection (y) and the percentage of center deflection (y_p) with different thickness at a maximum pressure of 1000Pa are given in Table 6.3. Thickness is varied from 1µm to 0.5µm, G_1 = G_2 = 130µm to 200µm, S = 600µm to 740µm.

Table 6.3 Load deflection analysis of single boss sculptured diaphragm (rectangle)

Shape	h (µm)	G_1 (µm)	G_2 (µm)	S (µm)	y (µm)	y_p (%)
Rectangular diaphragm (at a maximum pressure of 1000Pa)	1	200	200	600	0.342	34
	1	190	190	620	0.1892	18
	1	**180**	**180**	**640**	**0.1892**	**18**
	1	150	150	700	0.102	10
	0.9	180	180	640	0.259	29
	0.9	170	170	660	0.141	16
	0.85	180	180	640	0.307	36
	0.85	170	170	660	0.153	18
	0.85	150	150	700	0.167	20
	0.8	190	190	620	0.3691	46
	0.8	170	170	660	0.2007	25
	0.8	150	150	700	0.2007	25
	0.8	130	130	740	0.0759	10

The load deflection analysis shows that reduction in thickness is allowed by increase in the percentage of deflection. At the same time, variation in G_1 and G_2 should be within 20% of thickness of the diaphragm. The required percentage of deflection is achieved by varying the support width 'S' in respect to 'G_1' and 'G_2'. The deflection sensitivity with in SSD range is optimized for the single boss sculptured diaphragm with thickness h=0.9µm and G_1= G_2 = 160µm, S = 180 µm. This also reveals that, a rectangular diaphragm can be used with the thickness greater than the square diaphragm which will avoid burst condition. So rectangular diaphragms can be realizable in practice. The center deflection of the simulated square type single boss sculptured diaphragm is shown in Fig.6.5. The center deflection of rectangle type single boss sculptured diaphragm is also similar that of square type. The result shows that the center deflection takes place in the G_1 and G_2 region of the diaphragm as referred in Fig.6.4a. The blue colour indicates the maximum deflection.

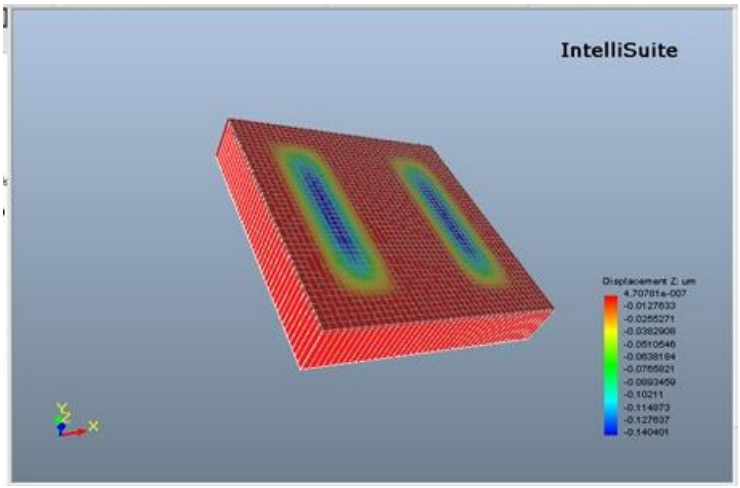

Fig.6.5 Simulated single boss sculptured diaphragm with center deflection at 1000Pa- square type

The feasibility of dimension optimization of double boss sculptured diaphragm is explored for square shape with thickness, center deflection (y) and percentage of center deflection (y_p) at a maximum pressure of 1000Pa is given in Table 6.4.

Table 6.4 Load deflection analysis of double boss sculptured diaphragm (square)

Shape	h (µm)	G_1 (µm)	G_2 (µm)	S_1 (µm)	S_2 (µm)	G_c (µm)	y (µm)	y_p (%)
Square diaphragm (at a maximum pressure of 1000Pa)	1	40	40	120	120	180	0.148	15
	1	40	40	140	140	140	0.277	28
	0.9	40	40	130	130	160	0.20	22
	0.9	40	40	140	140	140	0.0966	11
	0.85	40	40	140	140	140	0.1146	13
	0.85	40	40	130	130	160	0.2415	28
	0.8	**40**	**40**	**140**	**140**	**140**	**0.137**	**17**
	0.8	20	20	160	160	140	0.137	17
	0.8	20	20	150	150	160	0.137	17

The double boss diaphragm is used to increase sensitivity through reduction of the thickness of the diaphragm. The square diaphragm with 500µm×500µm×0.8µm shows that thickness has to be reduced much to increase deflection sensitivity. The center deflection of the simulated square type double boss sculptured diaphragm is shown in Fig.6.6. The center deflection of rectangle type double boss sculptured diaphragm is similar to the square type.

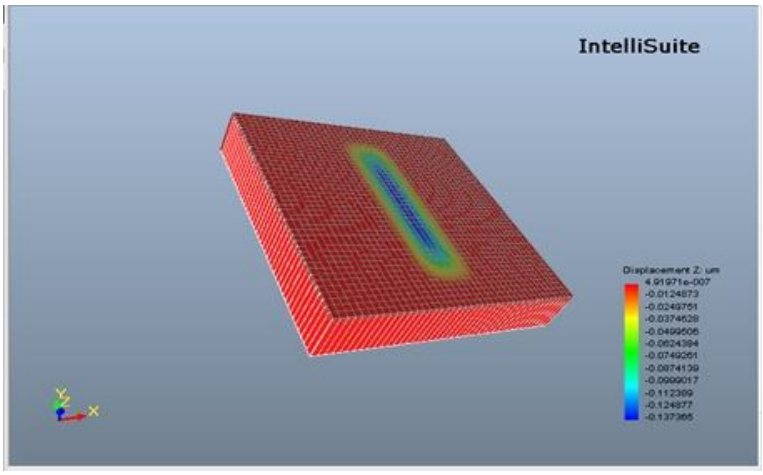

Fig.6.6 Simulated double boss sculptured diaphragm with center deflection at 1000Pa -square type

The feasibility of dimension optimization of double boss sculptured diaphragm is explored for rectangle shape with different thickness (h), center deflection (y) and percentage of center deflection (y_p) at a maximum pressure of 1000Pa is given in Table 6.5.

Table 6.5 Load deflection analysis of double boss sculptured diaphragm (rectangle)

Shape	h (µm)	G_1 (µm)	G_2 (µm)	S_1 (µm)	S_2 (µm)	G_c (µm)	y (µm)	y_p (%)
Rectangular diaphragm (at a maximum pressure of 1000Pa)	1	20	20	380	380	200	0.314	31
	1	20	20	370	370	220	0.3140	31
	1	20	20	390	390	180	0.0943	9
	0.9	20	20	380	380	200	0.431	48
	0.9	20	20	410	410	140	0.129	14
	0.9	100	100	330	330	140	0.13	14
	0.85	**20**	**20**	**400**	**400**	**160**	**0.153**	**18**
	0.8	40	40	380	380	160	0.18	23

The double boss rectangular diaphragm shows increase in deflection sensitivity as more than 30% with 1µm thickness. In order to reduce the percentage of deflection to less than 20% thickness is to be reduced to 0.85µm. The thickness of the rectangular diaphragm is greater than that of the square diaphragm. The deflection produced by rectangular is also greater than that of the square diaphragm. It shows

that, square diaphragm needs less thickness than rectangular diaphragm which tends to break very easily at maximum pressure. This reveals that rectangular diaphragm can be considered as the best suitable shape for sensing low pressures and also can be designed with thickness greater than the square type to avoid breakage of the diaphragm. More than that, when there is packaging constraints limit vis-à-vis the length, there rectangular diaphragms are the suitable choice of shape [89]. The optimized dimension of the single boss and double boss diaphragm from the load deflection analysis is given in Table 6.6a and Table 6.6b.

Table 6.6a Single boss sculptured diaphragm with optimized dimensions

Shape	h (µm)	G_1 (µm)	G_2 (µm)	S (µm)	y (µm)	y_p (%)
Square	0.9	170	170	160	0.1525	17
Rectangle	1	180	180	640	0.1892	18

Table 6.6b Double boss sculptured diaphragm with optimized dimensions

Shape	h (µm)	G_1 (µm)	G_2 (µm)	S_1 (µm)	S_2 (µm)	G_c (µm)	y (µm)	y_p (%)
Square	0.8	20	20	160	160	140	0.137	17
Rectangle	0.85	20	20	400	400	160	0.153	18

6.5 STRESS ANALYSIS AND PIEZORESISTIVE ANALYSIS

The maximum longitudinal and transverse stress regions estimated at 1000Pa for the optimized single boss diaphragm from the previous section have been analyzed and are shown in Fig.6.7 and 6.8. Figure 6.7 shows that, the maximum longitudinal stress S_{xx} (highlighted red) occurs at (90µm, 250µm) and (160µm, 250µm) from the center of the diaphragm in the vertical direction.

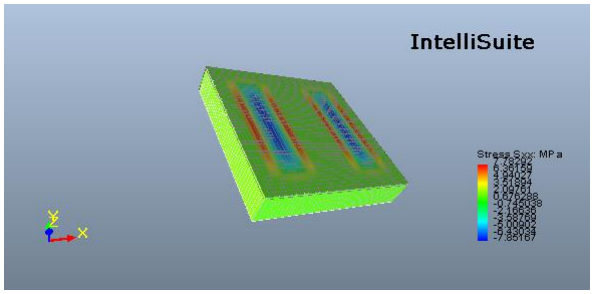

Fig.6.7 Maximum longitudinal stress distribution of simulated single boss sculptured diaphragm at 1000Pa

Similarly, Fig.6.8 shows that the maximum transverse stress S_{yy} occurs (highlighted red) at (170μm, 250μm) in the horizontal direction.

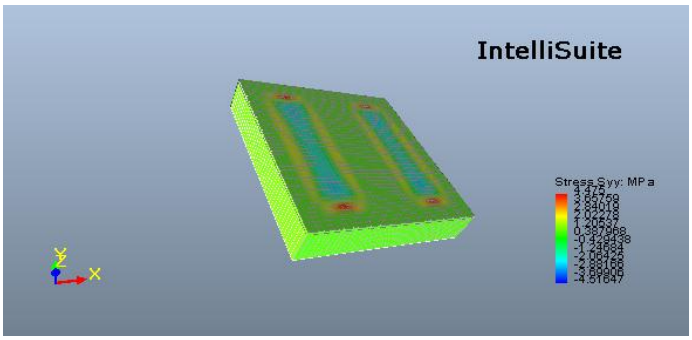

Fig.6.8 Maximum transverse stress distribution of simulated single boss sculptured diaphragm at 1000Pa

The maximum longitudinal and transverse stress regions estimated at 1000Pa for the optimized double boss diaphragm were analyzed and shown in Fig.6.9 and 6.10.

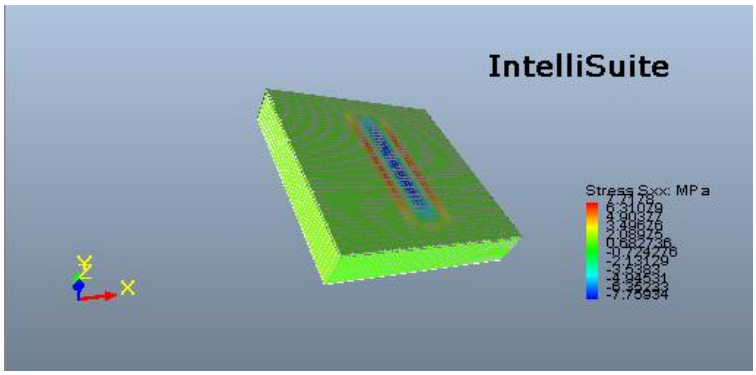

Fig.6.9 Maximum longitudinal stress distribution of simulated double boss sculptured diaphragm at 1000Pa

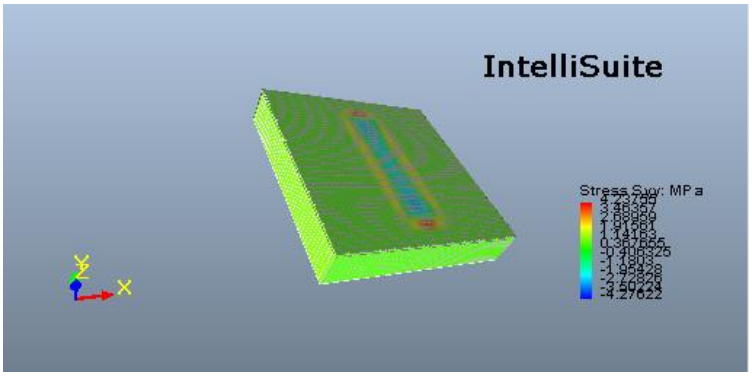

Fig.6.10 Maximum transverse stress distribution of simulated double boss sculptured diaphragm at 1000Pa

Figure 6.9 shows that, the maximum longitudinal stress S_{xx} (highlighted red) occurs at (70μm, 250μm) from the center of the diaphragm in the vertical direction. Similarly, Fig.6.10 shows that the maximum transverse stress S_{yy} occurs (highlighted red) at (0μm, 250μm) in the horizontal direction.

The maximum stress regions are identified for the proper placement of the four piezoresistors in such a way that two resistors experience tensile stress and exhibit increase in resistance and two resistors experience compressive stress and exhibit decrease in resistance. The piezoresistors placement for single and double boss diaphragms is shown in the Fig.6.11 and 6.12.

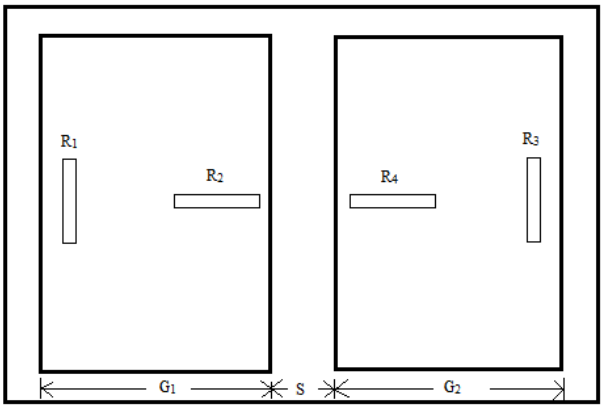

Fig.6.11 Piezoresistors placement of single boss sculptured diaphragm

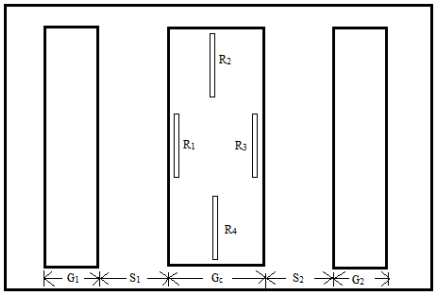

Fig.6.12 Piezoresistors placement of double boss sculptured diaphragm

The piezoresistors are of poly silicon material. The smith piezoresistive coefficients [13] used in the simulation are as follows: $\pi_{11} = 6.6\times10^{-11}$ Pa^{-1}; $\pi_{12} = -1.1\times10^{-11}$ Pa^{-1}; $\pi_{44} = 138\times10^{-11}$ Pa^{-1}. The dimensions of the piezoresistors used

were 20μm×10μm×0.5μm. The sheet resistance of p-type silicon resistor is 25Ω/square.cm and temperature = 20°C.

6.6 COMPARISON OF SIMULATED AND ANALYTICAL RESULTS

The electrical output is estimated with a wheat stone bridge assembly for the piezoresistors. The bridge is excited with the supply voltage of 5V. The longitudinal stress, transverse stress and electrical output for four types of sculptured diaphragm were compared in Table 6.7 at a maximum pressure of 1000Pa.

Table 6.7 Comparison of center deflection, longitudinal stress, transverse stress and electrical output at a maximum pressure of 1000Pa (Simulated results)

Number of boss	Thickness h(μm)	Diaphragm shape L(μm) × W (μm)	Center deflection (μm)	Percentage of center deflection y_p (%)	Longitudinal stress S_{xx} (MPa)	Transverse stress S_{yy} (MPa)	V_o (mV/Pa)
Single	0.9	Square 500×500	0.1525	17	7.783	4.475	2.283
	1	Rectangle 1000×500	0.1892	18	7.279	5.150	1.469
Double	0.8	Square 500×500	0.1374	17	7.718	4.238	2.402
	0.85	Rectangle 1000×500	0.1533	18	7.582	4.496	2.130

On comparing the percentage deflection y_p and output voltage from Table 6.5, the double boss sculptured diaphragm yields better deflection sensitivity and voltage sensitivity than the single boss sculptured diaphragm. The single boss (square) is 2.283mV/Pa, single boss (rectangle) is 1.469mV/Pa whereas double boss (square) is 2.402mV/Pa and double boss (rectangle) is 2.130mV/Pa. The applied pressure versus output voltage is plotted in Fig.6.13 and 6.14.

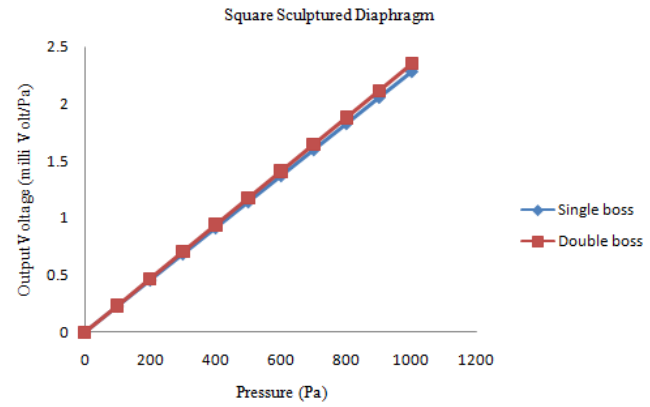

Fig.6.13 Applied pressure versus output voltage

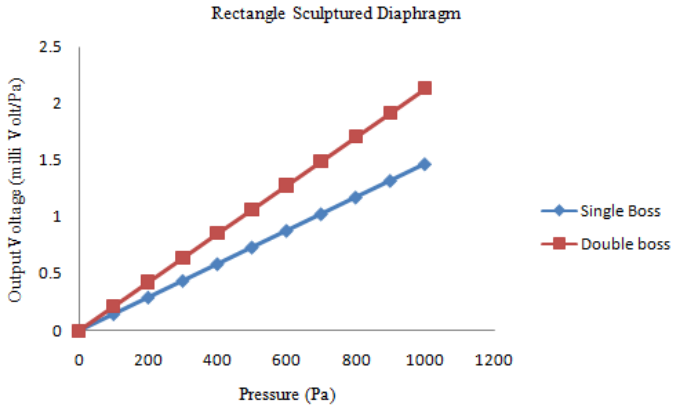

Fig.6.14 Applied pressure versus output voltage

On comparing shapes, the square yields better sensitivity than the rectangular type. Also, the square sculptured diaphragm needs smaller thickness to sense a low pressure range than the rectangle sculptured diaphragm which is difficult to realize practically. The rectangular diaphragms are suitable for realization in practice though sensitivity lags behind than a square diaphragm. On the whole, the double boss with rectangular sculptured diaphragms is more suitable to sense the low is proven here.

But, it is found that the longitudinal stress and transverse stress are almost the same for single and double sculptured diaphragm of square type. But the longitudinal stress increases for the double sculptured than single sculptured diaphragm and transverse stress decreases for the double sculptured than single sculptured diaphragm with reduced thickness. So it is necessary to maximize the stress by either SOI technique or non-uniform thickness which is discussed in next chapter. The single boss and double boss diaphragm with square and rectangle shape have been

analytically validated by using equations derived in the previous chapter. The analytical results of deflection, longitudinal stress, transverse stress and output voltage were compared for each case of diaphragm at a maximum pressure of 1000Pa is presented in Table 6.8.

Table 6.8 Comparison of center deflection, longitudinal stress, transverse stress and electrical output at a maximum pressure of 1000Pa (Analytical results)

Number of boss	Shape	Thickness h (μm)	Center deflection (μm)	Longitudinal stress S_{xx} (MPa)	Transverse stress S_{yy} (MPa)	Output voltage V_o (mV/Pa)
single	**Square**	0.9	0.1672	8.1682	4.7091	2.386
Single	**Rectangle**	1	0.1901	7.5761	5.351	1.536
Double	**Square**	0.8	0.1429	8.0312	4.3421	2.546
Double	**Rectangle**	0.85	0.1684	7.7491	4.5192	2.229

On comparing the analytical and simulated results, the analytical output voltage is higher than simulated output voltage. The output voltage is to be enhanced by analyzing the piezoresistors position and size which is discussed in next chapter.

6.7 SUMMARY

The output obtained shows that double boss sculptured diaphragm shows better sensitivity than the single boss sculptured diaphragm. On comparing shapes, square sculptured diaphragms yields better sensitivity than rectangular type. Though, sensitivity is better for square sculptured diaphragms, the thickness is less than the rectangular type, which means that it is not safe to realize in practice. But the rectangular diaphragms satisfy moderate sensitivity and ensure linearity together with 18% SSD. On the whole, the rectangular double sculptured diaphragm satisfies the sensitivity as well as acceptable linearity in output. The stress estimated using this rectangular sculptured diaphragm is to be improved by incorporating SOI approach with further reduction in thickness, proper sizing and positioning of piezoresistors is carried out in the next chapter.

CHAPTER 7

ENHANCEMENT OF SENSITIVITY

7.1 INTRODUCTION

Sculptured diaphragms are constructed to sense low pressures in the range of 0-1000Pa. Shapes in the diaphragm are also analyzed to yield better sensitivity with acceptable linearity. This is achieved by designing the diaphragm in such a way that stress is due to bending of the diaphragm and not due to stretching of the diaphragm as discussed in chapter 3. The rectangular sculptured diaphragm with two supports gives better sensitivity and acceptable linearity. The double support can withstand thickness less than 1μm and the optimized diaphragm is designed with 0.85μm achieves deflection sensitivity within 20% of h. The stress values had the major impact on the output voltage. But comparison of stress of the four cases in previous chapter shows that stress values are almost closer to one another. The sensitivity is improved from μV range to mV range by means of incorporating the following changes to enhance the stress

- Positioning of the piezoresistors for best sensitivity
- Size of piezoresistors
- Modifying the thickness of diaphragm to enhance the Stress
- Diaphragm with SOI
- Embossed diaphragm

7.2 POSITIONING OF THE PIEZORESISTOR FOR BEST SENSITIVITY

The piezoresistors are placed properly for the best sensitivity to be achieved by means of placing two resistors to experience tensile stress which exhibits increase in resistance and two resistors experience compressive stress which exhibits decrease in resistance. This type arrangement also gives better temperature compensation. The arrangement of resistors is estimated in eight different categories as shown in Fig.7.1.

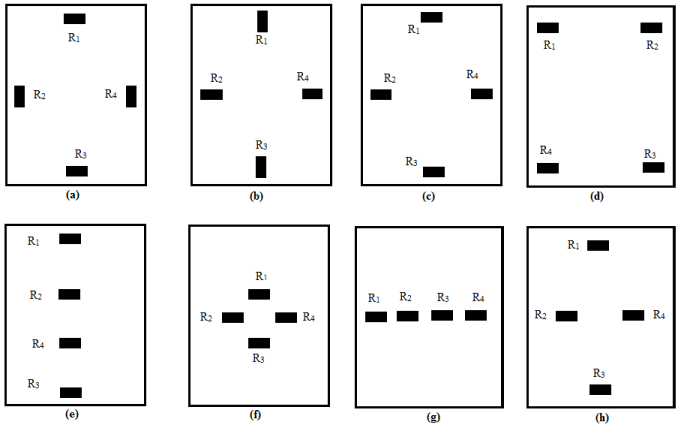

Fig.7.1 Different types of arrangement of piezoresistors placement

In pattern (a) four piezoresistors were placed parallel at the center of edge on the four sides. In pattern (b) four piezoresistors were placed perpendicular at the center of edge on the four sides. In pattern (c), two piezoresistors were placed perpendicular at the center of edge on two sides and two piezoresistors were placed parallel at the center of edge on two sides. In pattern (d), four piezoresistors were placed in four corners. In pattern (e), four piezoresistors placed parallel at the center. In pattern (f), four piezoresistors in pattern(c) were placed closer at the center of the diaphragm. In pattern (g), four piezoresistors were placed horizontally in the center. In pattern (h), the four piezoresistors were placed parallel and moved inside as similar to the pattern (c). The comparisons of the estimated output voltage at a maximum pressure of 1000Pa with respect to placement patterns of the piezoresistors were given in Table 7.1.

Table 7.1 Voltage output versus different placement pattern

Placement pattern	Output voltage (mV)
a	1.5mV
b	1.0mV
c	**3.5mV**
d	0.8 µV
e	10 µV
f	150µV
g	100µV
h	80µV

Among the eight patterns shown in Table 7.1, pattern (c) gives highest voltage sensitivity of 3.5mV at 1000Pa. The size of piezoresistors used to estimate the voltage is 40µm×20µm×1µm. It reveals that, pattern (c) is suitable and efficient in extracting the maximum stress into maximum change in resistance which in turn gives the highest voltage sensitivity. The maximum longitudinal stress S_{xx} and transverse stress S_{yy} distribution of double boss sculptured diaphragm referred in Fig.6.9 and 6.10 shows that stress is high in the center region as discussed in section 6.5.

7.3 IMPACT OF PIEZORESISTOR SIZE ON VOLTAGE SENSITIVITY

The next important key parameter is the size of piezoresistors to covert the maximum stress into resistance. The piezoresistors size is varied for different options and the output is estimated for the selected pattern (c). The results obtained show that the small size of piezoresistors gives the maximum sensitivity when compared with large size piezoresistors. The piezoresistors where designed with the resistance given by equation

$$R = \frac{\rho l}{A} \tag{7.1}$$

Where ρ is the resistivity, l is the length and A is the area which is equal to width×thickness of the piezoresistors. The length of the piezoresistors is to be decreased to improve the voltage sensitivity.

The four different sizes of piezoresistors are used to find the maximum sensitivity of change in resistance. The diaphragm and piezoresistors are made of polysilicon. The Table 7.2 represents the comparison of piezoresistors size versus output voltage.

Table 7.2 Piezoresistor size versus output voltage

Piezoresistor size	**Output voltage**
40µm×20µm×1µm	160µV
20µm×10µm×1µm	300 µV
16µm×2µm×1µm	**2.13mV**
10µm×5µm×0.5µm	3.0mV

The results reveal that the size of the piezoresistors is reduced to improve the voltage sensitivity. Also the length of the piezoresistors should be small to get higher output voltage. When the length is 40µm, the output voltage is 160µV which improves to 3.0mV by reducing the length to 10µm. The size cannot be reduced further due to constraint in fabrication which tends to break. So the size of the piezoresistors selected is 16µm×2µm×1µm with higher voltage output as 2.13mV.

7.4 MODIFYING THE THICKNESS OF DIAPHRAGM TO ENHANCE THE STRESS USING NON UNIFORM THICKNESS

The single and double boss sculptured diaphragms with uniform thickness indicated in the previous chapter show that the maximum stress is almost close to each other for all types of diaphragm. The new proposed structure for single and double boss sculptured diaphragm is created with optimized dimensions from Table 6.6a and 6.6b is shown in Fig.7.2.

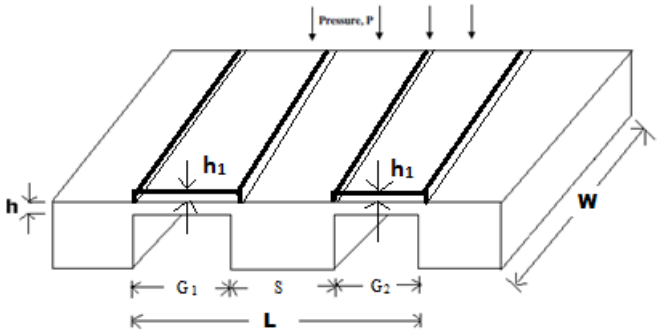

a. Single boss sculptured diaphragm

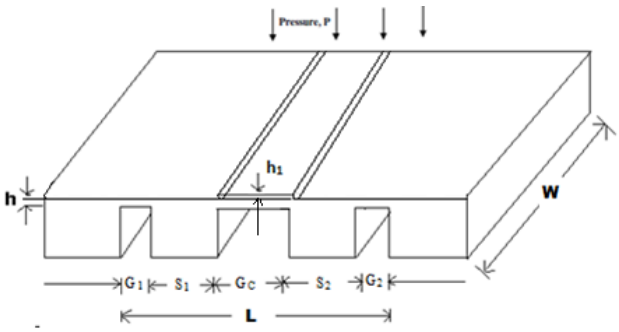

b. Double boss sculptured diaphragm

Fig.7.2 Cross sectional view of sculptured diaphragm with non uniform thickness

In order to maximize and concentrate on the stress in the supported region to improve the sensitivity, the total thickness is divided into two values as 'h' and 'h_1' where 'h' is the uniform thickness and 'h_1' is the thickness which is added only in the support regions which in turn increase the stress value. The center deflection regions are created with higher thickness to increase the stiffness at the center which in turn increases the stress as shown in Fig.7.2. The comparison of the improved longitudinal stress, transverse stress, center deflection, percentage of center deflection and voltage output for single and double boss sculptured diaphragm are given in Table 7.3. The output voltage is estimated by the piezoresistors placement using pattern (c) from the section 7.2. The dimension of single support square sculptured diaphragm created with: $G_1 = G_2 = 170\mu m$; $S = 160\mu m$ and their estimated output presented in Table 7.3a. The center deflection lower than 40% is considered as SSD to ensure linearity [109,110].

Table 7.3a Center deflection, longitudinal stress (S_{xx}), transverse stress (S_{yy}) and electrical output of the non uniform thickness for single boss square sculptured diaphragm at a maximum pressure of 1000Pa

Thickness (μm) $h=h+h_1$		**Center deflection (μm)**	**Percentage of center deflection y_p (%)**	**S_{xx} (MPa)**	**S_{yy} (MPa)**	**V_o (mV/Pa)**
h = 0.1	h_1= 0.5	0.4744	74	25.96	10.465	10.69
h =0.2	h_1= 0.5	0.3002	42	19.1	7.5393	7.979
h =0.3	**h_1= 0.5**	**0.2022**	**28**	**14.59**	**5.8165**	**6.051**

From the results obtained, 28% percentage deflection with thickness h=0.3μm and h_1 = 0.5μm is the enhanced sensitivity of 6.05mV using non uniform thickness. The other cases showing a percentage deflection greater than 30% were neglected. The dimension of single support rectangle sculptured diaphragm was created with: $G_1 = G_2 = 180\mu m$; $S = 640\mu m$ and their estimated output presented in Table 7.3b.

Table 7.3b Center deflection, longitudinal stress (S_{xx}), transverse stress (S_{yy}) and electrical output of the non uniform thickness for single boss rectangle sculptured diaphragm at a maximum pressure of 1000Pa

Thickness (μm) $h=h+h_1$		Center deflection (μm)	Percentage of center deflection y_p (%)	S_{xx} (MPa)	S_{yy} (MPa)	V_o (mV/Pa)
h = 0.3	h_1= 0.5	0.34373	42	16.378	8.2224	5.629
h =0.4	**h_1= 0.5**	**0.24229**	**27**	**12.891**	**6.5**	**4.413**
h =0.5	h_1= 0.5	0.17735	17	10.396	5.2629	3.544

From the results, 17% deflection with h=0.5μm and h_1 = 0.5μm is one for which the estimated output is 3.54mV and 27% deflection with h=0.4μm and h_1 = 0.5μm is one for which the estimated output is 4.4mV is the maximized sensitivity. The other cases showing a percentage deflection greater than 30% were neglected. The dimension of double support square sculptured diaphragm created with : G_1= G_2 =20μm;S_1 = S_2 = 160μm; G_c= 140μm and their estimated output presented in Table 7.3c.

Table 7.3c Center deflection, longitudinal stress (S_{xx}), transverse stress (S_{yy}) and electrical output of the non uniform thickness for double boss square sculptured diaphragm at a maximum pressure of 1000Pa

Thickness (μm) $h=h+h_1$		Center deflection (μm)	Percentage of center deflection y_p (%)	S_{xx} (MPa)	S_{yy} (MPa)	V_o (mV/Pa)
h = 0.4	h_1= 0.4	0.14003	18	9.5748	4.436	3.15
h =0.5	h_1= 0.2	0.29126	40	14.0437	6.9233	4.92
h =0.4	h_1= 0.3	0.29626	40	11.8228	6.9944	3.37
h =0.5	**h_1= 0.3**	**0.19488**	**24**	**10.8431**	**5.3824**	**3.77**

From the results the 24% deflection with h=0.5μm and h_1 = 0.3μm is one for which the estimated output is 4.4mV and 18% deflection with h=0.4μm and h_1 = 0.4μm is one for which the estimated output is 3.15mV. The other cases do not satisfy SSD. The dimension of double support rectangle sculptured diaphragm created with: G_1= G_2 =20μm;S_1 = S_2 = 400μm; G_c= 160μm and their estimated output presented in Table 7.3d.

Table 7.3d Center deflection, longitudinal stress (S_{xx}), transverse stress (S_{yy}) and electrical output of the non uniform thickness for double rectangle sculptured diaphragm at a maximum pressure of 1000Pa

Thickness (μm) $h=h+h_1$		Center deflection (μm)	Percentage of center deflection y_p (%)	S_{xx} (MPa)	S_{yy} (MPa)	V_o (mV/Pa)
h = 0.4	h_1= 0.5	0.162	20	9.6913	4.8053	3.372
h =0.4	**h_1= 0.4**	**0.1938**	**24**	**10.974**	**5.4084**	**3.842**
h =0.4	h_1= 0.3	0.2897	40	14.265	6.9594	5.044
h =0.5	h_1= 0.3	0.1949	24	10.843	5.3824	3.77

From the results, 24% deflection with h=0.5μm and h_1 = 0.3μm is one for which the estimated output is 3.77mV, 24% deflection with h=0.4μm and h_1 = 0.4μm is one for which the estimated output is 3.84mV and 20% deflection with h=0.4μm and h_1 = 0.5μm is one for which the estimated output is 3.372mV. The 24% deflection with 3.84mV is maximized sensitivity. The other cases do not satisfy SSD. The comparison of pressure versus output voltage for the selected structure for the pressure range of 0-1000Pa is shown in Fig.7.3 and 7.4.

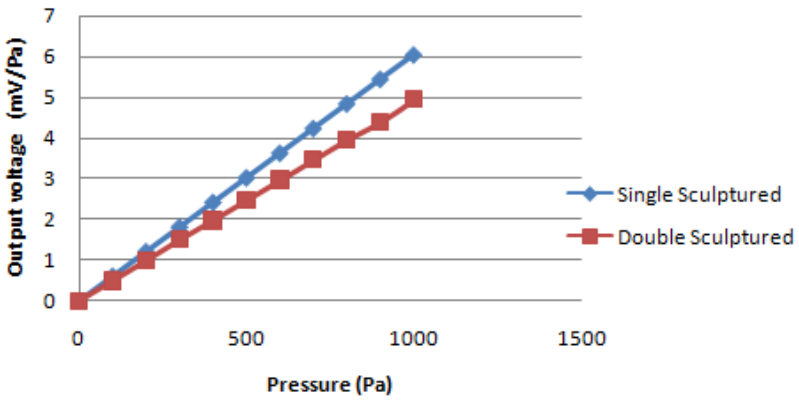

Fig.7.3 Comparison of pressure versus output voltage for non uniform thickness using square diaphragm

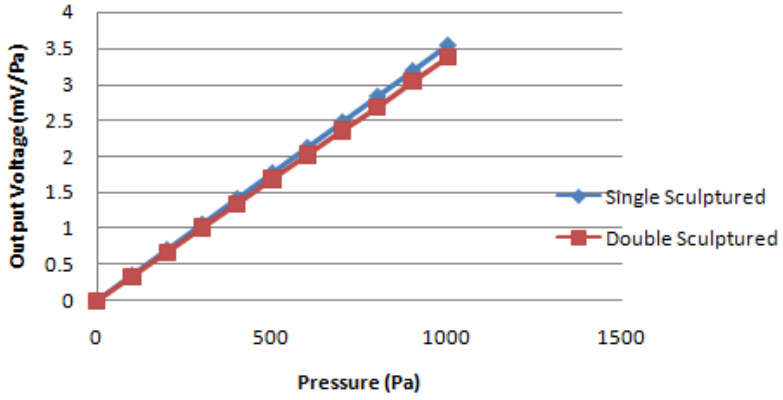

Fig.7.4 Comparison of pressure versus output voltage for non uniform thickness using rectangular diaphragm

The result shows that the modified thickness by stiffening the sculptured regions improved the stress from lower value to higher value and sensitivity is increased. In the case of square and rectangle types with non uniform thickness, single sculptured diaphragm yields the higher sensitivity but the double sculptured diaphragm satisfies both small scale deflection and sensitivity.

7.5 SENSITIVITY IMPROVEMENT USING SILICON-ON-INSULATOR (SOI)

The burst pressure analysis in chapter 6 shows that the minimum thickness for square diaphragm is 0.18µm and for the rectangle diaphragm is 0.2µm to achieve maximum sensitivity. But the thickness cannot be reduced beyond 0.6µm for square and 0.7µm for rectangle as referred in section 7.4 using non uniform thickness. In order to incorporate the minimum thickness, the silicon –on –insulator approach is used for double sculptured diaphragm to improve the sensitivity. Silicon on insulator (SOI) is an advanced variation of the conventional silicon wafer. In SOI wafer, a thin film of active single-crystalline silicon lies on a silicon dioxide dielectric layer at the top of a silicon wafer. This structure meets many of the drawbacks of conventional integrated circuits: sensibility to radiation, electrical consumption due to leakage currents, need of a minimum value of electrical voltage, limitation in the use of high voltages. SOI material has also been used to enhance Micro Electro Mechanical System (MEMS) performance. First, piezoresistive silicon pressure sensors have been achieved on SOI. The silicon strain gauges are etched in the surface single-crystalline

layer, electrically insulated from the bulk substrate, enhancing the temperature range. Moreover, junction noises are reduced for high dynamic detection. Industrial products are already available for avionics applications. More recently, it has been established that SOI is a very convenient substrate to provide single-crystalline silicon microstructures in surface micromachining processes [100,101,102,103]. The thickness of SOI layer plays an integral role in the sensor design. The fabrication of the SOI pressure sensor is carried out using the surface micromachining technique. Here The SOI wafer has been realized by bonded and etch back SOI (BESOI) technique [3, 4]. The SOI MEMS pressure sensor structure for single and double boss sculptured diaphragm created with optimized dimensions from Table 6.6a and 6.6b is shown in Fig.7.5 and 7.6.

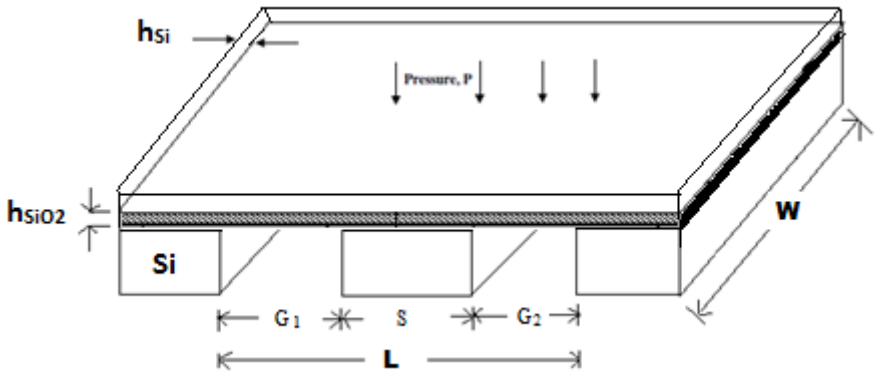

Fig.7.5 Single boss sculptured diaphragm with SOI

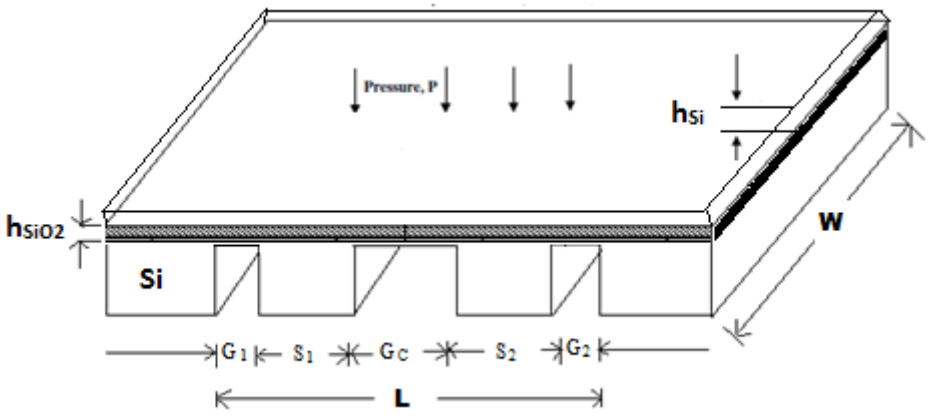

Fig.7.6 Double boss sculptured diaphragm with SOI

The Silicon-di-Oxide (SiO_2) box of standard thickness of 0.6μm is applied, and then the diaphragm of silicon is added on the top by surface micro machining

with minimum thickness from burst pressure analysis. The sculptured diaphragm with SOI is created and its comparison of the improved longitudinal stress, transverse stress, center deflection, percentage of center deflection and voltage output were estimated.

The dimensions of single boss square sculptured diaphragm with SOI: G_1= G_2 =170μm; S= 160μm and their estimated output is presented in Table 7.4a.

Table 7.4a Center deflection, longitudinal stress (S_{xx}), transverse stress (S_{yy}) and electrical output with SOI for single boss square sculptured diaphragm at a maximum pressure of 1000Pa

Thickness (μm) $h=h_{Si}+h_{SiO2}$		**Center deflection (μm)**	**Percentage of center deflection y_p (%)**	**S_{xx} (MPa)**	**S_{yy} (MPa)**	**V_o (mV/Pa)**
h_{Si} = 0.2	**h_{SiO2}= 0.6**	**0.334**	**40**	**12.37**	**4.9994**	**5.08**
h_{Si} =0.15	h_{SiO2}= 0.6	0.362	45	13.2	5.3369	5.428

The single boss square sculptured diaphragm with SOI yield a higher sensitivity of 5.08mV and small scale deflection is 40% with silicon diaphragm thickness 0.2μm. The other case yields 5.428mV but deflection is 45% not satisfying SSD with silicon diaphragm thickness 0.15μm. The dimensions of single boss rectangle sculptured diaphragm with SOI: G_1= G_2 =180μm; S= 640μm and their estimated output is presented in Table 7.4b.

Table 7.4b Center deflection, longitudinal stress (S_{xx}), transverse stress (S_{yy}) and electrical output with SOI for single boss rectangle sculptured diaphragm at a maximum pressure of 1000Pa

Thickness (μm) $h=h_{Si}+h_{SiO2}$		**Center deflection (μm)**	**Percentage of center deflection y_p (%)**	**S_{xx} (MPa)**	**S_{yy} (MPa)**	**V_o (mV/Pa)**
h_{Si} = 0.2	h_{SiO2}= 0.6	0.5703	70	15.44	6.749	6.001
h_{Si} =0.3	**h_{SiO2}= 0.6**	**0.3963**	**42**	**11.77**	**5.377**	**4.411**

The single boss rectangle sculptured diaphragm with SOI yield a higher sensitivity of 4.411 with 42% deflection and 6mV with 70% deflection. Both cases do not satisfy the SSD. The dimensions of double boss square sculptured diaphragm with

SOI: G_1= G_2 =20μm; S_1 = S_2 = 160μm; G_c= 140μm and their estimated output is presented in Table 7.4c.

Table 7.4c Center deflection, longitudinal stress (S_{xx}), transverse stress (S_{yy}) and electrical output with SOI for double boss square sculptured diaphragm at a maximum pressure of 1000Pa

Thickness (μm) $h=h_{Si}+h_{SiO2}$		**Center deflection (μm)**	**Percentage of center deflection y_p (%)**	**S_{xx} (MPa)**	**S_{yy} (MPa)**	**V_o (mV/Pa)**
h_{Si} = 0.2	**h_{SiO2}= 0.6**	**0.237**	**28**	**10.58**	**4.242**	**4.38**
h_{Si} =0.1	h_{SiO2}= 0.6	0.377	52	15.69	6.2924	6.48

The results show that, SOI with standard thickness of 0.6 μm reduced the thickness of silicon layer to its minimum thickness possible to achieve the maximum sensitivity. The double boss square sculptured diaphragm yields an output of 4.38mV with 28% deflection using 0.2μm silicon diaphragm thickness and 6.48mV with 52% deflection using 0.1μm thickness. 28% SSD is considered for which the maximum output voltage is 4.38mV which is greater than the conventional output 2.4mV. Similarly, the Double boss rectangle sculptured diaphragm with SOI is created and the output voltage is estimated.

The dimensions of double boss rectangle sculptured diaphragm with SOI: G_1= G_2 =20μm;S_1 = S_2 = 400μm; G_c= 160μm and their estimated output is presented in Table 7.4(d).

Table 7.4d Center deflection, longitudinal stress (S_{xx}), transverse stress (S_{yy}) and electrical output with SOI for double boss rectangle sculptured diaphragm at a maximum pressure of 1000Pa

Thickness (μm) $h=h_{Si}+h_{SiO2}$		**Center deflection (μm)**	**Percentage of center deflection y_p (%)**	**S_{xx} (MPa)**	**S_{yy} (MPa)**	**V_o (mV/Pa)**
h_{Si} = 0.2	**h_{SiO2}= 0.6**	**0.311**	**30**	**11.78**	**4.78**	**4.84**
h_{Si} =0.18	h_{SiO2}= 0.6	0.337	42	12.58	5.1	5.16

The result obtained shows that, the output voltage for sculptured diaphragm with SOI thickness of 0.6 μm and silicon thickness varied for 0.2 μm and 0.18 μm

which is the minimum thickness obtained using burst pressure approach is 4.84mV with 30% deflection. The other case is greater than 40% deflection with 5.16mV output. The SSD selected is 30% deflection with the output voltage by SOI method is improved to 4.84mV with minimum thickness which is greater than the conventional output of 2.13mV. The comparison of pressure versus output voltage for the selected structure in the pressure range of 0-1000Pa is shown in Fig.7.7 and 7.8.

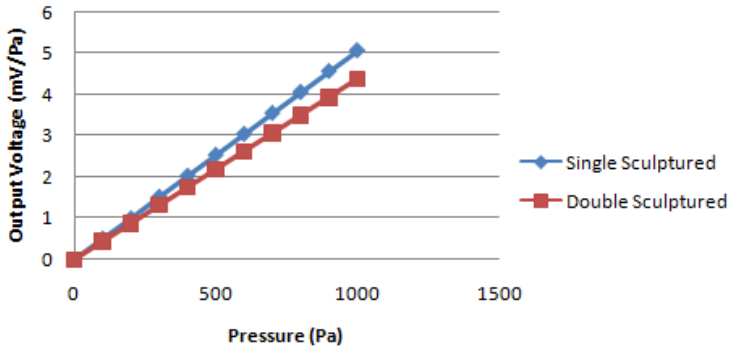

Fig.7.7 Comparison of pressure versus output voltage for square diaphragm with SOI

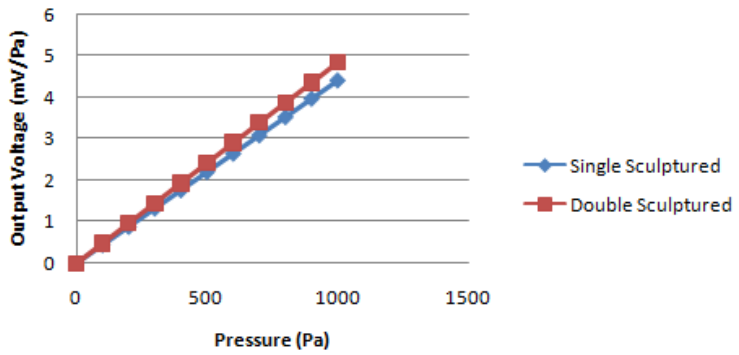

Fig.7.8 Comparison of pressure versus output voltage for rectangle diaphragm with SOI

From the graph, it is found that in square type sculptured diaphragm with SOI, single sculptured diaphragm yields a better sensitivity, but does not satisfy the small scale deflection condition of 40%. In the rectangle sculptured diaphragm with SOI, double boss sculptured diaphragm yields a higher sensitivity of 4.84mV which is twice the conventional type of 2.13mV and ensures linearity by satisfying percentage deflection of 30%. The thickness of silicon layer is 0.2µm and thickness of SiO_2 box is standard of 0.6µm.

7.6 DESIGN OF EMBOSSED DIAPHRAGM

The embossed diaphragm [87] is a special case of rigid diaphragms where solid supports are added in the bottom of the substrate. The structure of the embossed diaphragm of square type is shown in Fig.7.9.

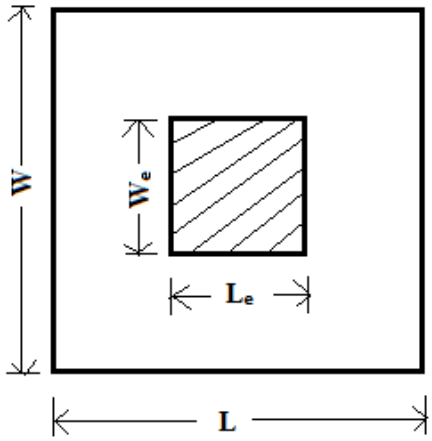

Fig.7.9 Top view of embossed diaphragm

In the diaphragm shown in Fig.7.9, L – length of the Diaphragm, L_e - Length of the embossed region, W_e – width of the embossed region and W – width of the diaphragm. The diaphragm thickness is uniform over the top of the substrate. All the dimensions are in µm. The sculptured diaphragms are those in which the supports of rectangular dimension are added, but in embossed diaphragm solid regions of that particular shape are added in the center. This type of embossed diaphragm is simulated with square and rectangular types with the following dimensions and their center deflection is analyzed for SSD.

Table 7.5 Dimensions of the embossed diaphragm

Dimensions	Square	Rectangular
Length of the outer region	700µm	1000 µm
Width of the Outer region	700µm	500 µm
Length of the embossed region	350 µm	600 µm
Width of the embossed region	350 µm	300 µm
Thickness of the diaphragm	1µm	1µm

The structure is simulated with the following dimension and the displacement and stress values at 1000Pa are compared in Table 7.6.

Table 7.6 Center deflection, percentage deflection, longitudinal stress and transverse stress of embossed diaphragm at a maximum pressure of 1000Pa

Type of embossed diaphragm	Center deflection (μm)	Percentage of deflection (%)	S_{xx} (MPa)	S_{yy}(MPa)
Square	0.193	19%	9.37	9.37
Rectangular	0.263	26%	8.515	6.5257

The square diaphragm satisfies the small scale deflection within 20%. The Longitudinal and transverse stress values are equal to 9.37MPa. The rectangular embossed diaphragm gives deflection which is greater than 20%. The longitudinal stress and transverse stress are not equal and they are less than the square embossed diaphragm. The center deflection obtained for both diaphragms are linear which is shown in Fig.7.10.

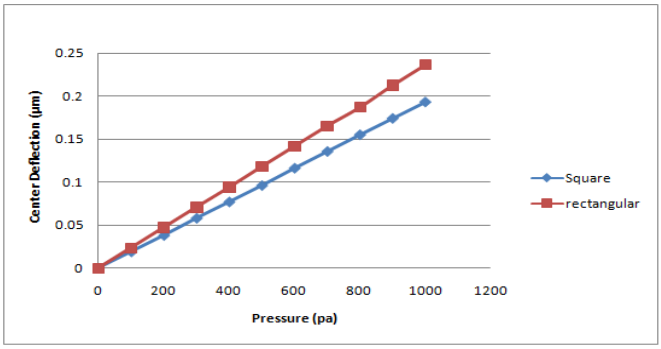

Fig.7.10 Pressure versus center deflection of embossed diaphragm

7.7 COMPARISON OF OUTPUT VOLTAGE FOR DIFFERENT PROPOSED STRUCTURE WITH EXISTING STRUCTURE

The sculptured diaphragms of square and rectangle shapes were created and their output for the pressure range of 0-1000Pa is compared and analyzed for different proposed methods. The three cases were uniform thickness of diaphragm, non-uniform thickness of diaphragm and SOI thickness diaphragm. The four different structures were square –single sculptured diaphragm, square – double sculptured diaphragm, rectangle – single sculptured diaphragm and rectangle- double sculptured diaphragm. The comparison graphs for four different structures with three cases were analyzed and presented as shown in Fig.7.11, 7.12, 7.13 and 7.14.

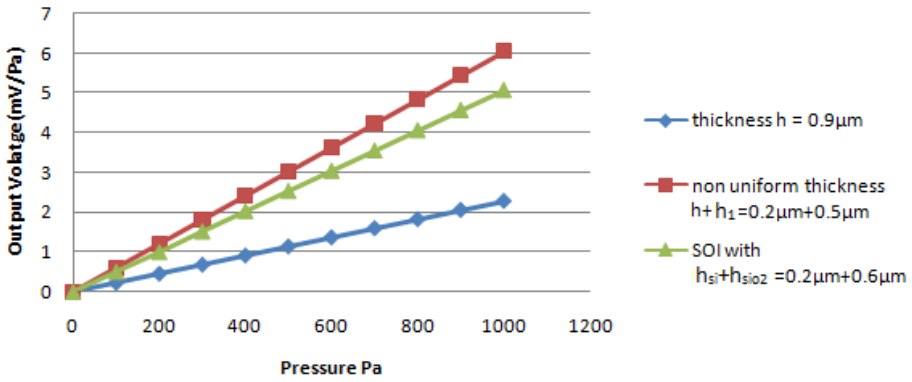

Fig.7.11 Comparison of output voltage for different proposed methods using square- single boss sculptured diaphragm

Fig.7.11 reveals that nonuniform thickness yields a higher sensitivity of 6.051mV than the uniform thickness and SOI thickness. Even though the square diaphragm gives a higher voltage output, percentage deflection exceeds 30% which shows that SSD is not satisfied. The square sculptured diaphragm with single boss can be chosen when the SSD is not a constraint.

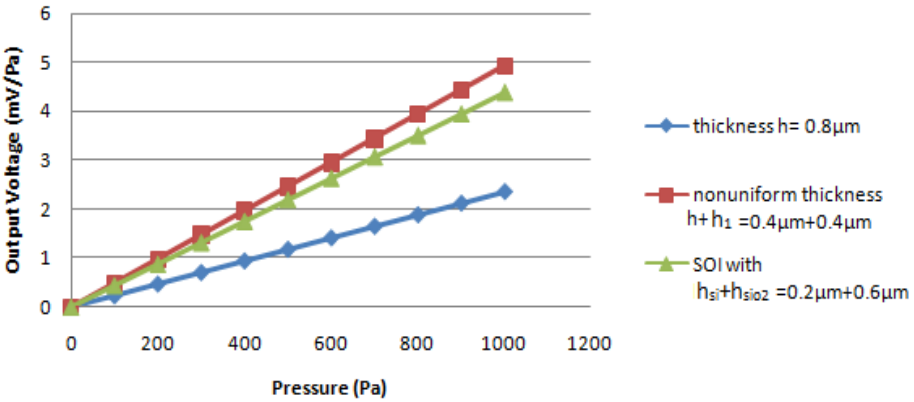

Fig.7.12 Comparison of output voltage for different proposed methods using rectangle -single boss sculptured diaphragm

Fig.7.12 reveals that nonuniform thickness yields the higher sensitivity of 4.93mV than the uniform thickness and SOI thickness. Similarly to the square single sculptured diaphragm, the square double diaphragm gives higher voltage output but percentage deflection exceeds 30% which shows that SSD is not satisfied. Therefore, double sculptured diaphragm of square type can be chosen when the SSD is not a constraint.

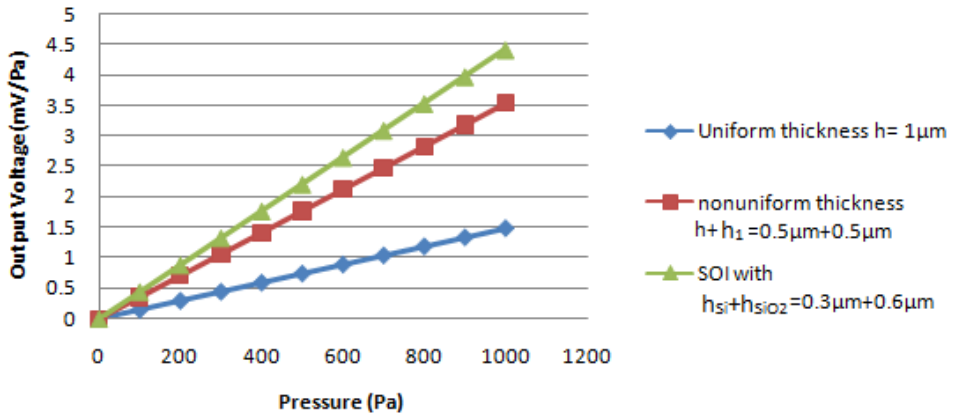

Fig.7.13 Comparison of output voltage for different proposed methods using square- double boss sculptured diaphragm

Fig.7.13 reveals that SOI thickness yields the higher sensitivity of 4.41mV than the uniform thickness and non-uniform thickness. The rectangle single sculptured diaphragm also satisfies the percentage of deflection within SSD range.

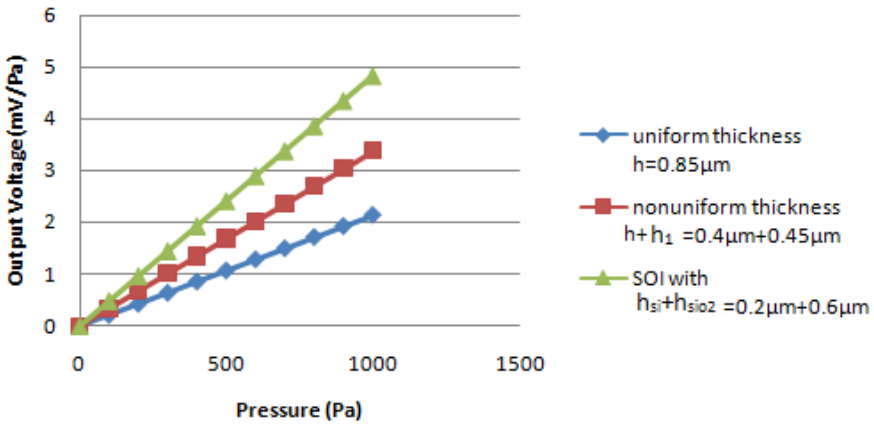

Fig.7.14 Comparison of output voltage for different proposed methods using rectangle-double boss sculptured diaphragm

Fig 7.14 reveals that SOI thickness yields the higher sensitivity of 4.84mV than the uniform thickness and non-uniform thickness. The rectangle single sculptured diaphragm also satisfies the percentage of deflection within SSD range with h = 0.2µm is used. The overall comparison of proposed diaphragm with existing diaphragm in terms of pressure range, shape, thickness, length, deflection, $\mathbf{S_{xx}}$, $\mathbf{S_{yy}}$ and voltage sensitivity are given in Table 7.7.

Table 7.7 Overall comparison of pressure range, center deflection, thickness, longitudinal stress, transverse stress and voltage sensitivity

Diaphragm type	Pressure range	Shape	Thickness of diaphragm (µm)	Length× width (µm)	Center deflection (µm)	Longitudinal stress S_{xx} (MPa)	Transverse stress S_{yy} (MPa)	Voltage sensitivity (mV/V/Pa)
Perforated diaphragm (40% perforation)	0-1kPa	Square	5µm	700 µm× 700 µm	0.211-0.402	8.1	11.9	0.216-0.387mV/V/Pa
Perforated diaphragm (40% perforation)	0-1kPa	Square	3µm	500 µm× 500 µm	0.200-0.406	8.4	12.2	0.258-0.406mV/V/Pa
Sculptured diaphragm (Proposed)	0-1 kPa	Square	0.8µm	500 µm× 500 µm	0.1374	7.718	4.238	2.402mV/V/Pa
Sculptured diaphragm (Proposed)	0-1 kPa	Rectangle	0.85µm	1000 µm ×500 µm	0.1533	7.582	4.496	2.130mV/V/Pa
Sculptured with non-uniform thickness (Proposed)	0-1 kPa	Square	0.8 µm	500 µm× 500 µm	0.237	10.58	4.242	4.38mV/V/Pa
Sculptured with non-uniform thickness (Proposed)	0-1 kPa	Rectangle	0.8 µm	1000 µm ×500 µm	0.311	11.78	4.78	4.84mV/V/Pa
Sculptured with SOI (Proposed)	0-1 kPa	Square	0.85 µm	500 µm× 500 µm	0.14003	11.5748	4.436	4.93mV/V/Pa
Sculptured with SOI (Proposed)	0-1 kPa	Rectangle	0.85 µm	1000 µm ×500 µm	0.162	9.6913	4.8053	3.372mV/V/Pa
Embossed (Proposed)	0-1 kPa	Square	1 µm	500 µm× 500 µm	0.193	9.37	9.37	2.9mV/V/Pa
Embossed (Proposed)	0-1 kPa	Rectangle	1 µm	1000 µm ×500 µm	0.263	8.5	6.5	2.7mV/V/Pa

7.8 SUMMARY

The diaphragms are constructed with smaller thickness to sense low pressure range 0-1000Pa. To avoid the balloon effect and reduce large scale deflection, diaphragms are created with supports. The improvement of output voltage by proper placement of piezoresistors, size of piezoresistors is analyzed. The two piezoresistors are placed to experience the longitudinal stress and show increase in resistance, other two piezoresistors are place to experience transverse stress and show decrease in resistance. The size of the piezoresistors is analyzed and good sensitivity from 16μm×2μm×1μm is the finding. The thickness optimized in the previous chapter is used here for the non-uniform thickness technique and voltage sensitivity is analyzed. The output of double sculptured rectangular diaphragm estimated is 3.842mV. The minimum thickness to achieve the maximum output is worked out by using SOI thickness. The thickness of silicon layer is 0.2μm and thickness of SiO_2 box is standard thickness of 0.6μm. The output voltage by SOI method is improved to 4.84mV with minimum thickness than the conventional output of 2.13mV. The result obtained reveals that, double sculptured with rectangle shape diaphragm with SOI thickness yields the maximum output and satisfies the small scale deflection which is more essential for low pressure sensing. The double sculptured with square shape using non uniform thickness yields 3.77mV, diaphragm with SOI yields 4.38mV than conventional diaphragm of 2.4mV. Though square shape gives a higher output but it does not satisfy the small scale deflection. The special case of embossed diaphragm is created and the output voltage is 2.7mV for rectangle type and 2.9mV for square type which is less than sculptured diaphragm. The proposed diaphragm with reduced thickness using non uniform thickness and SOI technique strongly establishes its superiority over all other existing diaphragms.

CHAPTER 8

CONCLUSION AND FUTURE SCOPE

8.1 FORE DEAL OF THE PROPOSED SCHEME

The diaphragm design is the major key part of any MEMS pressure sensor. This diaphragm should be designed to ensure high sensitivity with minimum thickness, acceptable linearity, physically realizable and does not break at the maximum pressure. The transduction mechanism should be properly selected to convert the displacement into electrical output. Since the invention of piezoresistance effect in silicon, piezoresistive transduction mechanism is more commonly recommended for pressure sensors. The piezoresistive method is linear, simple to fabricate. Wheat stone bridge arrangement for temperature compensation makes this more convenient for application. Thick diaphragms are suggested for very high pressure measurement [79, 89]. Perforated diaphragms are alternatives for thick non perforated diaphragms to sense medium and high pressure [97,98]. The thin diaphragms with supports are named as sculptured diaphragms were proposed for sensing low pressure.

8.2 RESEARCH CONTRIBUTIONS

The diaphragms designed for high pressures are thick flat ones. But this contradicts when the application is low pressure i.e. for low pressures it should be thin diaphragms to make it sensitive. But a thin diaphragm shows a balloon effect not satisfying small scale deflection or it may tend to break. With a view to overcome this problem, the flat diaphragms are modified in their structure with supports in the bottom named as sculptured diaphragms where thickness being reduced. This support protects the diaphragm from balloon effect and also tendency to break is reduced, simultaneously ensuring the small scale deflection within a range of 20 to 40%. This is because, at small deflections (<~10% diaphragm thickness) the pressure-deflection relationship will be linear. As the pressure increases, the rate of deflection decreases and the pressure-deflection relationship will become nonlinear. As a rule of thumb, a

deflection of 12% of diaphragm thickness will produce a terminal nonlinearity of 0.2%; a deflection of 30% produces a nonlinearity of 2% [4]. The suitability of the deflection range depends on the desired specification of the sensor and the acceptable degree of compensation. Due to these constraints to ensure linearity, the SSD is analyzed for less than 20% with respect to diaphragm thickness to ensure linearity within 0.5%. The different diaphragm materials are analyzed for the deflection sensitivity. Silicon is chosen for its excellent mechanical and electrical property, smaller hysteresis, smaller creep and elasticity. The three common shapes such as square, rectangle and circle are analyzed and square and rectangle results are found to have higher deflection sensitivity than the circular diaphragms. The importance of aspect ratio (h/L) thickness versus length is analyzed and reported. The thickness of the diaphragm should be selected as10% of diaphragm length. The diaphragms are created with bulk micromachining using wet etching with proper mask. The piezoresistors are realized by surface micromachining.

Initially the proposed single boss sculptured diaphragm created has three regions at the bottom of the substrate, namely, G_1, G_2 and S. The positioning of the boss by varying these regions to achieve the maximum deflection sensitivity within the SSD region for square shape (500μm×500μm) is analyzed and reported. The thickness of the diaphragm is 1μm. The maximum longitudinal stress and transverse stress is about 7.89MPa and 4.61MPa. The percentage of deflection is 15% and the output voltage estimated is 64.99μV/Pa. The analytical results show that the output is 68.7μV/Pa. Similarly, the rectangular single boss sculptured diaphragm created with 1μm thickness (500μm×300μm) and the feasibility of maximum deflection sensitivity is analyzed and reported. The maximum longitudinal stress and transverse stress is about 7.38MPa and 5.95MPa and the percentage of deflection is 14%. Deflection and stress are found to be comparatively low for a rectangular diaphragm which, however, ensures better linearity.

Similarly, the proposed double boss sculptured diaphragm created has five regions, namely, G_1, G_2, S_1, S_2 and G_c. The positioning of the boss by varying these regions to achieve the maximum deflection sensitivity within the SSD region for square shape (500μm×500μm) is analyzed and reported. The thickness used for this

diaphragm is 1μm. The maximum longitudinal stress and transverse stress is about 7.891MPa and 4.616MPa. The output voltage estimated is 64.99μV/Pa. The voltage sensitivity improved through use of SOI is around 104.9μV/Pa. The voltage sensitivity further improves through use of polysilicon piezoresistors with thickness reduced from 1μm to 0.5μm is about 154.9μV/Pa. Similarly, the rectangular double boss sculptured diaphragm created with 1μm thickness (500μm×300μm) and the feasibility of maximum deflection sensitivity is analyzed and reported. The maximum longitudinal stress and transverse stress is about 7.38MPa and 5.95MPa and the percentage of deflection is 14%. Here it shows that increasing the number of supports simultaneously reducing the diaphragm thickness improves the voltage sensitivity. At the same time, the dimension of rectangular diaphragm is not suitable to increase the sensitivity but it ensures linearity.

The output voltage obtained using thickness 1μm is in μV range. Improvement of output is done by reducing the thickness in the range of 0.5μm to 1μm incorporating the burst pressure approach. The burst pressure is the pressure at which the diaphragm exceeds the yield strength of the material. The length and width aspect ratio is twice the length of the diaphragm at which the stress getting maximized is reported. To enhance the sensitivity and linearity, square and rectangle shape with their dimensions are fixed at 500μm×500μm and 500μm×1000μm.

To enhance the sensitivity, the proposed sculptured diaphragms with square and rectangle using single and double supports were analyzed and reported in Table 6.6. The four different cases of diaphragms were analyzed for their electrical output using the diaphragm thickness of 0.9μm, 1.0μm, 0.8 μm and 0.85μm. The first case: Single boss square sculptured diaphragm gives 2.283mV. The longitudinal stress S_{xx} is 7.783MPa and transverse stress S_{yy} is 4.475MPa. The second case: Single boss rectangle sculptured diaphragm gives 1.469mV. The longitudinal stress S_{xx} is 7.279MPa and transverse stress S_{yy} is 5.150MPa. The third case: Double boss square sculptured diaphragm gives 2.402 mV. The longitudinal stress S_{xx} is 7.718MPa and transverse stress S_{yy} is 4.238MPa. The fourth case: Double boss rectangle sculptured gives output of 2.13mV. The longitudinal stress S_{xx} is 7.582MPa and transverse stress S_{yy} is 4.496MPa. It implies that, comparing square sculptured diaphragm, the

transverse stress increases for a rectangle sculptured diaphragm. But the longitudinal stress values are almost same. However, double boss sculptured diaphragms are better than single boss sculptured diaphragms in low pressure sensing.

The positioning of the piezoresistors is very essential in extracting the stress to convert into electrical output. The eight different positioning patterns were tested and analyzed for the maximum sensitivity reported in Table 7.1. At the same time, the length of the piezoresistors is another prime parameter essential to improve the voltage sensitivity which is analyzed and reported in Table 7.2.

The stress obtained by this uniform thickness is improved by using non-uniform thickness where stiffening of the diaphragm is done by increasing the thickness in the bossed regions. The first case: single boss square sculptured diaphragm gives the output 6.05mV with 28% deflection. The longitudinal stress S_{xx} is 14.59MPa and transverse stress S_{yy} is 5.8165MPa. The second case: single boss rectangle sculptured diaphragm gives output of 4.413mV with 27% deflection. The longitudinal stress S_{xx} is 12.891MPa and transverse stress S_{yy} is 6.5MPa. The third case: Double boss square sculptured diaphragm gives 3.77 mV with 24% deflection. The longitudinal stress S_{xx} is 10.84MPa and transverse stress S_{yy} is 5.38MPa. The fourth case: Double boss rectangle sculptured gives output of 3.84mV with 24% deflection. The longitudinal stress S_{xx} is 10.97MPa and transverse stress S_{yy} is 5.40MPa. On comparing four cases, the double boss rectangle sculptured diaphragm with 24% deflection satisfies the SSD and voltage sensitivity is 3.84mV/Pa using diaphragm thickness of 0.8μm.

The SOI layer proposed to improve the performance is analyzed for the above said cases. The first case: single boss square sculptured diaphragm gives the output 5.08mV with 40% deflection. The longitudinal stress S_{xx} is 12.37MPa and transverse stress S_{yy} is 4.999MPa. The second case: single boss rectangle sculptured diaphragm gives output of 4.41mV with 42% deflection. The longitudinal stress S_{xx} is 11.77MPa and transverse stress S_{yy} is 5.37MPa. The third case: Double boss square sculptured diaphragm gives 4.38 mV with 28% deflection. The longitudinal stress S_{xx} is 10.58MPa and transverse stress S_{yy} is 4.242MPa. The fourth case: Double boss

rectangle sculptured gives output of 4.84mV with 24% deflection. The longitudinal stress S_{xx} is 11.78MPa and transverse stress S_{yy} is 4.78MPa. The stress is improved within small scale deflection region. On comparing four cases, the double boss rectangle sculptured diaphragm with 24% deflection satisfies the SSD and voltage sensitivity is 4.84mV/Pa using diaphragm thickness of 0.2μm.

The embossed diaphragm is a special case of diaphragm where rigids are added to the lower thickness diaphragm to enhance stress and reduce nonlinearity arising due to ballooning effect. Such bossed diaphragms in which the center portion is solid with a dimension which made to deflect within small scale deflection region. The square and rectangular shapes are investigated with 1μm thickness and it is found that square gives best deflection than rectangular with respect to stress.

The rectangle double boss sculptured diaphragm with minimum thickness satisfies both small scale deflection and higher output voltage. The rectangle double boss sculptured diaphragm with the conventional method of using uniform thickness yields an output of 2.13mV. This is improved to 3.37mV by non-uniform thickness and 4.84mV by using SOI thickness. The stress concentration is improved from 7.582MPa to 11.78MPa. The thickness is reduced from 0.85 μm to 0.2 μm with SOI.

8.3 MERITS OF THE PROPOSED SCHEME

- The thin diaphragms with supports are constructed to give a linear output.
- The thin diaphragms with support minimize the balloon effect.
- The thin diaphragms with supports avoid breaking condition.
- They also increase flexural rigidity.
- The sensitivity is improved by reducing thickness to less than 1μm.
- Double boss sculptured diaphragm is constructed with smaller thickness than Single boss.
- Double boss sculptured diaphragm sense the low pressure with better sensitivity and linearity simultaneously than single boss.
- Square shape requires smaller thickness than rectangle shape.
- The sensitivity is enhanced by proper placement of piezoresistors.

- The sensitivity also depends on the size of the piezoresistors.
- Transduction mechanism is chosen as piezoresistive type as it is simple and linear.
- Square and rectangular sculptured diaphragm gives large deflection sensitivity.
- The non-uniform thickness method enhances the stress concentration in the supported regions.
- Electrical isolation by using SOI layer also reduces the thickness of the diaphragm, at the same time improves the voltage sensitivity and enhances the performance.

8.4 SUGGESTIONS FOR FUTURE WORK

There are numerous factors to be explored as an extension of this study,

i. The design of diaphragm for low pressure is a major issue which requires further mathematical analysis to get better performance.

ii. The longitudinal stress and transverse stress are not equal in magnitude, which is inconvenient to convert into electrical output. This can be further analyzed to equalize both stresses.

iii. The exact size of piezoresistors can be analyzed based on the stress graph.

iv. The mathematical models can be developed for non uniform thickness and SOI layer to get the better performance.

v. The different material for better maximized output which can withstand harsh environments.

vi. The packaging issues related to material for fabrication can be analyzed.

vii. The temperature compensation and sensitivity improvement by two wheat stone bridge arrangements can be analyzed.

viii. The structures can be fabricated and analyzed for their real time outputs with respect to different temperatures.

REFERENCES

[1] Madou, M., "Fundamentals of Microfabrication: The Science of Miniaturization", *Boca Raton, FL: second edition (revised), CRC*, 2002.

[2] W. P. Eaton and J. H. Smith, "Micromachined pressure sensors: review and recent developments", *Smart Materials and Structures*, vol. 6, pp.530–539, 1997.

[3] Julian W.Gardner, Vijay K.Varadhan and Osama O. Awadelkarim, "Microsensors, MEMS and Smart Devices", *John Wiley*, 2001.

[4] Stephen Beeby ,Graham Ensell, Michael Kraft and Neil White, "MEMS Mechanical Sensors", *Artech House, Inc*., Boston, London, 2004.

[5] G.K.Ananthasuresh, K.J.Vinoy, S.Gopalakrishnan, K.N.Bhat and V.K.Aatre, "Micro and Smart Systems", First Ed., *Wiley India Pvt. Ltd*, New Delhi, pp.122-125, 2010.

[6] R.S.MacKay, "Bio-Medical Telemetry", *IEEE Press*, Classic Reissue, 2nd Edition 1993.

[7] David S. Eddy and Douglas R Sparks, "Application of MEMS Technology in Automotive sensors and actuators", *Proceedings of the IEEE*, Vol. 86, N0 8, pp.1747 – 1755, August 1998.

[8] Sourabh Srivastav, Preetam Bhardwaj, Summit, "Fabrication, Sensing & Application of MEMS/NEMS Technology", *International Journal of Computational Engineering and Management*, Vol.12, pp.57-60, April 2011.

[9] Farbod Khoshnoud and Clarence W. De Silva, "Recent Advances in MEMS Sensor Technology – Mechanical Applications", *IEEE Instrumentation & Measurement Magazine*, pp.14-24, April 2012.

[10] Yong Zhang, Hohyun Keum, Kidong Park, Rashid Bashir, and Seok Kim, "Micro-Masonry of MEMS Sensors and Actuators", *Journal Of Microelectromechanical Systems*, Vol. 23, No. 2, pp.308-314, April 2014.

[11] Shengli Zhou, Fei Fei, Guanglie Zhang, John D. Mai, Yunhui Liu, Jay Y. J. Liou, and Wen J. Li, "2D Human Gesture Tracking and Recognition by the Fusion of MEMS Inertial and Vision Sensors", *IEEE Sensors Journal*, Vol.14, No.4, pp.1160-1170, April 2014.

[12] Chia-Ling Wei, Yu-Chen Lin, Tse-An Chen, Ren-Yi Lin, and Tin-Hao Liu, "Respiration Detection Chip With Integrated Temperature-Insensitive MEMS Sensors and CMOS Signal Processing Circuits", *IEEE Transactions On Biomedical Circuits And Systems*, Vol. 9, No. 1, pp.105-112 February 2015.

[13] Smith CS, "Piezoresistance effect in germanium and silicon", *Phys. Rev.*, Vol.94, pp.42–49, 1954.

[14] Mason WP, Thurston RN., "Use of piezoresistive materials in the measurement of displacement, force, and torque", *J Acous. Soc. of Am.*, Vol.29, pp.1096–1101,1957.

[15] Sanchez, JC.; Wright, WV., "Recent developments in flexible silicon strain gages, Semiconductor and Conventional Strain Gages", *New York: Academic Press*; pp.307-345, 1962.

[16] W.G. Pfann, R.N. Thurston, "Semiconducting stress transducers utilizing the transverse and shear piezoresistance effects", *J Appl. Phys.*, Vol.32, pp.2008–2019, 1961.

[17] O.N.Tufte , P.W. Chapman , Long D., "Silicon diffused-element piezoresistive diaphragms", *J Appl. Phys.*, Vol.33, pp.3322–3327, 1962.

[18] Petersen KE., "Silicon as a mechanical material", *Proc. IEEE* , Vol.70, pp.420–457,1982.

[19] Christel L, Petersen K, Barth P, Pourahmadi F, Mallon J, Bryzek J., "Single-crysytal silicon pressure sensors with 500× overpressure protection". *Sens. Actuators, A*, Vol.21, pp.84–88,1990.

[20] S.M. Spearing, "Materials issues in Micromechanical Systems (MEMS)", *Acta Matter*, Vol. 48, 79–196, 2000.

[21] J.P.Sullivan, T.A. Friedmann and K. Hjort, "Diamond and Amorphous Carbon MEMS", *MRS Bulletin, Special Issue on micromechanical Systems Technology and Application*, Vol. 26, No.4, pp.309-311, April 2001.

[22] Paul O, Gaspar J, Ruther P., "Advanced silicon microstructures, sensors, and systems". *IEEJ Trans.*, Vol.2, pp.199–215, 2007.

[23] Wise KD., "Integrated sensors, MEMS, and microsystems: Reflections on a fantastic voyage", *Sens Actuators A*, Vol.136, pp.39–50,2007.

[24] Xiaodong Wang, Baoqing Li, Onofrio L, Russo, Harry T.Roman, Ken K, Chin. R, Kenneth Farmer, "Diaphragm Design Guidelines and an optical

pressure sensor based on MEMS technique", *Microelectronic Journal*, Vol. 37, pp.50-56, 2006.

[25] Kwon K, Park S. "A bulk-micromachined three-axis accelerometer using silicon direct bonding technology and polysilicon layer", *Sensors and Actuators A. Physical*, Vol.66, pp.250–255, 1998.

[26] P.J. French, A.G.R. Evans, "Piezoresistance in ploysilicon and its properties applications to strain gauges", *Solid State-Electronics*, Vol.32, No.1, pp.1-10, 1989.

[27] Mallon JR, Pourahmadi F, Petersen K, Barth P, Vermeulen T, Bryzek J., "Low-pressure sensors employing bossed diaphragms and precision etch-stopping", *Sens. Actuators A* Vol. 21, pp. 89–95, 1990.

[28] Folkmer Bernd, SteinerPeter, LangWalter., "A pressure sensor based on a nitride membrane using single-crystalline piezoresistors", *Sens. Actuators A*, Vol.54, pp.488–492 1996.

[29] Esashi M, Sugiyama S, Ikeda K, Wang Y, Miyashita H., "Vacuum-sealed silicon micromachined pressure sensors", *Proc IEEE*, Vol.86, pp.1627–1639,1998.

[30] Hyeoncheol kim, Yong-Gwon Jeon and Kukjin Chun, "Improvement of the linearity of a capacitive pressure sensor using an interdigitated electrode structure", *Sensors and Actuators A*, Vol. 62, pp.586-590, 1997.

[31] R.E. Oosterbroek, T.S.J. Lammerink, J.W.Berenschot, G.J.M. Krijnen, M.C.Elwenspoek, A.Van den Berg, "A Micro Machined Pressure Flow Sensor", *Sensors and Actuators A*, Vol.77, pp.167 -177, 1999.

[32] Beeby, S. P., M. Stuttle, and N. M. White, "Design and Fabrication of a Low-Cost Microengineered Silicon Pressure Sensor with Linearized Output," *IEE Proc. Sci. Meas. Technol.*, Vol. 147, No. 3, pp. 127–130, 2000.

[33] P.D.Dimitropoulos, C.Kachris, D.P .Karampatzakis and G.I.Stamoulis, "A new SOI monolithic capacitive sensor for absolute and differential pressure measurements", *Sensors and Actuators A*, Vol.123-124, pp.36-43, April 2005.

[34] Li Chen, Mehran mehregany, "A silicon carbide capacitive pressure sensorfor in cylinder pressure measurement", *Sensors and Actuators A*, Vol.145-146, pp. 2-8, 2006.

[35] Fang He, Qing- An Huang, Ming Qin, "A Silicon directly bonded capacitive absolute pressure sensor", *Sensors and Actuators A*, Vol.135, pp. 507 – 514, 2007.

[36] Cheng Pang, Zhan Zhao, Lidong Du, Zhen Fang, "Adhesive Bonding with SU -8 in a vacuum for capacitive pressure sensors", *Sensors and Actuators A*, Vol.147, pp.672 – 676, 2008.

[37] Youngmin Kim, Dean P. Neikirk, "Micromachined fabry-perot cavity pressure transducer", *IEEE Photonics Technology letters*, Vol. 7, No. 12, pp 1471 – 1473, 1995.

[38] Libor Rufer, Christian C.Domingues, Salvador Mir, Valerie Petrini, Jean-Claude Jeannot and Patrick Delobelle, "A CMOS Compatible Ultrasonic Transducer Fabricated With Deep Reactive Ion Etching", *J.of MicroElectroMechanical Systems*, Vol.15, No.6, pp.1766-1776, 2006.

[39] F.Ceyssans, M.Driesen, K.Wouters, R.Puers, K.U.Leuven, "A Low cost and highly integrated fiber optical pressure sensor system", Sensors and Actuators A, Vol.145-146, pp.81-86, 2008.

[40] Yixian Ge, Ming Wang, Xuxing Chen, Hua Rong, "An optical MEMS pressure sensor based on a phase demodulation method", *Sensors and Actuators A*, Vol.143, pp.224-229, 2008.

[41] Keith E. Holbert, James A Nessel, Steven S. McCready, A.Sharif Heger and Thomas H. Harlow, "Response of Piezoresistive MEMS Accelerometers and Pressure Transducers to High Gamma Dose", *IEEE Trans. on Nuclear Science*, Vol.50, No.6, pp.1852-1859, 2003.

[42] Berns A, Buder U, Obermeier E, Wolter A, Leder A.Aero, "MEMS sensor array for high-resolution wall pressure measurements", *Sens. Actuators A*, Vol.132, pp.104–111, 2006.

[43] A. Wisitsoraat, V.Patthanasetakul, T.Lomas and Tuantranont, "Low cost thin film based piezoresistive MEMS tactile sensor", *Sensors and Actuatrors*, Vol. 139, pp.17-22, 2007.

[44] Shyam Aravamudhan and Shekhar Bhansali, "Reinforced piezo-resistive pressure sensor for ocean depth measurements", *Sen. and Actuators A*, Vol.142, pp.111-117, 2008.

[45] M. Milon, Jevti, A. Miloljub and Smiliani, "Diagnostic of silicon piezoresistive pressure sensors by low frequency noise measurements", *Sensors and Actuators*, Vol. 144, pp.267-274, 2008.

[46] E.R.Peake, A.R.Zias and J.V.Egan, "Solid-State Digital Pressure Transducer", *IEEE Tran Electron Devices*, Vol.16, pp.870–876, 1969.

[47] Stedman, CK., "Transducers with substantially linear response characteristics", *US Patent*. 3 341 794, Sep 12, 1967.

[48] Samaun, S.; Wise, K.; Nielsen, E.; Angell, J. "An IC piezoresistive pressure sensor for biomedical instrumentation", *IEEE International Solid-State Circuits Conference*, pp. 104-105, 1971.

[49] Wilner, LB, "A diffused silicon pressure transducer with stress concentrated at transverse gages", *23rd International Instrumentation Symposium*, LasVegas, NV, pp.361-365, 1977.

[50] Wilner, LB, "Sculptured pressure diaphragm", *US Patent*. 4 093 933. Jun 6, 1978.

[51] Marshall, JF, "Fabrication of semiconductor devices utilizing ion implantation", 4 033 787, Jul 5, 1977.

[52] Kurtz, AD, Mallon, JR and Nunn, TA., "Semiconductor transducers employing flexure frames". *US Patent*, 4 236 137, Nov 25, 1980.

[53] Clark SK, Wise KD, "Pressure sensitivity in anisotropically etched thin-diaphragm pressure sensors", *IEEE Trans Electron Devices*, Vol.26, pp.1887–1896, 1979.

[54] Jackson TN, Tischler MA, Wise KD, "An electrochemical P-N junction etch-stop for the formation of silicon microstructures", *IEEE Electron Device Lett*., Vol.2, pp.44–45, 1981.

[55] Kim SC, Wise KD., "Temperature sensitivity in silicon piezoresistive pressure transducers", *IEEE Trans Electron Devices*, Vol. 30, pp.802–810, 1983.

[56] Petersen, K., Barth, P., Poydock, J., Brown, J., Mallon, JJ., Bryzek, J., "Silicon fusion bonding for pressure sensors", *Tech. Digest IEEE Solid-State Sensor and Actuator Workshop*, pp.144-147, 1988.

[57] Kloeck B, Collins SD, de Rooij NF, Smith RL., "Study of electrochemical etch-stop for high-precision thickness control of silicon membranes", *IEEE Trans Electron Devices*, Vol.36, pp.663–669, 1989.

[58] Spencer RR, Fleischer BM, Barth PW, Angell JB., "A theoretical study of transducer noise in piezoresistive and capacitive silicon pressure sensors", *IEEE Trans Microelectron. Reliab. Electron Devices,* Vol.35, pp.1289–1298, 1988.

[59] Pourahmadi F., Gee D., Petersen K., "Modelling of thermal and mechanical stresses in Si microstructures", *Sens Actuators, A21 –A23,* 850-855,1990.

.[60] H. Sandmaier, "Non-Linear Analytical Modeling of Bossed Diaphragms for Pressure Sensors", *Sensors and Actuators,* Vol. A25–27, pp. 815-819, 1991.

[61] Kanda Y, Yasukawa A. "Optimum design considerations for silicon piezoresistive pressure sensors", *Sens Actuators A,* Vol. 62, pp.539–542, 1997.

[62] Lin L and Yun, "Design, Optimization & Fabrication of surface micromachined Pressure Sensors", *Journal of Mechatronics*, Vol. 8, pp.505-519, 1998.

[63] Lin L, "A simulation program for the sensitivity and linearity of piezoresistive pressure sensors", *IIEEE/ASME Journal of EEE/ASME Journal of MEMS*, Vol. 8, pp.514-522, 1999.

[64] Mosser,V., Susuki,J.,Goss,J, & Obermeier, E., "Piezoresistive Pressure Sensors Based on Polycrystalline Silicon," *Sensors and Actuators A,*Vol.28, pp.113-132, 1991.

[65] Sun YC, Gao Z, Tian LQ, Zhang Y, "Modelling of the reverse current and its effects on the thermal drift of the offset voltage for piezoresistive pressure sensors", *Sens Actuators A,* Vol.116, pp.125–132, 2004.

[66] Bae B, Flachsbart BR, Park K, Shannon MA, "Design optimization of a piezoresistive pressure sensor considering the output signal-to-noise ratio", *J Micromech Microeng,* Vol. 14, pp.1597–1607, 2004.

[67] F. J. Morin, T. H. Geballe, and C. Herring, "Temperature dependence of the piezoresistance of high-purity silicon and germanium", *Phys. Rev.,* Vol. 10, no. 2, pp. 525–539, 1956.

[68] O. N. Tufte and E. L. Stelzer, "Piezoresistive properties of silicon diffused layers", *J. Appl. Phys.*, Vol. 34, No. 2, pp.3322–3327, Feb. 1963.

[69] O. N. Tufte and E. L. Stelzer, "Piezoresistive properties of heavily doped n-type silicon", *Phys. Rev.*, Vol. 133, No. 6a, pp. A1705–A1716, Mar. 16, 1964.

[70] Kanda Y, "A graphical representation of the piezoresistance coefficients in silicon", *IEEE Trans Electron Devices*, Vol. 29, pp.64–70, 1982.

[71] Gniazdowski and P. Kowalski, "Practical approach to extraction of piezoresistance coefficient", *Sens. Actuators*, pp. 329–332, 1998.

[72] Shih-Chin Gong and Chengkuo Lee, "Analytical Solutions of Sensitivity for Pressure Microsensors", *IEEE Sensors Journal*, Vol. 1, No. 4, pp.340-341, December 2001.

[73] Shih-Chin Gong, "Effects of Pressure Sensor Dimensions on process window of membrane thickness", *Sensors and Actuators A*, Vol.112, pp.286-290, 2004.

[74] Henning A.K., Patel S., Selser M., Cozard B.A., "Factors Affecting silicon Membrane Burst Strength", *Proceedings of SPIE*, Vol. 5343, pp.145-153, 2004.

[75] Zhao Linlin, Xu Chen and Shen Guangdi, "Analysis for load limitations of square-shaped silicon diaphragms", *Solid-state Electronics*, Vol. 50, pp.1579-1583, 2006.

[76] Raman, M. S., Kifle, T., Bhattacharya, E., & Bhat, K. N., "Physical Model for the Resistivity and Temperature Coefficient of Resistivity in Heavily Doped Polysilicon", *IEEE Transactions on Electron Devices*, Vol.53, No.8, pp.1885-1892, 2006.

[77] K. Sivakumar, N.Dasgupta and K..N.Bhat, "Sensitivity enhancement of polysilicon piezo-resistive pressure sensors with phosporous diffused resistors", *Journal of Physics: Conference series*, Vol.34, pp216-221, 2006.

[78] Ingelin Clausen and Ola Sveen, "Die separation and packaging of a surface micromachined piezoresistive pressure sensor", *Sensors and Actuators A*, Vol.133, pp.457- 466, 2007.

[79] K . N. Bhat, "Reviews -Silicon Micromachined Pressure Sensors", *Journal of IISc*, Vol.87, No.1, pp.115-131, 2007.

[80] Lee W. S. and Lee S.S., "Piezoelectric Microphone built on circular Diaphragm", *Sensors and Actuators A*, Vol.144, pp.367-373, 2008.

[81] Xin Zhang, Seungbae Park and Michael W. Judy, "Accurate Assessment of Packaging Stress Effects on MEMS Sensors by Measurement and Sensor-Package Interaction Simulation", *J. of MicroElectroMechanical Systems*, Vol. 16, No 3, pp.639-649, 2007.

[82] Chun-Hyung Cho, Richard C.Jaeger and Jeffrey C.Suhling, "Characterization of the Dependence of the piezoresistive coefficients of Silicon From -150°C to 125°C", *IEEE Sensors Journal*, Vol.8, No.8, pp.1455-1468, 2008.

[83] Usmah Kawoos, Mohammad-Reza Tofighi, Ruchi Warty, Francis A. Kralick, and Arye Rosen, *"In-Vitro* and *In-Vivo* Trans-Scalp Evaluation of an Intracranial Pressure Implant at 2.4 GHz", *IEEE Transactions on Microwave Theory And Techniques*, Vol. 56, No. 10, pp.2356-2365, October 2008.

[84] Jong M. Park, Allan T. Evans, Kristian Rasmussen, Tyler R. Brosten, Gregory F. Nellis, Sanford A. Klein, and Yogesh B. Gianchandani, "A Microvalve with Integrated Sensors and Customizable Normal State for Low-Temperature Operation", *Journal Of Microelectromechanical Systems*, Vol. 18, No. 4, pp.868-877, August 2009.

[85] Giulio Fragiacomo, Kasper Reck, Lasse Lorenzen and Erik V.Thomsen, "Novel Design for Application Specific MEMS pressure sensors", *Sensors*, Vol.10, pp.9541-9563, 2010.

[86] Joel Soman and Chad B.O'Neal, "Fabrication and Testing of A PZT Strain Sensor For Soil Applications", *IEEE Sensors Journal*, Vol. 11, No. 1, pp. 78-85, 2011.

[87] Ivan Padron, Anthony T. Fiory and Nuggehalli M.Ravindra, "Integrated Optical and Electronic Pressure Sensor", *IEEE Sensors Journal*, Vol. 11, No. 2, pp.343-349, 2011.

[88] Yang Chuan and Li Chen, "The Compensation for Hysteresis of Silicon Piezoresistive Pressure Sensor", *IEEE Sensors Journal*, Vol. 11, No. 9, pp.2016-2021, September 2011.

[89] Vidhya Balaji and K.N. Bhat, "A Comparison of Burst Strength and Linearity of Pressure
Sensors having Thin Diaphragms of Different Shapes", *J.ISSS*, Vol.2, No.2, pp.18-26, 2012.

[90] Nitin R Panse1 and Dhananjay Panchgade, "Load-Deflection Analysis of Flat and Corrugated, Stainless Steel Diaphragms", *International Journal of Applied Engineering Research*, ISSN 0973-4562, Vol.8, No.15, pp.1833-1838, 2013.

[91] Gawade S.S and Chavan D.S., "Load Deflection Analysis of Flat and Corrugated Stainless Steel Diaphragms by Theoretical & Finite Element

Method", *Int.J, Engineering Research and Applications*, Vol.3, No. 4, pp.799-802, 2013.

[92] M. Shahiri-Tabarestani, B. A. Ganji and R. Sabbaghi-Nadooshan, "Design and Simulation of New Micro-Electromechanical Pressure Sensor for Measuring Intraocular Pressure", *IEEE conference*, pp.208-211, 2012.

[93] Moinuddin Ahmed, Donald P. Butler and Zeynep Celik-Butler, "MEMS Absolute Pressure Sensor on a Flexible Substrate", *IEEE MEMS Conference*, Paris, pp. 575-578, 2012.

[94] Suja K J, E Surya Raveendran and Rama Komaragiri, "Investigation on better Sensitive Silicon based MEMS Pressure Sensor for High Pressure Measurement", *International Journal of Computer Applications*, ISSN 0975 – 8887, Vol.72, No.8, May 2013.

[95] K.Y Madhavi, M.Krishna and C.S.Chandrasekhara, "Design of Piezoresistive Micropressure Sensor Using Finite Element Analysis", *Int.J of Computer Applications*, Vol. 70, No. 3, pp.20-26, 2013.

[96] Sarath S, Rama Komaragiri, "Feasibility Study of AC Bridges in MEMS Pressure Sensors", *IEEE Students' Conference on Electronics and Computer Science*, 2012.

[97] M.Rajavelu, D.Sivakumar,R.Joseph Daniel and K.Sumangala, "Feasibility Studies on MEMS Oxygen Flow Sensors by Differential Pressure Method for Pediatric Ventilators", *J.ISSS*, Vol.1, No.1, pp. 34-45, 2012.

[98] M.Rajavelu, D.Sivakumar,R.Joseph Daniel and K.Sumangala, "Perforated Diaphragms employed piezoresistive MEMS pressure sensor for sensitivity enhancement in gas flow measurement", *Flow Measurement and Instrumentation*, Vol. 35, pp.63-75, 2014.

[99] K . N. Bhat and M.M.Nayak, "MEMS pressure sensors –An overview of challenges in technology and Packaging", *J.ISSS*, Vol.2, No.1, pp. 39-71, 2013.

[100] M. Narayanaswamy, R. Joseph Daniel, K. Sumangala and C. Antony Jeyasehar, "Computer aided modelling and diaphragm design approach for high sensitivity silicon-on-insulator pressure sensors", *Measurement*, Vol. 44, pp.1924 -1936, 2011.

[101] M. Narayanaswamy, R.Joseph Daniel and K.Sumangala : "Peizoresistor size and placement effect on sensitivity of silicon-on-insulator piezoresistive pressure sensor", *J. ISOI*, Vol.43, No.3, pp.208-211, 2013.

[102] St´ephane Renard, "Industrial MEMS on SOI", *Journal of Micromech. Microeng*, Vol. 10, pp.245–249, 2000.

[103] Veljko Milanovic, "Multilevel Beam SOI-MEMS Fabrication and Applications", *Journal of Microelectromechanical Systems*", Vol. 13, No. 1, pp.19-29, February 2004.

[104] Mahanth Prasad, Vineet sahula, Vinod Kumar Khanna, " Design and Fabrication of Si Diaphragm , ZnO Piezoelectric Film-Based Acoustic Sensor Using SOI Wafers" *IEEE Trans. on Semiconductor Manufacturing*, Vol 26, No2, pp.233 – 241, 2013.

[105] Jin Xie, "Fabrication challenges and test structures for high-aspect-ratio SOI MEMS devices with refilled electrical isolation trenches", *Micro Systems Technology*, Springer, 2014.

[106] Thomas Helbling, Cosmin Roman, Lukas Durrer, Christoph Stampfer, and Christofer Hierold, "Gauge Factor Tuning, Long-Term Stability, and Miniaturization of Nanoelectromechanical Carbon-Nanotube Sensors", *IEEE Transactions on Electron Devices*, Vol. 58, No. 11, pp.4053-4060, November 2011.

[107] Saúl M. Domínguez-Nicolás, Raúl Juárez-Aguirre, Pedro J. García-Ramírez, and Agustin L. Herrera-May, "Signal Conditioning System With a 4–20 mA Output for a Resonant Magnetic Field Sensor Based on MEMS Technology", *IEEE Sensors Journal*, Vol. 12, No. 5, pp.935-942, May 2012.

[108] Liang Lou, Hongkang yan, Woo-Tae Park, Dim-Lee Kwong and Chengkuo Lee, "Characterization of Piezoresistive Si Nano Wires Based Pressure Sensors by Dynamic Cycling Test with Extra Large Compressive Strain", *IEEE Trans. Electron Devices*, Vol. 59, No.11, pp. 3097-3103, 2012.

[109] S. Timoshenko and S. Woinowsky-Krieger, "Theory of Plates and Shells", *McGraw-Hill*, New York, pp.4-32, 1959.

[110] Eduard Ventsel, Theodor Krauthammer, "Thin Plates and Shells, Theory, Analysis, and Applications", The Pennsylvania State University, University Park, Pennsylvania, *Marcel Dekker, Inc.*, New York, Basel, 2001.

LIST OF PUBLICATIONS

INTERNATIONAL JOURNALS

1. D.Sindhanaiselvi, R.Ananda Natarajan, "Design and Optimization of Low Pressure Sculptured Diaphragm with Burst Pressure, Stress Analysis and its Enhancement", *International Journal of Applied Engineering Research (IJAR),* ISSN 0973-4562, Vol. 10, No.24, pp.21075-21081, 2015.

2. D.Sindhanaiselvi, R.Ananda Natarajan, "Performance Analysis of Sculptured Diaphragm for Low Pressure MEMS Sensors", *International Journal of Applied Mechanics and Materials* , Vol. 592-594, pp.2193-2198, 2014.

INTERNATIONAL CONFERENCES

1. D.Sindhanaiselvi and R.Ananda Natarajan, "Design and Optimization of Low Pressure Sculptured Diaphragm with Burst Pressure and Stress Analysis", presented in the *International Conference on Advances in Design and Manufacturing (ICADM'14)* at National Institute of Technology, Tiruchirapalli, ISBN 978-93-84743-15-4, Vol.3, pp.1399-1404, Dec' 2014.

2. D.Sindhanaiselvi and R.Ananda Natarajan, "Design of Sculptured Diaphragm for Low Pressure MEMS Sensors ", presented in the *International Mechanical Engineering Congress"* at National Institute of Technology, Tiruchirapalli, ISBN 978-93-84389-01-7, June 2014.